

Copyright

by

David Samuel Simmons

2009

The Dissertation Committee for David Samuel Simmons
certifies that this is the approved version of the following dissertation:

**Phase and Conformational Behavior of LCST-Driven
Stimuli Responsive Polymers**

Committee:

Isaac Sanchez, Supervisor

Nicholas Peppas

Krishnendu Roy

Venkat Ganesan

Thomas Truskett

**Phase and Conformational Behavior of LCST-Driven
Stimuli Responsive Polymers**

by

David Samuel Simmons, B.S.

Dissertation

Presented to the Faculty of the Graduate School of

The University of Texas at Austin

in Partial Fulfillment

of the Requirements

for the Degree of

Doctor of Philosophy

The University of Texas at Austin

December, 2009

To my grandfather,
who made me an engineer
before I knew the word

and

to my wife, Carey,
for being my partner
on my good days and bad.

Acknowledgements

I am extraordinarily fortunate in the support I have received on the path to this accomplishment. My adviser, Dr. Isaac Sanchez, has made this publication possible with his advice, support, and willingness to field my ideas at random times in the afternoon; he has my deep appreciation for his outstanding guidance. My thanks also go to the members of my Ph.D. committee for their valuable feedback in improving my research and exploring new directions. I am likewise grateful to the other members of Dr. Sanchez' research group – Xiaoyan Wang, Yingying Jiang, Xiaochu Wang, and Frank Willmore – who have shared their ideas and provided valuable sounding boards for my mine. I would particularly like to express appreciation for Frank's donation of his own post-graduation time in assisting my research. I'd furthermore like to thank Dr. Gabriel Luna-Barcenas, with whom I had many educational conversations during his time visiting our group. I also have the great fortune of having received receiving invaluable mentorship in my undergraduate years and before. My great thanks go to Dr. Anuj Chauhan for preparing me for graduate school and beyond, and for teaching me the importance of scientific rigor. I am likewise deeply grateful to Dr. Leonard Pinchuk, whose mentorship began in my high school years and who opened many doors that led me to a career in engineering research. My final thanks go to the Cockrell School of Engineering and Mr. John W. Bartholow, Jr. for their generous financial support through the Thrust 2000 Endowed Graduate Fellowship.

“Gratitude” cannot begin to express my appreciation for the support of my family, which has made all things possible. My parents’ profound faith in me has given me the confidence to pursue my dreams. My sister’s certain belief in my character has driven me to live up to what she sees in me. My wife’s daily encouragement, trust, and example have helped me grow into the person I had always hoped to become. Moreover, her graceful patience with the glow of a laptop at odd hours of the night has been essential to the timely completion of this work.

Phase and Conformational Behavior of LCST-Driven Stimuli Responsive Polymers

David Samuel Simmons, Ph.D.

The University of Texas at Austin, 2009

Supervisor: Isaac C. Sanchez

Several analytical mean field models are presented for the class of stimuli responsive polymers that are driven by the lower critical solution temperature (LCST) transition. For solutions above the polymer crossover concentration, a hybrid model combines lattice-fluid excluded volume and van-der-Waals interactions with a combinatorial approach for the statistics of hydrogen bonding, hydration, and ionic bonding. This approach yields models for the LCST of both neutral polymers and lightly charged polyelectrolytes in aqueous salt solution. The results are shown to be in semi-quantitative agreement with experimental data for the cloud point of polyethylene oxide (PEO) in aqueous solution with various salts, and some aspects of the lyotropic series are reproduced. Results for lightly charged polyelectrolytes are compared to and shown to be in qualitative agreement with aspects of experimentally observed behavior. Finally, a framework is established for extension of these models to further aspects of the lyotropic series and polyelectrolyte behavior.

At the nanoscale, lattice fluid (LF) and scaled particle theory (SPT) approaches are employed to model the LCST-related coil-globule-transition (CGT) of isolated

polymer chains in highly dilute solution. The predicted CGT behavior semi-quantitatively correlates with experimental results for several polymer-solvent systems and over a range of pressures. Both the LF and SPT models exhibit a heating induced coil-to-globule transition (HCGT) temperature that increases with pressure until it merges with a cooling induced coil-to-globule transition (CCGT). The point at which the CCGT and HCGT meet is a hypercritical point that also corresponds to a merging of the lower critical and upper critical solution temperatures. Theoretical results are discussed in terms of a generalized polymer/solvent phase diagram that possesses three hypercritical points. Within the lattice model, a dimensionless transition temperature $\tilde{\Theta}$ is given for a long chain simply by the equation $\tilde{\Theta} = 1 - \eta_s^B(\Theta)$, where $\eta_s^B(\Theta)$ is the bulk solvent occupied volume fraction at the transition temperature. Furthermore, there is a critical value of the ratio of polymer to solvent S-L characteristic temperature below which no HCGT transition is predicted for an infinite chain.

Table of Contents

List of Tables	xi
List of Figures.....	xii
Chapter 1. Introduction.....	1
1.1. Polymer Solution Phase Behavior	1
1.1.1. Characteristics.....	1
1.1.2. Physics of the LCST	7
1.2. The Coil-Globule Transition.....	10
1.3. Charges in Solution.....	14
1.3.1. Effects on stability: the lyotropic series.....	14
1.3.2. The Debye-Huckel model.....	17
1.3.3. Polyelectrolytes.....	18
1.4. Approaches to the Chemical Potential.....	23
Chapter 2. The Lower Critical Solution Temperature.....	26
2.1. Review	27
2.1.1. Lattice fluid model.....	27
2.1.2. Hydrogen bonding lattice fluid model.....	30
2.2. Theory.....	35
2.2.1. Aqueous polymers in the presence of free salt	35
2.2.2. Polyelectrolytes.....	42
2.2.3. Solution Stability	54
2.3. Applications, Results, and Discussion.....	60
2.3.1. Neutral polymer in aqueous salt solution	60
2.3.2. Polyelectrolyte	67
2.4. Conclusions.....	73
Chapter 3. Single Chain Conformational Behavior.....	75
3.1. Theory.....	76
3.1.1. General model.....	76

3.1.2.	Lattice model	79
3.1.3.	Scaled particle theory	84
3.2.	Results.....	89
3.2.1.	Overall pressure-temperature behavior.....	89
3.2.2.	Physics of the transition.....	92
3.2.3.	The high pressure hypercritical point	95
3.2.4.	The CGT near the solvent vapor pressure	96
3.2.5.	Chain conformation through the CGT.....	101
3.3.	Conclusions.....	104
Chapter 4. Towards a Model for the Aqueous CGT		107
4.1.	CGT with Veytsman Statistics.....	107
4.1.1.	Physical contribution	109
4.1.2.	Hydrogen bonding contribution.....	109
4.1.3.	Chain gyration radius and coil-globule transition	110
4.2.	Basis for a Consistent Approach.....	112
Chapter 5. Conclusions.....		115
Appendix 1. Nomenclature.....		116
Appendix 2. Extended Derivations.....		123
A.2.1.	Solution Stability	123
A.2.2.	Scaled Particle Theory Coil-Globule Transition.....	124
Appendix 3. Mathematica code		129
A.3.1.	LCST in Aqueous Solution with Salt.....	129
A.3.2.	Lattice Fluid CGT	160
References.....		168
Vita	179

List of Tables

- Table 1: Comparison of theoretical HCGT temperatures at solvent vapor pressure with experimental and theoretical LCSTs for polyisobutylene in various solvents. Solvents are grouped by carbon number. SPT results are unavailable for some solutions due to present limitations on parameter availability for this model. 99
- Table 2: Comparison of theoretical and experimental results for $\partial\Theta/\partial P|_{P=0}$ for various systems. For the LF model, theoretical calculations are based on polymer molecular weights chosen to match those associated with each experimental result. For the SPT model, calculations are at infinite molecular weight, which is expected to cause little error due to the large size of the chain. SPT results are unavailable for some solutions due to present limitations on parameter availability for this model. 100

List of Figures

Figure 1: Temperature-composition phase diagram for weakly interacting polymer solution. The striped gray area is the metastable region and the solid gray area is the unstable region.....	3
Figure 2: Effect of polymer molecular weight on solution phase behavior. Curves may represent either spinodal or binodal loci. Dashed curves correspond to increasing chain molecular weight in the direct of the dotted line.	3
Figure 3: Polymer solution and blend phase diagrams. Behaviors include LCST only (a), UCST only (b), LCST and UCST curves with multiple extrema (c and d). merged LCST and UCST (e), closed immiscibility loops (f), and combinations of LCST, UCST, and closed immiscibility loop behavior (g and h). Curves may represent either spinodal or binodal curves.	4
Figure 4: Schematic master curve of polymer solution phase behavior in pressure-temperature space. The curve represents the spinodal or binodal curve of the system. The gray area denotes two-phase states whereas the white region denotes single-phase states. Dashed lines indicate phase boundaries lacking definitive experimental confirmation.	6
Figure 5: Qualitative schematic of mixture entropy of as a function of composition for a system above the LCST. The dotted straight line denotes the unmixed entropy. The curved dashed line denotes the mixture entropy neglecting equation of state effects. The solid curve represents the actual mixture entropy, with equation of state effects.	9
Figure 6: Schematic proposed master curve for pressure- temperature behavior of the CGT. The white region corresponds to a coil state, the gray to a globule state, and the curve to the CGT itself. Points to the left of P_{min} and to the right of P_{max} correspond to a CCGT, while points between P_{min} and P_{max} correspond to an HCGT.....	12
Figure 7: Plot from work by Florin et. al. ⁸⁰ showing early experimental results for the lyotropic series. Points denote cloud-point measurements for PEO / water solutions with varying concentrations of salts. Triangles correspond to data with KI, circles to KBr, squares to KCl, and diamonds to KF. Curves are simply a visual aid.	15

Figure 8: Conformational diagram of a weak polyelectrolyte based on Monte-Carlo simulations ¹⁰⁵ . The x-axis, ϵ_{vdW} , is the van der Waals interaction in units of $k_B T$ and is thus an inverse temperature axis. Yellow spheres denote charged monomers whereas blue sphere denote uncharged monomers.....	20
Figure 9: Spinodal curves for aqueous PEO in the presence of salt at various concentrations. Salt properties have been manually adjusted to approximate experimental results for the LCST of PEO with KI. Numbers on curves are salt occupied volume fraction corresponding to that curve. Note that the apparent meeting point of the three curves is not truly a single point upon closer inspection.	62
Figure 10: Cutout of isothermal ternary phase diagram for water-PEO-salt system, shown in Figure 11. Curves denote spinodals at indicated temperatures. The vertical axis corresponds to anion occupied volume fraction while the horizontal axis corresponds to polymer occupied volume fraction. Salt properties have been manually adjusted to approximate experimental results for the LCST of PEO with KBr. Numbers on curves denote the system temperature for that curve. Dashed line denotes an isothermal salt-induced LCST transition at 370 K.	63
Figure 11: The ternary phase diagram for the present system. The white region corresponds to the region shown in Figure 10. Results have not been obtained for the grey region, and the present model would likely be inappropriate for treatment of the region corresponding to higher salt concentration due to breakdown of the Debye-Huckel model.	64
Figure 12: Schematic of possible associations in PEO-water-free salt system. Heavy dashed lined denote hydrogen bond types, which are present in the absence of free ions. Light dashed lines denote ion-dipole bond types. Bonds that share a locus compete with one another for use of that type of site. The heavy curve denotes a PEO chain, with a particular oxygen site note. C+ and A- denote free cation and anion, respectively.	65
Figure 13: Experimental cloud points ⁸⁰ (points) and manual LCST fits (curves) based on the above theory, for aqueous PEO as a function of salt concentration for various salts. Black curve and points correspond to the LCST in the presence of KI, green to KBr, blue to NaCl, and red to KF. The purple line demonstrates a typical salting-in case as predicted by this model for a hypothetical salt characterized by a strong favorable	

cation-water hydration interaction and weak anion-water and cation-polymer interactions.	66
Figure 14: Effect of fraction of electrolytic monomers on PEO LCST, for monomers with a very low pK_0 corresponding to a strong electrolyte, in 0.05 molar aqueous salt solution. The properties of the salt do not correspond exactly to any real salt but fall within the range of lyotropic salting-out behavior.	70
Figure 15: LCST of aqueous PEO with electrolytic subunits substituted for 0.1% of its monomers, as a function of the pK_0 of the electrolyte subunits. The vertical dashed line indicates the pC of the solution (the negative base ten logarithm of the counterion concentration) in solution. The free ions do not correspond to any real salt, but are hypothetical ions constructed to fall into the typical range of salting out behavior described above.....	71
Figure 16: LCST of PEO with strong electrolytic subunits substituted for 0.1% of its monomers, as a function of anion volume fraction. The equivalent range of salt molarity is zero to about 0.7.....	72
Figure 17: Plot of dimensionless CGT pressure versus temperature as predicted by equation (3.32) for an infinite chain in solution with $r_s = 10$ and $\zeta = \tilde{T}_p^*/\tilde{T}_s^* = 2.0$. Because $\tilde{\Theta} \equiv \Theta/2T_p^* = (\tilde{T}_p/2) _{\alpha=1}$, the scaling of the temperature axis is such that the temperature value given for any point on the curve corresponds to the value of $\tilde{\Theta}$ at that pressure. The solid square denotes the critical point of the solvent. Values to the left of the hypercritical point P_{\max} correspond to an HCGT while values to the right correspond to a CCGT.	90
Figure 18: Plot of CGT of polyisobutylene in n-pentane. The solid line is the lattice fluid prediction, while the blue line is the scaled particle theory prediction.	91
Figure 19: P - T plot of the HCGT of polyisobutylene ($M_w = 1.66 \times 10^6$ g/mol) in various solvents. Solid lines correspond to predictions based upon equation (3.32) for the lattice fluid model for an infinite chain. Dashed lines correspond to predictions based upon equation (3.54) for the SPT model for an infinite chain. Points correspond to experimental data ¹¹	92
Figure 20: Qualitative contributions by excluded volume and polymer self-interaction energy to the RHS of equation (3.22) as a function of temperature for a system in which the polymer S-L characteristic	

temperature is greater than the solvent S-L characteristic temperature. Coil-globule transitions occur when the sum of these contributions is zero.⁹³

- Figure 21: LCST and CGT data for polyisobutylene in various solvents as a function of solvent density..... 94
- Figure 22: Contour plot of temperature $\tilde{\Theta}_{P_{\max}}$ at the high pressure hypercritical point as a function of interaction ratio ζ and solvent size r_s , for the LF model in the limit of infinite chain length. The numbered lines indicate the value of $\tilde{\Theta}_{P_{\max}}$ along that contour. White points indicate the position of various polymer / solvent systems. Each vertical triplet of points corresponds, from top to bottom, to polystyrene, polyisobutylene, and PDMS in the labeled solvent..... 96
- Figure 23: Quantitative plot of dimensionless transition temperature vs. the ratio of the S-L characteristic temperatures of the polymer and solvent for infinite chain length. The vertical axis is the dimensionless transition temperature $\tilde{\Theta}$. Figure 23a is for infinite r_s while Figure 23b is for r_s equal to 10. The point marked in red on each plot is the liquid-vapor critical point of the solvent. The green curve denotes the critical point of the solvent as a function of ζ . Each branch from the critical point corresponds to a coil globule transition for a chain in a different solvent phase, as labeled on the plots. Note that in the limit of infinite r_s (Figure 23b) both the gas and supercritical phases are at zero solvent density. Sub-critical data is at the solvent saturated vapor pressure while supercritical data is at the solvent critical pressure..... 98
- Figure 24: Plot of theoretical vs experimental values of $\partial\Theta/\partial P|_{P=0}$ for systems shown in Table 2. Black diamonds denote LF-CGT results while blue squares denote SPT-CGT results. The 45 degree line indicates the locus of points along which theoretical and experimental values would agree..... 101
- Figure 25: Expansion factor as a function of temperature for various molecular weights of polyisobutylene in n-pentane near the HCGT. The red line corresponds to a molecular weight of 10^6 , the blue to a molecular weight of 10^7 , and the black to a molecular weight of 10^8 103
- Figure 26: Polymer volume fraction as a function of temperature for various molecular weights of polyisobutylene in n-pentane near the HCGT. The red line corresponds to a molecular weight of 10^6 , the blue to a molecular weight of 10^7 , and the black to a molecular weight of 10^8 103

Figure 27: Typical plot of chain expansion factor through the pressure induced globule-to-coil transition as predicted by this model, shown as calculated for the system polyisobutylene / n-pentane. Curves correspond to different temperatures. From leftmost to rightmost curve, corresponding temperatures are 353 K, 354 K, 355 K, 356 K, and 357 K. 104

Chapter 1. Introduction

The lower critical solution temperature (LCST) transition is a ubiquitous and fundamental mechanism by which many stimuli responsive polymers react to environmental changes. This mechanism has drawn great interest in the development of synthetic ‘smart polymers,’ and it is believed to contribute to the function of many biopolymers. LCST physics drive two qualitatively distinct but related behaviors. For solutions of uncrosslinked polymers above the chain overlap concentration, the LCST presents as a macro-scale phase separation. On the other hand, in macromolecular systems that are either highly dilute or are covalently constrained from phase separation, the LCST takes the form of a swelling transition at the scale of the molecule or covalently constrained network. These behaviors exist over a wide range of polymer solution properties, from nonpolar polymers in organic solvents to polyelectrolytes in aqueous solution. Despite this extensive applicability, a predictive and even qualitative theoretical understanding of these phenomena is lacking in many cases. Accordingly, this work presents a new set of models extending theoretical understanding and semi-quantitative prediction of LCST phenomena to a range of previously unaddressed systems.

1.1. Polymer Solution Phase Behavior

1.1.1. Characteristics

It has long been understood that polymer solutions exhibit rich phase behavior that is qualitatively distinct from that of small molecule mixtures. Whereas small molecule solutions exhibit thermally induced mixing, as early as 1960 Freeman and Rowlinson reported thermally induced phase separation in polymer solutions¹. The modern picture of binary polymer solution phase behavior is of a variety of possible phase diagrams. The typical temperature-composition phase diagram for a weakly interacting polymer solution includes two phase boundaries, the lower corresponding to thermally induced mixing and the upper corresponding to thermally induced demixing, as

shown in Figure 1²⁻⁴. For the lower boundary, the maximum temperature at which thermally induced mixing occurs is known as an upper critical solution temperature (UCST). For the upper boundary, the minimum temperature at which thermally induced demixing occurs is known as a lower critical solution temperature (LCST). Alternatively, these terms are sometimes used to refer to the infinite molecular weight limit of these extrema or to the entire corresponding spinodal or binodal curve. The asymmetry in the critical curves in Figure 1 originates from the asymmetry in component size; in general, the more dissimilar the molecular size of the components, the greater the asymmetry in the phase diagram. As shown in Figure 2, as the polymer molecular weight goes to infinity and the solvent molecular weight is held constant, the LCST and UCST move to zero composition at a condition corresponding to the Flory theta point.

Beyond this typical behavior for weakly interacting polymers, many other T-x phase diagrams exist for polymer solutions in general^{2,3,5,6}, particularly in the presence of strong intermolecular interactions. Solutions may exhibit LCST or UCST behavior only (Figure 3 a, b), and these critical curves may possess multiple extrema⁷ (Figure 3 c, d). Merging of an LCST and a UCST curve may result in a necked immiscible region, as in Figure 3e. Closed immiscibility loops are also observed (Figure 3f), as are such loops in the presence of other typical or atypical LCST and UCST curves (Figure 3 g, h). Furthermore, the system pressure and component molecular weights may control which such behavior is observed.^{4,8}

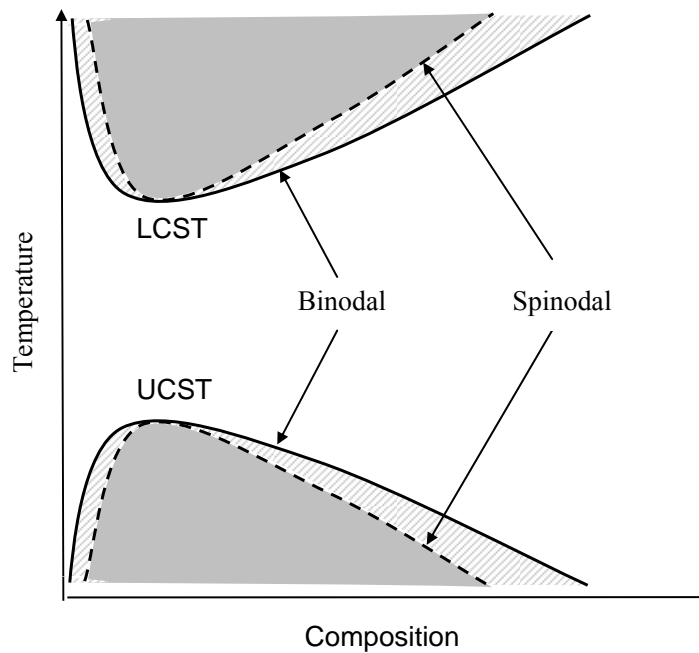


Figure 1: Temperature-composition phase diagram for weakly interacting polymer solution. The striped gray area is the metastable region and the solid gray area is the unstable region.

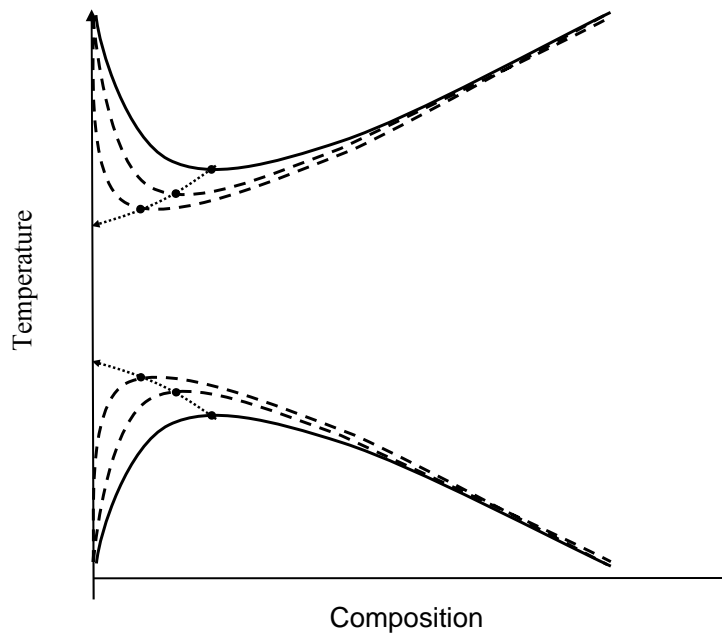


Figure 2: Effect of polymer molecular weight on solution phase behavior. Curves may represent either spinodal or binodal loci. Dashed curves correspond to increasing chain molecular weight in the direct of the dotted line.

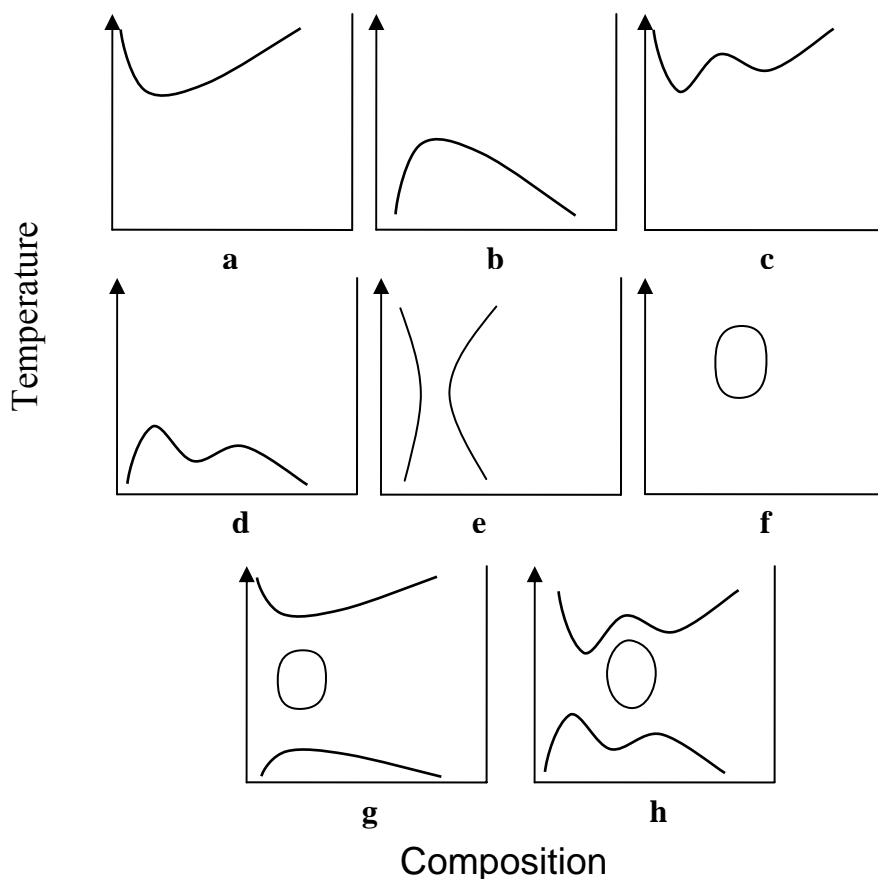


Figure 3: Polymer solution and blend phase diagrams. Behaviors include LCST only (a), UCST only (b), LCST and UCST curves with multiple extrema (c and d), merged LCST and UCST (e), closed immiscibility loops (f), and combinations of LCST, UCST, and closed immiscibility loop behavior (g and h). Curves may represent either spinodal or binodal curves.

The pressure-temperature behavior of these phase boundaries in polymer solutions has likewise been the subject of great interest. For weakly interacting polymer solutions where the T-x phase behavior is generally of the form of Figure 1, the LCST is observed to have a universally positive slope with pressure. The UCST, on the other hand, may have a positive or negative slope, or both in different pressure ranges. Furthermore, at low pressure the UCST and LCST may meet at a so-called hypercritical point³. In a seminal work⁹, Konyenburg and Scott in 1968 (republished in 1980)

presented a theoretical development of the possible critical behaviors of binary van der Waals mixtures. This work has been applied^{3, 10} for classifying the pressure-temperature phase behaviors of various weakly interacting polymer solutions.

More recently, Imre and associates have proposed^{3, 4, 8, 10} that a single ‘master curve’ may combine the behavior of the various Konyenburg and Scott classifications for weakly interacting polymer solutions. In particular, they argue that apparently different classifications appear only because the liquid-liquid phase boundary sometimes extends into a metastable region with respect to liquid-vapor or liquid-solid phase stability. The proposed master curve, displayed in Figure 4, includes three ‘hypercritical points’: one at a minimum temperature T_{min} , one at a minimum pressure P_{min} , and one at a local pressure maximum P_{max} . Points on the curve to the left of P_{min} correspond to the UCST in Figure 1, while points between P_{min} and P_{max} correspond to the LCST. The high pressure hypercritical point P_{max} , and the UCST to its right have not been experimentally confirmed, likely due to polymer degradation at elevated temperatures^{3, 11}. However, evidence for such a maximum and ensuing UCST exists in several forms. From a theoretical standpoint, the possibility of a high temperature closed immiscibility loop has been shown based on the Sanchez-Lacombe (S-L) lattice fluid model⁵. Experimentally, results in polymer-solvent systems have exhibited distinct negative curvature in the LCST, indicating the possibility of a maximum^{11, 12}. In addition, the phase lines of several small molecule systems¹³ as well as systems of hydrocarbons in CO₂¹⁴ have been experimentally shown to exhibit a maximum in pressure.

Differences in the positions of the hypercritical points of Figure 4 in different systems then explain the appearance of qualitatively different behaviors in previous studies. When the metastable liquid state found at pressures below the vapor-liquid equilibrium pressure (including at negative pressures) is not considered, systems with P_{min} below this curve appear are incorrectly taken to have separate and non-contacting LCST and UCST phase boundaries. Similarly, when T_{min} is at negative pressure, the UCST would appear to have a purely positive slope, and when it is at extremely high

pressure the system would appear to have a purely negative slope. Furthermore, T_{min} may be experimentally inaccessible if it falls below the freezing temperature of the solvent. In support of this perspective, Imre and associates have demonstrated experimental results in which the LCST and UCST cloud point curves continue into the negative pressure domain and meet at a previously unknown low pressure hypercritical point⁸.

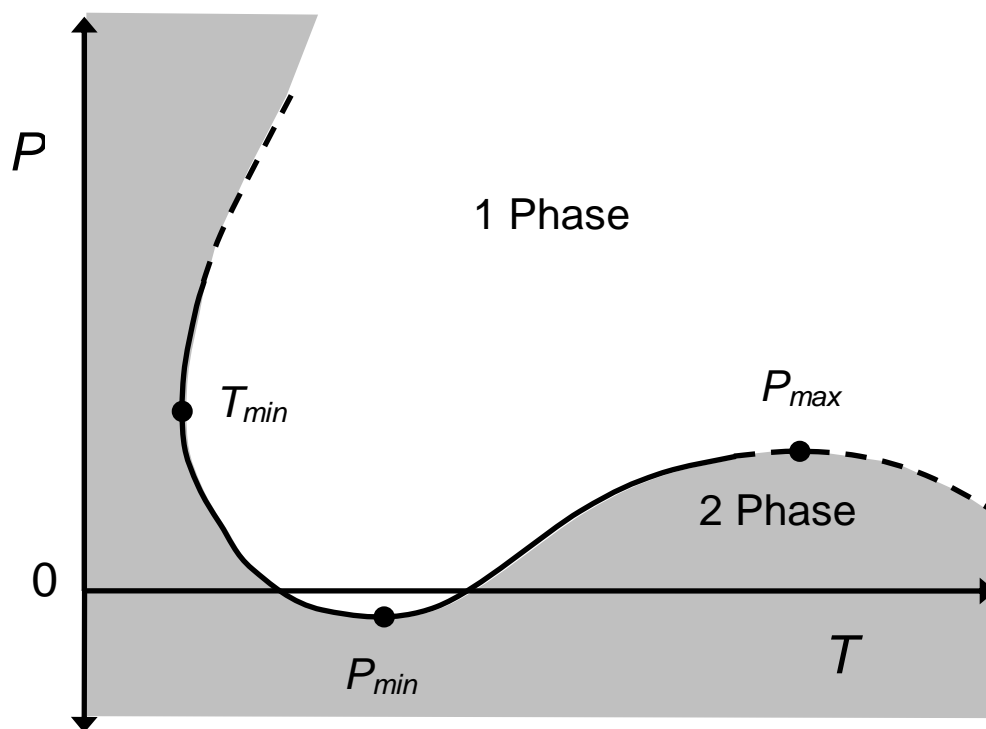


Figure 4: Schematic master curve of polymer solution phase behavior in pressure-temperature space. The curve represents the spinodal or binodal curve of the system. The gray area denotes two-phase states whereas the white region denotes single-phase states. Dashed lines indicate phase boundaries lacking definitive experimental confirmation.

1.1.2. Physics of the LCST

The LCST can be viewed superficially as an inverse of the UCST in that it is characterized by a chain collapse or phase separation with increasing temperature. However, the physical basis of the LCST transition is quite different from that of the UCST. Whereas UCST phase separation is driven by attractive enthalpic considerations, the LCST phase separation is driven by entropy. In particular, above the LCST, the separation is actually entropically favorable. This reversal of the usual role of entropy can be understood, depending on the system, as stemming either from so-called ‘equation of state’ (EOS) effects or from specific interactions such as hydrogen bonding.

The entropically driven nature of the LCST was rigorously demonstrated for a two component mixture by Sanchez in the following way¹⁵. The limit of stability for a two phase mixture is defined by the condition

$$g_{xx} = 0, \quad (1.1)$$

where g is intensive free energy, and

$$g_{xx} \equiv \left(\frac{\partial^2 g}{\partial x^2} \right)_{P,x}, \quad (1.2)$$

and where x is a composition fraction conjugate to the definition of the intensive free energy. Since the two-component condition for stability is

$$g_{xx} > 0, \quad (1.3)$$

g_{xx} is negative within the spinodal and positive without it. By definition of the LCST and UCST we then have that

$$\left(\frac{\partial g_{xx}}{\partial T} \right)_{P,x} = \begin{cases} > 0 & \text{at a UCST} \\ < 0 & \text{at an LCST} \end{cases}. \quad (1.4)$$

Applying the definition of entropy,

$$s = - \left(\frac{\partial g}{\partial T} \right)_{P,x}, \quad (1.5)$$

and inverting the order of differentiation in equation (1.4) reveals that s_{xx} is always positive at an LCST and negative at a UCST. At the spinodal

$$g_{xx} = h_{xx} - Ts_{xx} = 0, \quad (1.6)$$

where h is intensive enthalpy. Consequently, at the LCST s_{xx} are h_{xx} are both positive; thus for the LCST entropics are universally destabilizing and the phase separation is purely entropically driven. This is in contrast to the UCST, at which entropics are universally stabilizing and the phase separation is driven purely and universally by enthalpics.

More recently, Sanchez also demonstrated formally that solution compressibility is always destabilizing (ie. a compressible solution is always less stable than the corresponding incompressible solution) and that this effect is a central element of the LCST transition¹⁵. This fact is shown simply by separating the free energy into incompressible and compressible parts:

$$g_{xx} = a_{xx} - v\kappa_T a_{vx}^2, \quad (1.7)$$

where v is intensive volume, a is the intensive Helmholtz free energy, and κ_T is the isothermal compressibility. The first term is the constant volume contribution to the stability, and the second term is the compressible contribution. Since the second term is always positive, and remembering equation (1.3) for binary stability, solution compressibility always detracts from system phase stability. This is the thermodynamic origin of the so-called ‘equation of state effects’.

The physics of the above arguments are shown at a thermodynamic level in Figure 5 for a system above the LCST. In particular, the inclusion of equation of state effects can reveal a local minimum in the mixture entropy. Since the curvature of the entropy will become positive in this region, this typically yields an unstable region of negative curvature in the free energy, leading to phase separation. Put another way, the maximum system entropy will be obtained by phase separation into two partially demixed states.

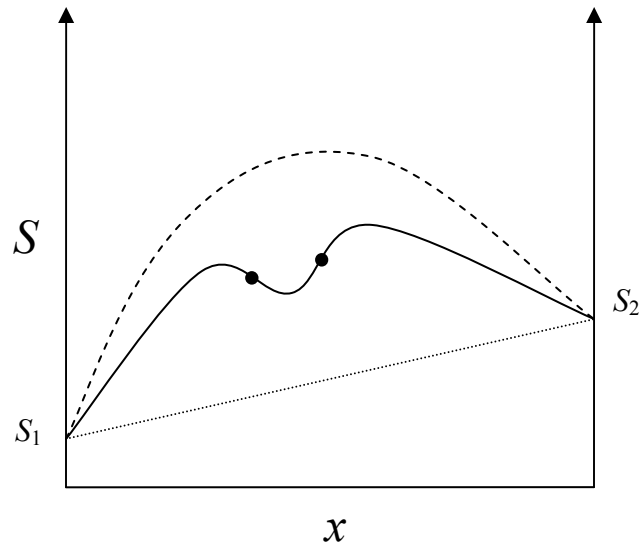


Figure 5: Qualitative schematic of mixture entropy of as a function of composition for a system above the LCST. The dotted straight line denotes the unmixed entropy. The curved dashed line denotes the mixture entropy neglecting equation of state effects. The solid curve represents the actual mixture entropy, with equation of state effects.

From a molecular standpoint, equation of state effects emerge from differences in size and packing between solution components. In essence, for mixtures of components that differ greatly in interaction and/or size, there can be a densification on mixing that is entropically unfavorable. A simple example of this effect can be seen in a system of two types of hard spheres of greatly differing diameters. In this case, the smaller spheres can pack easily in the spaces between the larger spheres, yielding a densification and overall loss of free volume. This, in turn, yields an unfavorable contribution to the free energy of mixing.

In addition to the compressibility-related origin of the LCST, the LCST can also emerge from strong directional interactions such as hydrogen bonding. As in the compressibility origin, this mechanism is entropically driven. In this case, the entropic loss emerges from the reduction in degrees of freedom with hydrogen bond formation.

Above some temperature, it becomes more favorable for the system to phase separate in order to reduce this penalty. This second class of LCST is particularly relevant in the aqueous ‘smart’ polymer systems that are of great interest in biological settings. For example, a hydrogen-bonding-based LCST transition near physiological temperatures drives the stimuli-responsive behavior of Poly(*N*-isopropylacrylamide) (PNIPAAm), making it an excellent candidate for use in biological systems.

The above distinctions between the LCST and UCST initially emerged from the inability of the Flory-Huggins lattice fluid model to capture LCST behavior. Because this model included no vacancies, it did not allow for variable density and hence had no equation of state and could not predict the LCST. In response to this limitation, Flory and associates developed a simple mean field theory that qualitatively predicted the presence of an LCST via the introduction of equation of state effects in the form of variable density¹⁶⁻¹⁸. Some years later, Sanchez and Lacombe incorporated equation of state effects into the original Flory-Huggins lattice framework by introducing vacant lattice sites^{5, 19, 20}. The Sanchez-Lacombe lattice fluid model semi-quantitatively predicted LCST transitions for a wide range of polymer solutions and became the gold standard for this purpose. This model accordingly provides the basis for much of the theoretical development in the present study. However, although this model effectively addresses compressibility driven LCST phenomenon, it does not in its original form reproduce the hydrogen bonding-driven LCST. Some more recent extensions of this model will thus be invoked in order to allow consideration of aqueous systems.

1.2. The Coil-Globule Transition

A parallel issue to that of polymer solution phase behavior is that of polymer spatial conformation. In particular, how does the conformation of an isolated chain in solution below the chain crossover concentration reflect phase transitions in the analogous semi-dilute or concentrated solution? Flory began to address this question from a theoretical standpoint with the observation that there should be a ‘theta’ condition

at which the solvent quality is such that the polymer's attractive and excluded volume interactions exactly cancel out. Flory argued that in this state the chain would assume the ideal Gaussian Configuration of a random flight^{21,22}, with its radius scaling as the root of chain length²³. Under solvent conditions better than this theta condition, he argued that the chain would assume a more extended configuration in which its radius scales as the chain length to the three fifths power²³. Stockmayer later noted²⁴ that all chains should assume a collapsed conformation when their effective self interaction becomes strong enough; such a collapse occurs for solvent conditions significantly poorer than the theta condition, with the collapsed globule radius scaling as chain length to the one third power.

It has since been shown that although the second virial coefficient vanishes as expected at the theta point, the chain conformation is perturbed by the retention of a nonzero third virial coefficient²⁵. It has likewise been argued that ternary interactions cannot be neglected at the theta point and that it thus does not strictly correspond to the ideal chain state²⁶. Nevertheless, for many purposes the chain configuration can be treated as essentially ideal in the dilute theta state. Indeed, this essential concept that emerged from Flory's work – a coil-to-globule transition (CGT) as the solvent quality drops through the Theta point – forms the basis of the present investigations regarding single-chain conformational behavior near the LCST.

The above picture of the CGT immediately suggests a strong link with phase transition behavior; in particular, both the UCST and associated cooling-induced CGT (CCGT) occur at or near the Flory theta condition. Similarly, in 1979, Sanchez pointed out that there should be a heating induced CGT (HCGT) closely related to the LCST²⁷. Based on this close correspondence, the qualitative form of the master phase diagram shown in Figure 4 for weak polymers can likely be applied to the CGT as well, as shown in Figure 6. In this conception, an HCGT locus lies between high pressure and low pressure hypercritical points P_{max} and P_{min} , while CCGT loci are found at temperatures outside of these points. In fact, simulation^{28,29} and experimental³⁰ studies of oligomers in

supercritical solvents that have suggested the presence of a high-temperature CCGT at temperatures above the HCGT, and drawing this parallel between conformation and phase behavior thus lends further support for the existence of a high temperature UCST in polymers.

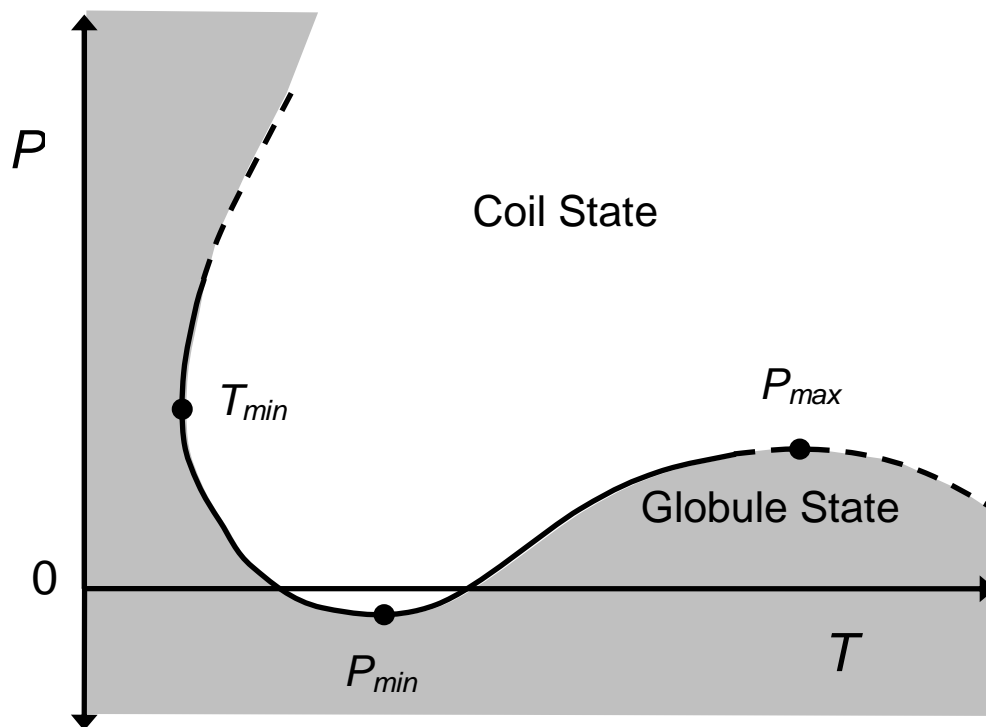


Figure 6: Schematic proposed master curve for pressure- temperature behavior of the CGT. The white region corresponds to a coil state, the gray to a globule state, and the curve to the CGT itself. Points to the left of P_{min} and to the right of P_{max} correspond to a CCGT, while points between P_{min} and P_{max} correspond to an HCGT.

Possibly as a result of its relative tractability, the CCGT to the left of P_{min} has long been the focus of theory³¹⁻³⁵, experiment³⁶⁻⁴⁴, and simulation^{45, 46}. However, the HCGT has recently received increased attention, particularly due to its connection with the functionality of biological macromolecules. Early studies in this area indicated that CGTs are of relevance in the functionality of DNA^{47, 48}. More recent results have

confirmed the presence of a coil-globule transition in DNA⁴⁹⁻⁵¹ and have demonstrated a relationship between protein coil-globule transitions and folding⁵²⁻⁵⁵. Numerous studies have also documented high pressure denaturation or conformational changes in proteins⁵⁶⁻⁵⁸ that can be understood as a pressure induced CGT. Computer simulation^{28, 29, 59-62} and experiment⁶³⁻⁶⁵ have confirmed the existence of this ‘inverse’ collapse transition, and further studies have suggested that it may be the dominant mechanism in many applications. Indeed, Urry argued that the LCST “transition provides a fundamental mechanism whereby proteins fold and function and whereby the energy conversions that sustain living organisms can occur at constant temperature.”⁶⁶ Within the context of many dilute biological systems, this crucial LCST mechanism must take the form of an HCGT.

In addition to direct applications in single molecule systems, the CGT has useful parallels with the swelling behavior of polymer networks. Flory commented that, despite quantitative differences between the two, the single chain case “may quite properly be regarded as a submicroscopic prototype” of polymer networks, and that “qualitatively..., the two situations are strikingly similar.” In particular, both types of system are subject to the essential forces that would otherwise drive phase separation, but they are covalently restricted from doing so. Many proposed applications for synthetic stimuli responsive polymers seek to harness these underlying physics. The LCST-driven behavior of PNIPAAm, for example, is commonly applied as a swelling transition that can be triggered by physiological temperatures⁶⁷⁻⁷¹. Via this mechanism, such materials have been proposed for use in controlled drug delivery due to their ability to release an absorbed drug in response to physiological triggers⁷². Their utility has likewise been demonstrated as prototype sensors⁷³, actuators, and micro-scale valves⁷⁴ for use in micro-fluidic systems.

Recently, a limited model for an HCGT has been developed for the case of a symmetric solvent—one in which the solvent-polymer interaction, the polymer self interaction, and the solvent self interaction are all equal.⁷⁵ However, to our knowledge

no general model exists that predicts HCGT temperature and behavior for arbitrary combinations of polymer and solvent. A more general model, however, is available for the CCGT. Sanchez, in 1979, showed that a lattice based model for a polymer chain in vacuum could predict the gyration radius of the chain given the experimental CCGT temperature²⁷. The present work on dilute chain conformational behavior centers on extensions of this model to the HCGT.

1.3. Charges in Solution

1.3.1. Effects on stability: the lyotropic series

The presence of free salt has been shown to strongly affect⁷⁶⁻⁸⁰ and even induce⁸¹⁻⁸⁴ phase and swelling transitions both in biological⁸⁵ and synthetic polymers. To complicate matters, differing salts, even among those with equal valencies, have been shown to produce qualitatively different affects on the solubility of macromolecules. Certain salts have a monotonic salting out effect, whereas other salts exhibit a ‘salting in’ effect at low concentrations and a ‘salting out effect’ at high concentrations. The lyotropic (or Hofmeister’s) series ranks ions in terms of relative salting-out effect. For example, the lyotropic series for the anions fluorine, chlorine, bromine, and iodine is typically $F^- > Cl^- > Br^- > I^-$ ⁸⁶. This series is demonstrated by Figure 7 from early work by Florin and associates on the cloud point of PEO in the presence of various salts⁸⁰. A central observation regarding this behavior is that in most cases the lyotropic series for anions contains far more variation of behavior than that for cations; put another way, the effect of a salt on solution stability is typically controlled much more strongly by its anion than cation. This experimental result has formed the basis for much of the investigation of the underlying physics of the lyotropic series.

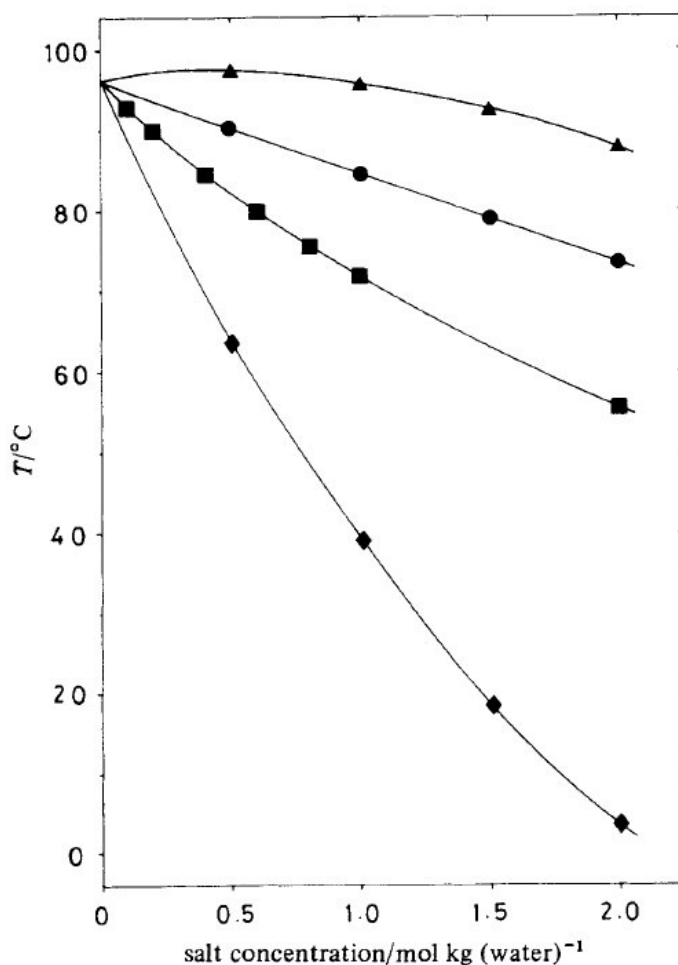


Figure 7: Plot from work by Florin et. al.⁸⁰ showing early experimental results for the lyotropic series. Points denote cloud-point measurements for PEO / water solutions with varying concentrations of salts. Triangles correspond to data with KI, circles to KBr, squares to KCl, and diamonds to KF. Curves are simply a visual aid.

At the simplest level, the salting out behavior observed in the lyotropic series could be ascribed to occupation by ions of water sites needed for macromolecule hydration. In this vein, Park and Hoffman have argued⁸¹, based on experiments with PNIPAAm, that direct interactions between the cation and the polymer chain drive the lyotropic series in at least some systems. Such explanations are recommended by their simplicity in that they consider only binary interactions. However, they do not clearly

explain the salting-in effect of some salts, and it has been argued that they also do not explain the dominance of anion identity in determining salt effects⁸⁶.

An alternative set of models have focused on ions' effects on hydrophobic hydration of the macromolecule. Melander and Horvath have developed a highly cited such theory based on salt-induced changes in solvent surface tension and on electrostatic interactions, which they argue naturally yields a theoretical lyotropic series⁸⁵. Alternatively, Inomata and associates have noted an excellent correlation between the B coefficient of viscosity for the anion and the temperature depression of the LCST for a small range of selected salts, and on this basis they and others⁷⁸ argue that varying effects of anions on the 'icelike' hydration structure of water are responsible⁷⁷. The B coefficient of viscosity is a fitting parameter for highly dilute salt solutions that is a constant of the solute molecule and is understood to relate to the ion-water interaction^{78, 87, 88}. In particular, anions with a positive B coefficient (typically small and/or polyvalent ions) are understood to augment icelike water structure formation and therefore strengthen the hydrophobic interaction between the polymer and itself. On the other hand, those with negative B coefficients (typically large and/or monovalent ions) are understood to interfere with such structure formation and stabilize hydrophobic hydration.

In a third approach, Satoh and associates have argued that, for at least some systems, salt effects are determined by their role in hydrogen bonding hydration rather than in hydrophobic hydration of polymers⁸⁶. In particular, they argue that the ability of water molecules to hydrogen bond to the polymer is modified by their concurrent hydration of ions. In this mechanism, hydration of an anion is taken to decrease the positive charge on the water's hydrogen atoms and increase the negative charge on the water's oxygen. This, in turn, increases water's ability to act as a hydrogen bond proton acceptor and decreases its ability to act as a hydrogen bond proton donor. Hydration of a cation is taken to have the opposite effect. As a consequence, the hydrophilic hydration of a polymer that is a proton acceptor will be weakened by anions and strengthened by

cations, with the reverse holding true for a proton donating polymer. The balance of these effects is then said to control the effect of the salt on solution stability.

At this time, none of these approaches appears to have been strongly demonstrated to fully account for the experimental lyotropic effect. It seems likely that all of these mechanisms may play a role in various systems: straightforward occupation of hydrogen bonding hydration sites by ions; modification of hydrogen-bonding affinities as a consequence of ion hydration; and modification of hydrophobic hydration induced by ion-driven changes in the ice-like structure of solvating water. The first mechanism follows simply from binary interactions, whereas the latter two would seem to require the consideration of ternary or higher order interactions.

1.3.2. The Debye-Huckel model

At a far simpler level than the above, the most essential behavior of ions in electrolyte solution was captured by the early and still highly useful Debye-Huckel model for charge screening⁸⁹. At its core, the model constitutes a first order series expansion of the spherically symmetric Poisson-Boltzmann equation for an ion in a sea of charges. The central physical conclusion of the model is that any such ion will be surrounded by a relative scarcity of coions and relative glut of counterions, peaking at a screening length $1/\kappa$, given by

$$\kappa^2 = 8\pi I l_B \quad (1.8)$$

where I is ionic strength and l_B is the Bjerrum length, corresponding to the charge separation at which electrostatic energy equals thermal energy. This is given by

$$l_B = \frac{\beta q^2}{4\pi\epsilon_0\epsilon_r}, \quad (1.9)$$

where $\beta = 1/k_B T$, q is the elementary charge, ϵ_0 is the permittivity of free space, ϵ_r is the dielectric constant of the medium, k_B is Boltzmann's constant, and T is temperature. The screened electrostatic potential U_{ij} through which any two charges of type i and j in

solution will interact at distances greater than the screening length is then shown to be given by

$$\beta U = l_B z_i z_j \frac{\exp(-\kappa r)}{r}, \quad (1.10)$$

where z_k is the valency of ion k and r is the spacing between the ions. The electrostatic free energy u_i of any particular free ion of type i is likewise shown to be given by

$$\beta u_i = -z_i^2 \kappa l_B \frac{1}{1 + \kappa \sigma_i^I}, \quad (1.11)$$

where σ_i^I is the ionic diameter of an ion of species i . Equation (1.11) may then be summed over all ions to yield the total electrostatic energy of the solution, and the activity of each ion species may likewise be obtained.

The Debye-Huckel model is effective only within significant limitations. First, it is restricted to fairly low charge densities, above which a first order solution of the Poisson-Boltzmann equation becomes inadequate. This limit can be stretched by using a higher order solution at the cost of significantly increased complexity. On the other hand, the approach fundamentally fails to address phenomena related to strong correlations between ions such as ion bridging; similarly, it fails to properly address multivalent ion behavior. Several studies have indicated that such phenomena can play a strong role in polyelectrolyte phase and conformational behavior⁹⁰⁻⁹². Finally, it can be inadequate in the presence of closely fixed charges as such arrangements render invalid the assumption of spherical symmetry on which the above solution is based. This last limitation in particular has led to the development of ion distribution models for the special case of polyelectrolyte systems, to be discussed in the following section.

1.3.3. Polyelectrolytes

Polyelectrolyte phase and conformational behavior present unique challenges relative to that of uncharged polymers. The underlying origin of these challenges is the presence of charges, both free in solution and fixed on the polymer chains themselves.

The long range nature of the Coulombic interactions between these charges yields behavior qualitatively different from that of polymer solutions without charges. In an excellent review paper⁹³, Dobrynin and Rubinstein have given a modern view of many of the relevant issues.

Phase and conformational behavior

The introduction of charges to the chain backbone introduces a rich array of conformational behavior not seen in uncharged polymers. Extensive theoretical attention has been focused over the course of several decades on the electrostatic persistence length and modifications of chain stiffness with addition of charges to a chain⁹⁴⁻¹⁰⁰. Moreover, it has long been understood that Coulombic self-repulsion can cause polyelectrolyte chains to assume a more expanded conformation than the equivalent neutral chain¹⁰¹. As early as 1952 Hill further noted that such interactions may in fact distort the chain from a spherical shape¹⁰². More recently, Dobrynin, Rubinstein, and Obukhov have shown that sufficiently charged polyelectrolyte chains in poor solvent will assume a ‘bead necklace’ conformation consisting of multiple spherical globules attached by strings of polymer^{103, 104}. Both conformations are essentially adaptations to maintain the local collapsed globular conformation demanded by the solvent quality while progressively increasing the average distance between like charges on the polymer backbone so as to reduce the associated unfavorable interaction energy. A recent simulation study¹⁰⁵ by Ulrich and coworkers has demonstrated these and other conformational behaviors, as shown in Figure 8. At high effective charges, the chain assumes a highly extended conformation for good solvents and a bead necklace conformation for poor solvents. At intermediate charge fractions, a ‘cigar’ conformation is found. Finally, as expected, at low effective charge fractions the standard uncharged globule and coil conformations are observed. However, it is important to note that Figure 8 omits an expected high temperature transition back to a collapsed globule as the LCST is encountered at low ionization fraction.

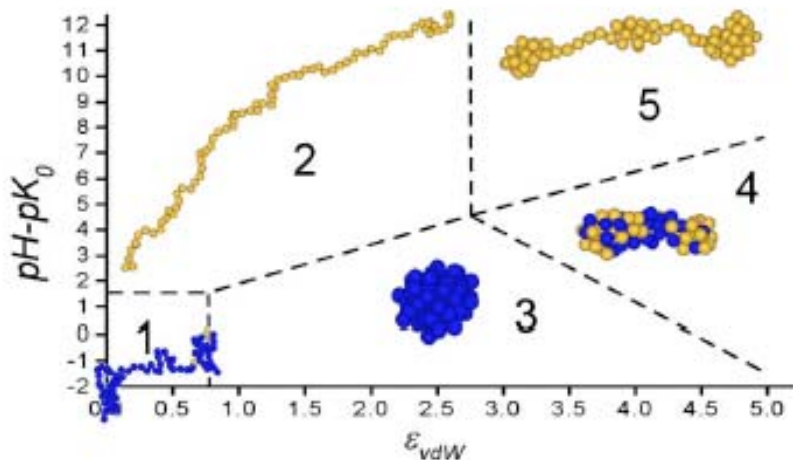


Figure 8: Conformational diagram of a weak polyelectrolyte based on Monte-Carlo simulations¹⁰⁵. The x-axis, ϵ_{vdW} , is the van der Waals interaction in units of $k_B T$ and is thus an inverse temperature axis. Yellow spheres denote charged monomers whereas blue sphere denote uncharged monomers.

As suggested by Figure 8, the inclusion of charges on the polymer causes its phase and conformational behavior to become sensitive to qualitatively new environmental stimuli. For example, dissociable subunits such as acrylic and methacrylic acid have been copolymerized with PNIPAAm in order to yield a pH sensitive LCST¹⁰⁶⁻¹⁰⁸. This mechanism has been proposed for use in controlled pH triggered drug delivery⁷² as well as in pH based sensors⁷³. For polyelectrolytes that are polyacids or polybases, the mechanism of this sensitivity is actually counterion dissociation equilibrium. As a separate issue, solution ionic strength affects polyelectrolyte behavior due to charge screening. Furthermore, electrical fields have also been shown to induce conformational changes in polyelectrolytes^{109, 110}, and such effects have been proposed for use in drug delivery¹¹¹, artificial pumps and muscles¹¹², and so on.

Relative to an uncharged polymer, the inclusion of charges in the chain may either stabilize or destabilize the solution, and this effect is determined by the balance of several mechanisms. Perhaps the most intuitive such mechanism is that of Coulombic repulsion between like charges on the chain. Such repulsions are typically expected to lead to

enhanced solution stability as the polymer imbibes more solvent in order to increase the separation between charges. With increasingly unfavorable electrostatics, this effect is expected to result in more expanded chain conformations exhibiting the emergence of non-isometry and longer range order. However, this mechanism may be mitigated by charge screening, and it may not be the dominant mechanism at low polymer charge densities or high screening. Furthermore, at high counterion concentrations, the backbone charges may be effectively neutralized, eliminating this effect entirely.

A second mechanism for modulation of solution stability is then altered chain hydration. In particular, fixed ions on the charge backbone are expected to be hydrophilic and to increase the net interaction between the chain and water. However, it has been shown that this effect can be reversed if the relevant counterion concentration is sufficiently high so as to lead to a low dissociation fraction of ionizable groups on the chain^{113, 114}. For example, in random copolymers of N-isopropylacrylamide and acrylic acid, the solution is destabilized relative to the neutral polymer at low pH¹¹⁵. This effect is attributed to intrachain hydrogen bonding¹¹³ or attractive interactions between the proton acceptor sites on the isopropylacrylamide subunits and the non-dissociated acidic sites on the acrylic acid subunits¹¹⁵. Furthermore, this explanation is qualitatively consistent with theoretical¹¹⁶ and simulation¹¹⁷ results pinpointing counterion condensation and ensuing intramolecular interactions as an origin of chain collapse.

Free ion distribution

A key element of the behavior of charges in solution is the balance between dissociated and associated ions, characterized by the ionization fraction. For weak electrolytes, this balance is given at infinite charge dilution by the commonly tabulated dissociation constant pK_0 . However, at finite charge concentrations, which are present almost by default in the case of a polyelectrolyte wherein dissociable groups are covalently connected, the actual ionization fraction α_k is altered by electrostatic interactions, such that^{105, 118-120}

$$pK_0 = pH + \log \left[\frac{1 - \alpha_k}{\alpha_k} \right] + \frac{1}{kT \ln 10} \frac{\partial g_{el}}{\partial \alpha_k}, \quad (1.12)$$

where g_{el} is the intensive electrostatic free energy of the system and where K_0 is called the intrinsic dissociation constant, corresponding to the value of the dissociation constant in the limit of zero charge density. In general, pH here is the negative base ten logarithm of the relevant counterion concentration rather than simply of the hydrogen cation concentration. Equation (1.12) can be understood as a modified Henderson-Hasselbalch equation that accounts for long-range electrostatic interaction between charge. In principle, this equation is all that is needed to rigorously calculate the ionization fraction of charges in a polyelectrolyte. However, determining $\partial g_{el} / \partial f$ exactly can be quite challenging, particularly in the case where the Debye-Huckel approach is inadequate. A number of alternative approaches to determining ion distribution vis-à-vis a polyelectrolyte chain have thus been developed.

One of the earliest and most influential such attempts was the Manning condensation model¹²¹. As in the Debye-Huckel case, this model employs the Poisson-Boltzmann equation, but it replaces the spherical symmetry of that earlier approach with a cylindrical geometry centered on a charged rod-like chain. Its key conclusion is that there is a critical linear charge density upon a rodlike polymer above which counterions condense into the immediately surrounding region to neutralize some of its effective charge. For monovalent counterions and monovalent dissociable groups upon the chain, this limit is at the point where the Bjerrum length equals the mean distance between charges. The practical effect of this phenomenon is to render the effective charge of highly ionized polymers significantly less than would be predicted from intrinsic dissociation constants alone.

Recently, more advanced models for ion distribution about the chain have been proposed. A three domain extension of the Manning model has been devised which establishes three phases of counterion behavior¹²². The principle of this model is that a Manning-like cylindrical region around a stiff polymer chain is further embedded within

a much larger spherical region. Despite such improvements, however, the application of a model based on a rodlike polymer to flexible chains clearly presents certain limitations. In order to address this problem, Muthukumar has more recently proposed a model for counterion distribution around flexible polyelectrolytes¹²³, and has shown that the behavior in this case is qualitatively different than that predicted by the Manning model. Furthermore, he and Kundagrami more recently demonstrated that the dielectric mismatch between the bulk solvent and the domain immediately surrounding the polyelectrolyte may have a strong effect in biasing counterions toward the condensation on the chain¹²⁴. Several studies have also indicated the importance of counterion valency in counterion and polyelectrolyte behavior, with evidence of ion bridging by multivalent salts^{91, 92, 124, 125}.

1.4. Approaches to the Chemical Potential

There are two general statistical mechanical approaches to obtaining the chemical potential of a component in solution. The most common method is to begin by calculating the Gibbs partition function Ω or Gibbs free energy G of the system. The chemical potential of a component k is then the derivative of the free energy with respect to the number of molecules of k :

$$\mu_k = \left(\frac{\partial G}{\partial N_k} \right)_{T, P, \{N_{j \neq k}\}}, \quad (1.13)$$

where T is temperature, P is pressure, and $\{N_{j \neq k}\}$ denotes the number of molecules of all species other than k .

A second approach to the chemical potential, initially developed by Benjamin Widom in 1963¹²⁶, is the insertion method. The key to this approach is the separation of the contribution of one particle within the configurational partition function. For a one-component fluid of N particles, the configuration partition function may be written as

$$Q_N = \int_V \dots \int_V \exp(-\beta W_N) d\tau_1 \dots d\tau_N, \quad (1.14)$$

where W_N is the interaction energy of the N particles within volume V , and β is the inverse of the product of Boltzmann's constant and temperature. Separating out the N^{th} particle gives

$$\begin{aligned} Q_N &= \int_V \dots \int_V \exp(-\beta\psi) \exp(-\beta W_{N-1}) d\tau_1 \dots d\tau_N, \\ &= Q_{N-1} V \langle \exp(-\beta\psi) \rangle \end{aligned} \quad (1.15)$$

where ψ is the interaction energy of the one selected particle with all the remaining $N-1$ particles as a function of their position. The brackets denote an average over all possible positions of this particle. The activity a_i of the particle of species i is then given by

$$a_i = \frac{\rho_i}{\langle \exp(-\beta\psi_i) \rangle}, \quad (1.16)$$

where ρ_i is the number density of species i . The chemical potential can then be written as

$$\beta\mu_i = \ln \frac{\rho_i \lambda_i^3}{\mathbf{B}_i}, \quad (1.17)$$

where λ_i is the thermal wavelength and \mathbf{B}_i is called the insertion parameter and is given by

$$\mathbf{B}_i = \langle \exp(-\beta\psi_i) \rangle. \quad (1.18)$$

For systems with a hard core repulsion, the above may be simplified. For any inserted position at which the particle overlaps with another, the interaction energy ψ_i will be infinite and the contribution of these configurations thus will be zero. It follows that equation (1.18) can be written for hard spheres as

$$\mathbf{B}_i = \mathbf{P}_i \langle \exp(-\beta\psi_i) \rangle. \quad (1.19)$$

This may be rewritten exactly as

$$\mathbf{B}_i = \mathbf{P}_i \exp(-\beta\langle\psi_i\rangle) \langle \exp[-\beta(\psi_i - \langle\psi_i\rangle)] \rangle. \quad (1.20)$$

Within a mean field approximation, the latter factor in equation (1.20) is neglected, obtaining

$$\mathbf{B}_i = \mathbf{P}_i \exp(-\beta \langle \psi_i \rangle) \quad (1.21)$$

for a hard sphere fluid within a mean field model. Furthermore, Sanchez, Truskett, and in 't Veld showed¹²⁷ in 1999 that equation (1.21) may be applied even to non-hard sphere fluids under most circumstances by taking acceptable insertions to be only those resulting in a negative interaction energy.

Although in principle both of these approaches will yield valid component properties in any system, in practice one or the other often offers considerable simplification. Furthermore, they often yield different and even contradictory results as a consequence of differences in the way conceptually equivalent approximations play out in each approach. For example, the mean field approximation used in the insertion approach may yield quantitatively and even qualitatively different results than a mean field approximation used in directly calculating the system partition function. As a result, the choice of approach can be quite important, and attempts to mix results stemming from the two approaches may be problematic.

Chapter 2. The Lower Critical Solution Temperature

A model for the LCST of charge-containing aqueous polymer solutions is needed in order to facilitate understanding and design of such systems in a variety of applications. Such a model must encompass several physical interactions: excluded volume interactions; weak van der Waals interactions including dispersion forces and fixed dipole interactions; hydrogen bonding; ion-dipole interactions, and ion-ion interactions. Furthermore, it should account for competition and cooperation between the ion-ion, ion-dipole, and hydrogen bonding interactions, so as to reproduce and elucidate the physics of the lyotropic series of salts as described in section 1.3.1.

The hydrogen bonding lattice fluid model¹²⁸ for the LCST incorporates the excluded volume, van der Waals, and hydrogen bonding interactions from the above list. The present development extends this model to interactions involving charge, subject to several limitations. The first such limitation is that, with one exception, only binary interactions will be considered. As discussed in section 1.3.1, this may omit some proposed mechanisms for the lyotropic effect that rely upon ternary or higher interactions. Secondly, the extension will focus on monovalent salts and will not be directly amenable to treating many of the phenomena, such as ion bridging, that are believed to occur with higher valency salts. In fact, these two limitations are related, and a framework developed for treatment of ternary interactions could possibly be modified to achieve better treatment of multivalent ions. For the present, however, the primarily binary approach is recommended by its relative simplicity, and it should facilitate a useful investigation of the extent to which binary interactions play a role in establishing lyotropic behavior.

An extension to polyelectrolytes is offered that addresses the basic physics by which incorporation of charges into the polymer backbone introduces new sensitivities of the LCST to environmental properties. Consideration is made of the unfavorable Coulombic interactions between polymer charges that can stabilize the system at

sufficiently high polymer charge density and low screening. Enhanced hydration of polymer chains with addition of charges is explicitly addressed. Furthermore, a framework is provided for treating interactions between non-dissociated charges on the polymer with each other and with the chain backbone; such interactions are posited to drive destabilization of polyelectrolyte solutions at high counterion concentration.

2.1. Review

Two existing models provide many of the underpinnings for the current development of the LCST. The Sanchez-Lacombe (SL) lattice fluid (LF) model^{5, 19, 20, 128} provides the basic mean field approach for predicting the LCST in weakly interacting polymers. The hydrogen bonding lattice fluid (HBLF) model extends this approach to treat hydrogen bonds via Veytsmann statistics¹²⁹. A brief recapitulation of these models follows.

2.1.1. Lattice fluid model

Consider a mixture consisting of t components with N_k molecules of each component k , at temperature T and pressure P . Further consider the system to be divided into a lattice of N_r sites. Each molecule of species k occupies r_k such sites, with each site occupying v_k^* volume in the pure state. The total number of sites occupied is

$$Nr \equiv \sum_{k=1}^t N_k r_k, \quad (2.1)$$

leaving N_0 sites unoccupied such that the total number of sites is

$$N_r = Nr + N_0. \quad (2.2)$$

The fraction of occupied sites is then given by

$$\tilde{\rho} = \frac{Nr}{Nr + N_0}. \quad (2.3)$$

The volume fraction occupied by species k in the mixture is then defined as

$$\phi_k \equiv \frac{r_k N_k}{rN} = x_k \frac{r_k}{r}, \quad (2.4)$$

where $x_k \equiv N_k/N$ is the mole fraction of species k . Similarly, component surface fractions may be defined as

$$\theta_k = \phi_k s_k / \sum_{j=1}^t \phi_j s_j = \phi_k s_k / s, \quad (2.5)$$

where s_k is a surface to volume ratio characteristic of the molecule, equal to the number of contact sites per segment of molecule k . This ratio was treated as unity in the original development of the lattice fluid model; however, it is included here in the interest of consistency with recent work and results in the literature. The average interaction energy of a site of species k in its pure state is

$$\varepsilon_k^* = \frac{s_k}{2} \varepsilon_{kk}, \quad (2.6)$$

where ε_{kk} is the interaction energy between two adjacent sites of species k .

The following mixing rules are applied:

$$v^* = \sum_{k=1}^t \phi_k v_k^*; \quad (2.7)$$

$$\varepsilon^* = \frac{s}{2} \sum_{k=1}^t \sum_{l=1}^t \theta_k \theta_l \varepsilon_{kl}; \quad (2.8)$$

and a Berthelot-type rule is applied for the cross-interaction terms, given by

$$\varepsilon_{kl} = \xi_{kl} (\varepsilon_{kk} \varepsilon_{ll})^{1/2}, \quad (2.9)$$

where ξ_{kl} is a dimensionless parameter expected to have value close to one. The combination of equations (2.8) and (2.9) indicates that only ratios rather than absolute values of s_k 's are important. Furthermore, both s_k 's and ξ_{kl} 's have been taken to be unity successfully in a number of applications^{15, 19, 20, 127}.

The system volume is

$$V = rNv^* \tilde{v}, \quad (2.10)$$

where \tilde{v} is the reduced volume, which is the inverse of the reduced density $\tilde{\rho}$.

Similarly, the total energetic contribution from physical interactions is given by

$$E_p = -rN\tilde{\rho}\varepsilon^*. \quad (2.11)$$

The physical partition function is then given by¹²⁸

$$Q_p(T, N_0, N_k) = (1 - \tilde{\rho})^{N_0} \tilde{\rho}^{-N} \prod_{k=1}^t (\omega_k / \phi_k)^{N_k} \exp(\beta r N \tilde{\rho} \varepsilon^*), \quad (2.12)$$

where ω_k is the number of configurations available to a chain of species k in the close packed state. This is treated as a constant of the molecule and will drop out in calculations of phase stability.

The Gibbs partition function is given by

$$\Psi(T, P, \{N_k\}) = \sum_{N_0=0}^{\infty} Q_p(T, N_0, \{N_k\}) \exp(-\beta PV). \quad (2.13)$$

The Gibbs free energy is related to the Gibbs partition function by

$$G = kT \ln \Psi. \quad (2.14)$$

The maximum term approximation may be applied to the Gibbs partition function as usual; the equivalent minimization condition on the free energy is

$$(\partial G / \partial \tilde{v})_{T, P, \{N_k\}} = 0. \quad (2.15)$$

The free energy of the system is then given by

$$\beta G = rN \left[-\tilde{\rho} / \tilde{T} + \tilde{P} / \tilde{\rho} \tilde{T} - (1 - 1 / \tilde{\rho}) \ln \left(1 - \tilde{\rho} + \frac{1}{r} \ln \tilde{\rho} + \sum_{k=1}^t \frac{\phi_k}{r_k} \ln \frac{\phi_k}{\omega_k} \right) \right], \quad (2.16)$$

where

$$\tilde{T} = \frac{T}{T^*} = \frac{k_B T}{\varepsilon^*}, \quad (2.17)$$

and

$$\tilde{P} = \frac{P}{P^*} = \frac{v^* P}{\varepsilon^*}. \quad (2.18)$$

From equations (2.15) and (2.16), the equation of state (EOS) of the system is

$$\tilde{\rho}^2 + \tilde{P} + \tilde{T} \left\{ \ln(1 - \tilde{\rho}) + \tilde{\rho} \left(1 - \frac{1}{r} \right) \right\} = 0. \quad (2.19)$$

The chemical potential of component k from equation (2.16) is

$$\begin{aligned} \beta\mu_k = & \ln \phi_k + 1 - \frac{r_k}{r} + r_k \left[-\frac{\tilde{\rho}}{\tilde{T}_k} + \frac{\tilde{P}_k}{\tilde{T}_k \tilde{\rho}} - \left(1 - \frac{1}{\tilde{\rho}} \right) \ln(1 - \tilde{\rho}) + \frac{1}{r_k} \ln \tilde{\rho} \right], \\ & + r_k \tilde{\rho} \left[\sum_{i=1}^t \theta_i X_{ki} - \sum_{j=1}^t \sum_{i=1}^{j-1} \theta_i \theta_j \frac{S_k}{S_i} X_{ij} \right], \end{aligned} \quad (2.20)$$

where X_{ij} is the Flory χ parameter modified to account for the surface to volume ratio parameters included in this version of the lattice-fluid model:

$$X_{ij} = \beta \left(\varepsilon_i^* + \frac{S_i}{S_j} \varepsilon_j^* - 2 \left(\frac{S_i}{S_j} \right)^{1/2} \varepsilon_{ij}^* \right). \quad (2.21)$$

2.1.2. Hydrogen bonding lattice fluid model

Consider a mixture consisting of t components with N_k molecules of each component k , at temperature T and pressure P . The system contains m_d types of proton donors and m_a types of proton acceptors. Each molecule of species k contains d_i^k such donor sites of type i and a_j^k such acceptor sites of type j . The total number of donors of type i is then

$$N_d^i = \sum_{k=1}^t N_k d_i^k, \quad (2.22)$$

while the total number of acceptors of type j is

$$N_a^j = \sum_{k=1}^t N_k a_j^k. \quad (2.23)$$

The configurational partition function of the system is then assumed to be factorable. One factor, Q_{HB} , considers only hydrogen bonding interactions. A second factor, Q_P , considers only ‘physical’ interactions such as excluded volume, induced

dipole, and weak polar interactions. Each factor explicitly ignores the presence of the interactions captured in the other factors, although they are linked implicitly. The canonical partition function can thus be written as

$$Q = Q_{HB}Q_P. \quad (2.24)$$

This decoupling of interactions is clearly an approximation; however, its success has been demonstrated in a number of papers¹²⁸⁻¹³¹. In fact, a recent work has further decoupled the above approach in the charge free case by splitting the ‘physical’ contribution into random and nonrandom contributions in order to facilitate a quasi-chemical approach to the physical interactions¹³⁰.

The physical contribution to the partition function of this system is given by the lattice fluid model, above. The hydrogen bonding contribution is given as follows. The system will contain a number of bonds between donors of type i and acceptors of type j equal to N_{ij} . The total number of unbonded donors of type i and unbonded acceptors of type j , respectively, are then given by

$$N_{i0} = N_d^i - \sum_{j=1}^m N_{ij} \quad (2.25)$$

and

$$N_{0j} = N_a^j - \sum_{i=1}^n N_{ij}. \quad (2.26)$$

The total number of hydrogen bonds in the system is

$$N_{HB} = \sum_{i=1}^n \sum_{j=1}^m N_{ij}. \quad (2.27)$$

The hydrogen bonding partition function will have several contributions. The first, $Q_{HB,C}$, is an entropic combinatorial factor accounting for the number of possible ways of forming N_{ij} bonds for all i - j pairs. This has been shown via the Veytsman approach, which is based on straightforward combinatorial considerations¹²⁸, to be given by

$$Q_{HB,C} = \prod_{i=1}^{m_d} \frac{N_d^i!}{N_{i0}!} \prod_{j=1}^{m_a} \frac{N_a^j!}{N_{0j}!} \prod_i \prod_j \frac{1}{N_{ij}!}. \quad (2.28)$$

The second contribution to the hydrogen bonding partition function, $Q_{HB,G}$, is a geometric probability factor accounting for the probability that each of the pairs considered in the combinatoric factor $Q_{HB,C}$ are actually spatially proximate to one another. Equivalently, this term can be understood to account for the loss of translational entropy with bond formation. For any particular pair, this contribution will scale as the ratio of the volume of an ion to the volume of an entire system; there is one such factor for each association pair in the system. In terms of lattice fluid parameters, this factor is thus

$$Q_{HB,G} = \left(\frac{\tilde{\rho}}{rN} \right)^{N_{ij}} . \quad (2.29)$$

The third contribution to the hydrogen bonding partition function, $Q_{HB,S}$, will be an entropic loss factor accounting for the loss of rotational degrees of freedom with bond formation and for local steric considerations. Alternatively, it may be understood as the probability that all pairs are correctly oriented and aligned to form hydrogen bonds. It may be written in terms of an entropy change of hydrogen bond formation S_{ij}^0 as

$$Q_{HB,S} = \left(\beta T S_{ij}^0 \right)^{N_{ij}} . \quad (2.30)$$

The final contribution, $Q_{HB,E}$, will be an energetic factor accounting for the energy of formation of all associative bonds in the system. It may be written in terms of the energy of hydrogen bond formation E_{ij}^0 as

$$Q_{HB,E} = \left(\beta E_{ij}^0 \right)^{N_{ij}} . \quad (2.31)$$

Combining equations (2.28) through (2.31) yields

$$Q_{HB} = \prod_{i=1}^{m_d} \frac{N_d^i}{N_{i0}!} \prod_{j=1}^{m_a} \frac{N_a^j}{N_{0j}!} \prod_i \prod_j \frac{(\beta F_{ij}^0)^{N_{ij}}}{N_{ij}!} \left(\frac{\tilde{\rho}}{rN} \right)^{N_{ij}} , \quad (2.32)$$

where

$$F_{ij}^0 = E_{ij}^0 - T S_{ij}^0 . \quad (2.33)$$

The Gibbs free energy is obtained as in the lattice fluid model, with the modification that the Gibbs partition function is now given by

$$\Psi(T, P, \{N_k\}) = \sum_{N_0=0}^{\infty} \left[\frac{Q_P(T, N_0, \{N_k\})}{Q_{HB}(T, N_0, \{N_k\}, \{N_{ij}\})} \right] \exp(-\beta PV), \quad (2.34)$$

and the system volume is now

$$V = rNv^* \tilde{v} + \sum_{i=1}^{m_d} \sum_{j=1}^{m_a} N_{ij} V_{ij}^0. \quad (2.35)$$

It follows that the Gibbs free energy may also be partitioned into contributions from each of the above groups:

$$G = G_P + G_{HB}. \quad (2.36)$$

The physical contribution to free energy is given by equation (2.16) from the lattice fluid model. The hydrogen bonding contribution is:

$$\beta G_{HB} = rN \left[\sum_{i=1}^{m_d} \sum_{j=1}^{m_a} v_{ij} \left(1 + \beta G_{ij}^0 + \ln \frac{v_{ij}}{\tilde{\rho} v_{i0} v_{0j}} \right) + \sum_{i=1}^{m_d} v_d^i \ln \frac{v_{i0}}{v_d^i} + \sum_{j=1}^{m_a} v_a^j \ln \frac{v_{0j}}{v_a^j} \right], \quad (2.37)$$

where $G_{ij}^0 = F_{ij}^0 + PV_{ij}^0$, and $v_d^i = \frac{N_d^i}{rN}$, $v_{i0} = \frac{N_{i0}}{rN}$, $v_{0j} = \frac{N_{0j}}{rN}$, and so on.

The free energy minimization condition on the density is essentially the same as that in the lattice model:

$$\left(\frac{\partial G}{\partial \tilde{v}} \right)_{T, P, \{N_k\}, \{N_{ij}\}} = 0. \quad (2.38)$$

However, an additional set of free energy minimization conditions now constrain the hydrogen bonding numbers:

$$\left(\frac{\partial G}{\partial N_{ij}} \right)_{T, P, \tilde{v}, \{N_k\}, \{N_{lu \neq ij}\}} = 0 \quad (2.39)$$

for all i and j . From equation (2.38), the density equation of state is now given by

$$\tilde{\rho}^2 + \tilde{P} + \tilde{T} \left\{ \ln(1 - \tilde{\rho}) + \tilde{\rho} \left(1 - \frac{1}{\tilde{r}} \right) \right\} = 0, \quad (2.40)$$

where

$$\frac{1}{\tilde{r}} \equiv \frac{1}{r} - \sum_{i=1}^{m_d} \sum_{j=1}^{m_a} v_{ij}. \quad (2.41)$$

Note that equation (2.40) is of the same functional form as the density EOS for the pure lattice fluid EOS, given by equation (2.19). The effect of hydrogen bonding on the density equation of state is simply to modify the effective average molecular size. However, there is now an additional set of equations of state on the hydrogen bond numbers, deriving from equations (2.39):

$$\beta G_{ij}^0 + \ln \left(\frac{v_{ij}}{\tilde{\rho} v_{i0} v_{0j}} \right) = 0. \quad (2.42)$$

The chemical potential of component k is in general given by

$$\begin{aligned} \mu_k = & \left. \frac{\partial G}{\partial N_k} \right)_{T,P,\{N_{l \neq k}\}, \tilde{v}, \{N_{ij}\}} + \left. \frac{\partial G}{\partial \tilde{v}} \right)_{T,P,\{N_k\}, \{N_{ij}\}} \left. \frac{\partial \tilde{v}}{\partial N_k} \right)_{T,P,\{N_{l \neq k}\}} \\ & + \sum_{i=1}^{m_d} \sum_{j=1}^{m_a} \left. \frac{\partial G}{\partial N_{ij}} \right)_{T,P,\{N_k\}, \tilde{v}} \left. \frac{\partial N_{ij}}{\partial N_k} \right)_{T,P,\{N_{l \neq k}\}}. \end{aligned} \quad (2.43)$$

However, by applying the minimization conditions of equations (2.38) and (2.39), equation (2.43) may be reduced to

$$\begin{aligned} \mu_k = & \left. \frac{\partial G_P}{\partial N_k} \right)_{T,P,\{N_{l \neq k}\}, \tilde{v}, \{N_{ij}\}} + \left. \frac{\partial G_{HB}}{\partial N_k} \right)_{T,P,\{N_{l \neq k}\}, \tilde{v}, \{N_{ij}\}}. \\ = & \mu_{k,P} + \mu_{k,HB} \end{aligned} \quad (2.44)$$

The physical contribution to chemical potential is given by the lattice fluid result of equation (2.20). The hydrogen bonding contribution is given by

$$\beta \mu_{k,HB} = r_k \sum_{i=1}^n \sum_{j=1}^m v_{ij} + \sum_{i=1}^n d_i^k \ln \frac{v_{i0}}{v_d^i} + \sum_{j=1}^m a_j^k \ln \frac{v_{0j}}{v_a^j}. \quad (2.45)$$

2.2. Theory

2.2.1. Aqueous polymers in the presence of free salt

Model description

As discussed in the introduction, it is well known that the LCST of aqueous polymers may be considerably altered by the presence of modest concentrations of free salt. A significant limitation of the hydrogen bonding lattice fluid model is its inability to account for this effect. The present model remedies this deficiency through a simple approach. The electrostatic interactions characteristic of ions are divided into two types: short range ion-dipole interactions (ex. ion hydration), and long range ion-ion interactions. The long range interactions will be addressed by including an electrostatic factor in the partition function based on the Debye-Huckel approximation. The short range interactions will be addressed by applying Veytsman¹²⁹ statistics to the combined network of ion-dipole and hydrogen bonds. Note that ionic bonding is not considered in this model; hence it is not applicable to solutions containing weak electrolytes. The later model for polyelectrolytes presented in section 2.2.2 specifically considers ionic bonding and could be applied in a simplified form to non-polyelectrolytic systems containing weak free salts.

As in the hydrogen bonding lattice fluid model, the system partition function is treated as factorable. A factor Q_P will account for physical interactions as before. A second factor, Q_A , will replace Q_{HB} and will account for specific ‘associating’ interactions including hydrogen bonding and ion-dipole interactions. A final factor, Q_E , accounts for long range electrostatic interactions between ions. The canonical partition function can thus be written as

$$Q = Q_E Q_A Q_P. \quad (2.46)$$

Physical partition function

In general, the physical partition function may be based on any number of theories. As noted above, for example, a quasi-chemical approach has recently been applied for physical interactions in the charge-free case¹³⁰. However, as in the hydrogen bonding lattice fluid model¹²⁸ and in the interest of simplicity, the present development is based upon the lattice fluid model, above. The physical partition function is then given as before by equation (2.16).

Associating partition function

The associating partition function follows the same development as that for the hydrogen bonding lattice fluid model, albeit with alterations to account for ion-dipole interactions. Namely, hydrogen and ion-dipole bonds are ‘lumped together’ as ‘association bonds’. As such, m_d and m_a express the number of ‘association’ donors and acceptors rather than simply the number of types of hydrogen bond donors and acceptors. Each molecule of species k then contains d_i^k such association donor sites of type i and a_j^k such association acceptor sites of type j .

Other than these changes of definition, the derivation for the hydrogen bonding partition function applies exactly. Equations (2.22) and (2.23) apply for the total number of association donors and acceptors, respectively. The number of association bonds between donors of type i and acceptors of type j is equal to N_{ij} , where ion-dipole interactions are now included in the $\{N_{ij}\}$. The total number of association bonds is then given by

$$N_A = \sum_{i=1}^{m_d} \sum_{j=1}^{m_a} N_{ij} . \quad (2.47)$$

The associating partition function is of the same form as that of the hydrogen bonding contribution in the prior model:

$$Q_A = \prod_{i=1}^{m_d} \frac{N_d^i!}{N_{i0}!} \prod_{j=1}^{m_a} \frac{N_a^j!}{N_{0j}!} \prod_{i=1}^{m_d} \prod_{j=1}^{m_a} \frac{(\beta F_{ij}^0)^{N_{ij}}}{N_{ij}!} \left(\frac{\tilde{\rho}}{rN} \right)^{N_{ij}}, \quad (2.48)$$

where

$$F_{ij}^0 = E_{ij}^0 - TS_{ij}^0. \quad (2.49)$$

Electrostatic partition function

The dimensionless ionic strength of the present system is given in lattice fluid terms by

$$\tilde{I} \equiv v^* I = \frac{1}{2} \frac{\tilde{\rho}}{rN} \sum_{k=1}^l N_k z_k^2 = \frac{1}{2} \tilde{\rho} \sum_{k=1}^l \frac{\phi_k}{r_k} z_k^2, \quad (2.50)$$

where z_k is the charge valency of species k and I is dimensional ionic strength. For sufficiently low ionic strengths, the interaction energy u_l of any selected free ion of type l with the surrounding cloud of free ions is given by the Debye-Huckel theory⁸⁹:

$$\beta u_l = - \frac{\tilde{\kappa}^3}{8\pi\tilde{I}} \frac{z_l^2}{1 + \kappa\sigma_l^l}, \quad (2.51)$$

where σ_l^l is the diameter of the ion and $\tilde{\kappa}$ is a dimensionless Debye-Huckel inverse screening length, given in lattice-fluid terms by

$$\tilde{\kappa}^3 \equiv v^* \kappa^3 = (8\pi\tilde{I})^{3/2} \left(\frac{l_B^3}{v^*} \right)^{1/2}, \quad (2.52)$$

where κ is the usual Debye-Huckel inverse screening length, l_B is the Bjerrum length, q is the electron charge, ε_0 is the vacuum permittivity, and ε_r is the dielectric constant of the medium. The ion's diameter σ_l^l may be based upon its van der Waals radius or, as an approximation, upon its pure state lattice spacing $v_l^{*1/3}$. In general, the dielectric constant is a function of composition, density, and temperature:

$$\varepsilon_r = \varepsilon_r[\tilde{\rho}, \{\phi_k\}, T]. \quad (2.53)$$

However, this development will neglect the density and composition dependencies of the dielectric constant.

The electrostatic potential energy is simply the sum of the per-ion electrostatic energy given in equation (2.51) over all ions in the system, halving to prevent double-counting:

$$E_E = \frac{1}{2} \sum_{k=1}^l N_k u_k. \quad (2.54)$$

Combining equations (2.51) and (2.54) gives the contribution to potential energy from electrostatic interactions:

$$\beta E_E = -rN \frac{\tilde{\kappa}^3 \tilde{I}_\kappa}{8\pi\tilde{\rho}\tilde{I}}, \quad (2.55)$$

where \tilde{I}_κ can be understood as a screening-adjusted ionic strength, given by

$$\tilde{I}_\kappa \equiv \frac{1}{2} \tilde{\rho} \sum_{k=1}^l \frac{\phi_k}{r_k} \frac{z_k^2}{1 + \kappa\sigma_k}. \quad (2.56)$$

It then follows from equation (2.55) that the electrostatic partition function is given by

$$Q_E = \exp \left[rN \frac{\tilde{\kappa}^3 \tilde{I}_\kappa}{8\pi\tilde{\rho}\tilde{I}} \right]. \quad (2.57)$$

Note also that the component mole numbers are constrained by the requirement of electrical neutrality:

$$\sum_{l=1}^{m_C} N_l z_l = 0. \quad (2.58)$$

Free energy

The Gibbs free energy is obtained as in equation (2.14). The Gibbs partition function is now given by

$$\Psi(T, P, \{N_k\}) = \sum_{N_0=0}^{\infty} \left[\frac{Q_P(T, N_0, \{N_k\}) Q_A(T, N_0, \{N_k\}, \{N_{ij}\})}{Q_E(T, N_0, \{N_k\}) \exp(-\beta PV)} \right], \quad (2.59)$$

where V is given by equation (2.35), with the modification that V_{ij}^0 now applies to formation of ion-dipole bonds as well as hydrogen bonds. As in the HBLF model, it follows that the Gibbs free energy may also be partitioned into contributions from each of the above groups:

$$G = G_p + G_A + G_E. \quad (2.60)$$

The physical contribution to free energy is given by equations (2.16) from the SL model. The associating contribution is of the same form as equation (2.37) from the HBLF model, albeit with the altered variable definitions described above. The electrostatic contribution is given, from equation (2.57), by

$$\beta G_E = -rN \frac{\tilde{\kappa}^3 \tilde{I}_\kappa}{8\pi\tilde{\rho}\tilde{I}}. \quad (2.61)$$

Equations of state

The minimization conditions on free energy, as in the HBLF model, are given by equations (2.38) and (2.39). The associating equations of state are given by equation (2.42) from the HBLF model. The density equation of state is now

$$\tilde{\rho}^2 + \tilde{P} + \tilde{T} \left\{ \ln(1 - \tilde{\rho}) + \tilde{\rho} \left(1 - \frac{1}{\bar{r}} \right) + \frac{\tilde{\kappa}^3 (\tilde{I}_\kappa - \tilde{I}_{2\kappa})}{16\pi\tilde{I}} \right\} = 0, \quad (2.62)$$

where

$$\tilde{I}_{2\kappa} = \frac{1}{2} \tilde{\rho} \sum_{k=1}^l \frac{\phi_k}{r_k} \frac{\tilde{\kappa} \sigma_k^l}{v^{*1/3}} \frac{z_k^2}{\left(1 + \tilde{\kappa} \sigma_k^l / v^{*1/3} \right)^2}, \quad (2.63)$$

and where \bar{r} is given by equation (2.41) as in the HBLF model. Note that equation (2.62) is of the same functional form as that of the lattice fluid and hydrogen bonding lattice fluid models, albeit with an additional term for Coulombic interactions between free ions. Furthermore, the electrostatic term will be negligibly small at most charge concentrations of interest and can thus usually be neglected. This result emerges from the $\tilde{\kappa}^3$ scaling of this interaction, which in essence is the cube of the ratio of the lattice spacing to the Debye-Huckel screening length. As the lattice spacing is of the length

scale of atoms and the screening length is considerably larger for modest charge concentrations, the order of this term is much less than one.

Chemical potential

As before, the chemical potential may be divided into contributions from the various partition function factors:

$$\begin{aligned}\mu_k &= \left. \frac{\partial G}{\partial N_k} \right)_{T,P,\{N_{l \neq k}\}, \tilde{v}, \{N_{ij}\}} \cdot \\ &= \mu_{k,P} + \mu_{k,A} + \mu_{k,E}\end{aligned}\quad (2.64)$$

The physical and associating contributions are given by equations (2.20) and (2.45) from the LF and HBLF models. The electrostatic contribution is given by

$$\beta\mu_{k,E} = -\frac{\tilde{\kappa}^3}{16\pi\tilde{I}} \left(z_k^2 \left(\frac{1}{1+\kappa a_k} + \frac{1}{2} \frac{\tilde{I}_\kappa - \tilde{I}_{2\kappa}}{\tilde{I}} \right) - (\tilde{I}_\kappa - \tilde{I}_{2\kappa}) \frac{r_k v_k^*}{\tilde{\rho} v^*} \right). \quad (2.65)$$

Note that for uncharged species, the electrostatic contribution to chemical potential reduces to

$$\beta\mu_{k,E} = \frac{\tilde{\kappa}^3}{16\pi\tilde{I}} \left((\tilde{I}_\kappa - \tilde{I}_{2\kappa}) \frac{r_k v_k^*}{\tilde{\rho} v^*} \right). \quad (2.66)$$

Furthermore, as in the density equation of state, for most cases the contribution to chemical potential from electrostatics will be negligible due to its $\tilde{\kappa}^3$ scaling.

Heat of mixing

The heat of mixing is given by the difference in energies between the components in the pure states and the mixture. For covalent components such as solvents and polymers, the pure state energies may be calculated consistently via this model. However, for free ions for which the pure state is a crystalline ionic lattice, it is necessary to call upon some other theoretical or experimental data in order to determine the ionic lattice energy $E_{L,i}$ of the pure state solid. Given this quantity, the energy of mixing is

$$\Delta E_{mix} = -rN\varepsilon^* \tilde{\rho} + \sum_{i=1}^{m_d} \sum_{j=1}^{m_a} N_{ij} E_{ij}^0 - \sum_{k=\text{covalent species}} \left(-r_k N_k \varepsilon_k^* \tilde{\rho}_k^0 + \sum_{i=1}^{m_d} \sum_{j=1}^{m_a} N_{ij}^{k0} E_{ij}^0 \right) - \sum_{i=\text{salts}} N_{s,i} E_{L,i}, \quad (2.67)$$

where $\tilde{\rho}_k^0$ is the reduced density of component k in its pure state and N_{ij}^{k0} denotes association counts in pure component k . The sum of k over covalent species indicates a sum over components whose pure state is not an ionic crystal. The summation over salts is a summation over electrically neutral salt species, such as NaCl or HCl (rather than a summation over dissociated ion species such as Na, Cl, and H as other species sums in this paper are). Thus, $N_{s,i}$ is the number of salt molecules of type i necessary to provide the ions present in solution, and is related to the N_k 's of the ion species by stoichiometric considerations. For example, in a simple system containing ions dissociated from only a single salt species, $N_{s,i}$ would be given by

$$N_{s,i} = \frac{\sum_{k=\text{ion species}} N_k n_{k,i}}{\sum_{k=\text{ion species}} n_{k,i}} \quad (2.68)$$

where $n_{k,i}$ is the number of ions of species k per molecular unit of salt molecule i . For example, $n_{k,i} = 1$ for chlorine in NaCl or 2 for chlorine in MgCl₂.

Equation (2.67) for the heat of mixing provides an approach to obtaining associating parameters for ion hydration. Such an approach first requires an independent determination of lattice fluid parameters for ions, in order to obtain a physically meaningful separation of physical and associating interactions. Atomic ions' lattice fluid parameters may be obtained by approximating their physical interactions to be equal to those of a hypothetical Noble gas of equal van der Waals radius. The properties of this hypothetical Noble gas can, in turn, be determined via interpolation with respect to the van der Waals radius of real Noble gases. Once lattice fluid parameters are determined via this approach, the only remaining parameters are those for association interactions.

These can then be obtained by a best fit to heat of mixing data over a range of temperature and pressure.

The major hurdle in fitting *ion* association parameters to *salt* heats of solvation based on a single salt solution is that there is no basis for the establishment of independent parameters for the salt's constituent ions. This problem can be surmounted by simultaneously fitting to heat of solvation for four separate water-salt systems in which each cation and anion appears exactly twice. An ideal such set of systems would contain only strong 1:1 salts. One example reasonably satisfying these requirements would consist of the systems water-NaCl, water-HCl, water-HBr and water-NaBr. The effect of fitting all four ions contained in this set to all four systems at once would be to distinguish each ion from any particular ion pairing. Once parameters for these ions were established, they could be used to establish those of other ions by fitting to heat of solvation data for a salt consisting of one of these ions and the new desired ion.

An informative test of this model would be whether ion hydration parameters obtained from a heat of solvation optimization such as the one above are also able to yield LCSTs in agreement with experiment. Success in such a test would indicate that the model consistently captures the physics of both ion hydration and solution stability.

2.2.2. Polyelectrolytes

Model description

Two modifications must be made to the above model in order to treat polyelectrolytes. First, the electrostatic term must be modified to account for long range Coulombic interactions involving the charges fixed on the chain. Second, whereas the above model does not consider ionic bonding, many polyelectrolytes of interest only partially ionize at experimental pH, and it is thus necessary to incorporate this interaction explicitly.

Consider a system containing t species, in which there are N_k molecules of each species k . Of these species, t_p are polymeric or macromolecular and t_s are small molecules. All dissociable ionic species are considered to be fully dissociated into their constituent ions for the purpose of these counts. Each molecule of species k contains C_l^k cationic sites of type l and A_u^k anionic sites of type u ; the system contains m_C types of such cationic sites and m_A types of such anionic sites. The total number of cationic sites of type l is then

$$N_C^l = \sum_{k=1}^t N_k C_l^k, \quad (2.69)$$

and the total number of anionic sites of type u is

$$N_A^u = \sum_{k=1}^t N_k A_u^k. \quad (2.70)$$

Of these, N_{lu}^l pairs of a cationic group of type l and an anionic group of type u will be in a bound state. Each cationic site of type l has a charge valency z_l^C and an ionic radius a_l^C , and each anionic site of type u has a charge valency z_u^A and an ionic radius a_u^A .

The system also contains m_a types of association bond donor sites and m_a association bond acceptor sites, where ‘association bonds’ include hydrogen bonds and ion hydration or ion-dipole type bonds, and optionally may include some strong dipole-dipole bonds. Association donors include hydrogen bond proton donors and hydration sites on cationic sites and on some partial positive poles of dipoles. Association acceptors include hydrogen bond proton acceptors and hydration sites on anionic sites and some on partial negative poles of dipoles. Each molecule of species k presents d_i^k association bond donors sites of type i and a_j^k association bond acceptor sites of type j that are not associated with an ionic site. Furthermore, each charged site is associated uniquely with a single type of association site which by convention shall have the same index as the charged site type. Thus each cationic site of type i exhibits d_i^C association

donor sites of type i , and each anionic site of type j exhibits a_j^A association acceptor sites of type j .

Finally, bound pairs of a cation of type l with an anion of type u may exhibit d_i^{lu} association donors of type i and a_j^{lu} association acceptors of type j ; this represents dipole-dipole interactions between bound ion pairs and other dipoles and can often be neglected. However, note that, for bound ion pairs on a polyelectrolyte, this class of interactions has been posited to drive solution destabilization with respect to the neutral polymer at high counterion concentration^{113, 115}. Omission of such interactions may thus omit some polyelectrolyte physics. Furthermore, note that this contribution represents the introduction of a limited class of ternary interactions into the model; specifically, it accounts for ion-ion-dipole ternary interactions. This approach could be further extended to account for ternary interactions more generally. For example, water's hydrogen bonding-energy to the polymer could be modified if the water is also hydrating an ion. The ion-ion-dipole ternary interaction has been selected for special treatment in this model simply because the energy of ion pairing is so high as to be expected to have a far more significant ternary effect.

The total number of association donors of type i is

$$N_d^i = \sum_{k=1}^t N_k d_i^k + \alpha_i^C d_i^C N_C^i + \sum_{l=1}^{m_C} \sum_{u=1}^{m_A} N_{lu}^l d_i^{lu}, \quad (2.71)$$

and the number of association acceptors of type j is

$$N_a^j = \sum_{k=1}^t N_k a_j^k + \alpha_j^A a_j^A N_A^j + \sum_{l=1}^{m_C} \sum_{u=1}^{m_A} N_{lu}^l a_j^{lu}, \quad (2.72)$$

where α_i^C and α_j^A denote cation and anion ionization fractions, respectively, defined as

$$\alpha_i^C = 1 - \frac{1}{N_C^i} \sum_{u=1}^{m_A} N_{lu}^l \quad (2.73)$$

and

$$\alpha_u^A = 1 - \frac{1}{N_A^u} \sum_{l=1}^{m_C} N_{lu}^I. \quad (2.74)$$

The requirement of charge neutrality provides a constraint upon the molecule numbers:

$$\sum_{l=1}^{m_C} N_C^l z_l^C + \sum_{u=1}^{m_A} N_A^u z_u^A = 0. \quad (2.75)$$

As in previous models the partition function of this system is considered to be factorable. The first factor, Q_P , accounts for ‘physical’ interactions between molecules: excluded volume interaction, dispersion forces, and most dipole-dipole interactions. A second factor, Q_I , accounts for ionic bonding. The third factor, Q_A , accounts for associating interactions such as hydrogen bonds, ion-dipole bonds, and some strong dipole-dipole bonds. The final factor, Q_E , accounts for long range electrostatic interactions. The canonical partition function may thus be written as

$$Q = Q_P Q_I Q_A Q_E. \quad (2.76)$$

As in the previous model, the lattice fluid model result given by equation (2.12) will be used for the physical partition function. Similarly, equation (2.48) for associating interactions will be used for the associating partition function.

Ion-binding partition function

The ionic bonding partition function will follow the same development as the associating partition function. The number of unbonded cationic groups of type l and number of unbonded anionic groups of type u are

$$N_{l0}^I = N_C^l \alpha_l^C = N_C^l - \sum_{u=1}^{m_A} N_{lu}^I \quad (2.77)$$

and

$$N_{0u}^I = N_A^u \alpha_u^A = N_A^u - \sum_{l=1}^{m_C} N_{lu}^I. \quad (2.78)$$

As in the association contribution, this leads to an ionic bonding partition function of

$$Q_I = \prod_{l=1}^{m_C} \frac{N_C^l!}{N_{l0}^l!} \prod_{u=1}^{m_A} \frac{N_A^u!}{N_{0u}^u!} \prod_{l=1}^{m_C} \prod_{u=1}^{m_A} \frac{(\beta F_{lu}^I)^{N_{lu}^I}}{N_{lu}^I!} \left(\frac{\tilde{\rho}}{rN} \right)^{N_{lu}^I}, \quad (2.79)$$

where

$$F_{lu}^I = E_{lu}^I + TS_{lu}^I, \quad (2.80)$$

and where E_{lu}^I and S_{lu}^I are the energy and entropy, respectively, of pair formation between a cationic group of type l and an anionic group of type u .

Electrostatic partition function

For simplicity, note that the total number of types of ionic groups in the system is given by

$$m_I \equiv m_C + m_A. \quad (2.81)$$

Then define the number of ionic groups of type l per molecule of type k I_l^k such that

$$I_l^k \equiv \begin{cases} C_l^k & l \leq m_C \\ A_{l-m_C}^k & l > m_C \end{cases}. \quad (2.82)$$

Similarly,

$$\alpha_l \equiv \begin{cases} \alpha_l^C & l \leq m_C \\ \alpha_{l-m_C}^A & l > m_C \end{cases}, \quad (2.83)$$

$$z_l \equiv \begin{cases} z_l^C & l \leq m_C \\ z_{l-m_C}^A & l > m_C \end{cases}, \quad (2.84)$$

and

$$\sigma_l^I \equiv \begin{cases} \sigma_l^C & l \leq m_C \\ \sigma_{l-m_C}^A & l > m_C \end{cases}, \quad (2.85)$$

The ionic strength of this system may now be defined in dimensionless form as

$$\tilde{I} \equiv Iv^* = \frac{1}{2} \tilde{\rho} \sum_{k=1}^t \frac{\phi_k}{r_k} \sum_{l=1}^{m_l} \alpha_l I_l^k z_l^2. \quad (2.86)$$

The contribution from free ions to \tilde{I} is

$$\tilde{I}_f \equiv I_f v^* = \frac{1}{2} \tilde{\rho} \sum_{k=t_p+1}^t \frac{\phi_k}{r_k} \sum_{l=1}^{m_l} \alpha_l I_l^k z_l^2, \quad (2.87)$$

where the sum from $t_p + 1$ to t denotes a sum over small molecules only.

There will be two distinct types of long range electrostatic interactions. The first type includes interactions involving free ions (those on small molecules). Due to their small size, the spatial distribution of such ions is expected to be dominated by their electrostatic interactions, and these interactions are thus modeled via the Debye-Huckel theory. Within this framework, the interaction energy of any ion with the surrounding cloud of free ions is given by⁸⁹

$$\beta u_l^f = -\frac{\tilde{\kappa}^3}{8\pi\tilde{I}_f} \frac{z_l^2}{1 + \tilde{\kappa}\sigma_l^f / v^{*1/3}}, \quad (2.88)$$

where

$$\tilde{\kappa}^3 \equiv \kappa^3 v^* = \left(8\pi\tilde{I}_f\right)^{3/2} \left(\frac{l_B^3}{v^*}\right)^{1/2}, \quad (2.89)$$

and where κ is the Debye-Huckel inverse screening length and l_B is the Bjerrum length, defined as usual by

$$l_B \equiv \frac{\beta q^2}{4\pi\epsilon_0\epsilon_r}. \quad (2.90)$$

The second type of Coulombic interaction includes only those between fixed ions (those on macromolecules). The spatial distribution of such ions is taken to be dominated by considerations of the chain backbone rather than by electrostatics, and the charges thus do not participate in Debye-Huckel screening. They are however, still screened by the free ions, such that the interaction between two such fixed ions is given the Debye-Huckel screened pair interaction energy:

$$\beta u^{bb} = \frac{l_B}{r} \exp(-\kappa r). \quad (2.91)$$

Integrating equation (2.91) over all space (considering all other fixed charges) yields for the interaction energy u_l^b of a fixed charge of type l with all other fixed charges

$$\beta u_l^b = \frac{z_l \tilde{\rho}_l^p}{\tilde{I}_f}, \quad (2.92)$$

where $\tilde{\rho}_l^p$ is the total dimensionless charge density of fixed polymeric charges:

$$\tilde{\rho}_l^p \equiv \rho_l^p v^* = \frac{1}{2} \tilde{\rho} \sum_{k=1}^{t_p} \frac{\phi_k}{r_k} \sum_{l=1}^{m_l} \alpha_l I_l^k z_l. \quad (2.93)$$

The total electrostatic energy of the system is the sum of equations (2.88) and (2.92) over all applicable ions, halving as necessary to prevent double-counting:

$$\beta G_E = \frac{rN}{\tilde{\rho} \tilde{I}_f} \left[\left(\tilde{\rho}_l^p \right)^2 - \frac{\tilde{\kappa}^3}{8\pi} \left(\tilde{I}_{p\kappa} + \tilde{I}_\kappa \right) \right], \quad (2.94)$$

where \tilde{I}_κ is a screened ionic strength, given by

$$\tilde{I}_\kappa \equiv \frac{1}{2} \tilde{\rho} \sum_{k=1}^{t_p} \frac{\phi_k}{r_k} \sum_{l=1}^{m_l} \frac{\alpha_l I_l^k z_l^2}{1 + \tilde{\kappa} \sigma_l^I / v^{*1/3}}, \quad (2.95)$$

and $\tilde{I}_{p\kappa}$ is the contribution from polymeric charges to this screened ionic strength, given by

$$\tilde{I}_{p\kappa} \equiv \frac{1}{2} \tilde{\rho} \sum_{k=1}^{t_p} \frac{\phi_k}{r_k} \sum_{l=1}^{m_l} \frac{\alpha_l I_l^k z_l^2}{1 + \tilde{\kappa} \sigma_l^I / v^{*1/3}}. \quad (2.96)$$

The electrostatic contribution to the partition function is then

$$Q_E = \exp \left[-\frac{rN}{\tilde{\rho} \tilde{I}_f} \left[\left(\tilde{\rho}_l^p \right)^2 - \frac{\tilde{\kappa}^3}{8\pi} \left(\tilde{I}_{p\kappa} + \tilde{I}_\kappa \right) \right] \right]. \quad (2.97)$$

For modest salt concentrations, both terms in equation (2.97) will be considerably less than one and will thus be negligible relative to the physical, associating, and ion-binding contributions.

Free energy

The Gibbs partition function is given by

$$\Psi(T, P, \{N_k\}) = \sum_{N_0=0}^{\infty} \left[\frac{\mathcal{Q}_P(T, N_0, \{N_k\}) \mathcal{Q}_A(T, N_0, \{N_k\}, \{N_{ij}\}, \{N_{lu}^I\})}{\mathcal{Q}_I(T, N_0, \{N_k\}, \{N_{lu}^I\}) \mathcal{Q}_E(T, N_0, \{N_k\}, \{N_{lu}^I\})} \exp(-\beta PV) \right], \quad (2.98)$$

where the system volume V is given by

$$V = rNv^* \tilde{v} + \sum_{i=1}^{m_d} \sum_{j=1}^{m_a} N_{ij} V_{ij}^0 + \sum_{l=1}^{m_c} \sum_{u=1}^{m_A} N_{lu}^I V_{lu}^I, \quad (2.99)$$

and where V_{ij}^0 is the volume change of association formation between a donor of type i and an acceptor of type j and V_{lu}^I is the volume change of ionic bond formation between a cationic group of type of type l and an anionic group of type u .

As before, the Gibbs free energy is given by equation (2.14) and the free energy may be segregated into the same contributions as the partition function:

$$G = G_P + G_A + G_I + G_E. \quad (2.100)$$

The physical and associating contributions to free energy are given by equations (2.16) and (2.37), respectively, as in the HBLF model. The electrostatic contribution to free energy is given by

$$\beta G_E = \frac{rN}{\tilde{\rho} \tilde{I}_f} \left[\left(\tilde{\rho}_l^p \right)^2 - \frac{\tilde{K}^3}{8\pi} \left(\tilde{I}_{p\kappa} + \tilde{I}_\kappa \right) \right]. \quad (2.101)$$

The ionic bonding contribution is given by

$$\beta G_I = rN \left[\sum_{l=1}^{m_c} \sum_{u=1}^{m_A} v_{lu}^I \left(1 + \beta G_{lu}^I + \ln \frac{v_{lu}^I}{\tilde{\rho} v_{l0}^I v_{0u}^I} \right) + \sum_{l=1}^{m_c} v_C^I \ln \frac{v_{l0}^I}{v_C^I} + \sum_{u=1}^{m_A} v_A^u \ln \frac{v_{0u}^I}{v_A^u} \right], \quad (2.102)$$

where $G_{lu}^I = F_{lu}^I + PV_{lu}^I$ and $v_C^I = \frac{N_C^I}{rN}$, $v_{l0}^I = \frac{N_{l0}^I}{rN}$, $v_{lu}^I = \frac{N_{lu}^I}{rN}$, and so on.

Extra care must be taken in determining the maximum term of the partition function due to complications arising from interactions between the associating and

ionic-bonding contributions to the partition function. In particular, the maximum term is equivalent to minimizing the Gibbs free energy with respect to \tilde{v} and each of the N_{ij} and v_{lu}^I , where

$$v_{lu}^I = \frac{N_{lu}^I}{(N_C^I N_A^I)^{1/2}} = \frac{v_{lu}^I}{(v_C^I v_A^I)^{1/2}} \quad (2.103)$$

Minimizing with respect to a non-intensive measure of ionic bonding or to an intensive measure which is asymmetric for anions and cations results in a model that is not thermodynamically self consistent. In particular, for such a model the system free energy is not correctly recovered from the chemical potential. Accordingly, the correct minimization conditions are

$$\left(\frac{\partial G}{\partial \tilde{v}} \right)_{T,P,\{N_k\},\{v_{lu}^I\},\{N_{ij}\}} = 0, \quad (2.104)$$

$$\left(\frac{\partial G}{\partial N_{ij}} \right)_{T,P,\tilde{v},\{N_k\},\{v_{lu}^I\},\{N_{yz \neq ij}\}} = 0, \quad (2.105)$$

and

$$\left(\frac{\partial G}{\partial v_{lu}^I} \right)_{T,P,\tilde{v},\{N_k\},\{v_{yz \neq lu}^I\},\{N_{ij}\}} = 0, \quad (2.106)$$

for all i and j and all l and u for which N_{ij} and N_{lu}^I , respectively, are not identically zero due to the system definition (i.e. pairings of ions comprising a strong electrolyte).

Equations of state

The associating equations of state are given by equation (2.42) as in earlier models. Equation (2.104) yields the density EOS for the system:

$$\tilde{\rho}^2 + \tilde{P} + \tilde{T} \left\{ \ln(1 - \tilde{\rho}) + \tilde{\rho} \left(1 - \frac{1}{\tilde{r}} \right) + \frac{\tilde{K}^3}{16\pi \tilde{I}_f} (\tilde{I}_\kappa - \tilde{I}_{2\kappa} + \tilde{I}_{p\kappa} - \tilde{I}_{p2\kappa}) \right\} = 0, \quad (2.107)$$

where

$$\frac{1}{\tilde{r}} \equiv \frac{1}{r} - \sum_{i=1}^{m_d} \sum_{j=1}^{m_a} v_{ij} - \sum_{l=1}^{m_c} \sum_{u=1}^{m_A} v_{lu}^I, \quad (2.108)$$

$$\tilde{I}_{2\kappa} = \frac{1}{2} \tilde{\rho} \sum_{k=1}^i \frac{\phi_k}{r_k} \sum_{l=1}^{m_l} \frac{\tilde{\kappa} \sigma_l^I}{v^{*1/3}} \frac{\alpha_l I_l^k z_l^2}{\left(1 + \tilde{\kappa} \sigma_l^I / v^{*1/3}\right)^2}, \quad (2.109)$$

and

$$\tilde{I}_{p2\kappa} = \frac{1}{2} \tilde{\rho} \sum_{k=1}^{i_p} \frac{\phi_k}{r_k} \sum_{l=1}^{m_l} \frac{\tilde{\kappa} \sigma_l^I}{v^{*1/3}} \frac{\alpha_l I_l^k z_l^2}{\left(1 + \tilde{\kappa} \sigma_l^I / v^{*1/3}\right)^2}. \quad (2.110)$$

Note that long range electrostatic interactions do not play a significant role in the density equation of state of modest charge density solutions. This surprising conclusion emerges from two predictions. The first prediction, as in the previous model, is that the energy of Coulombic interactions involving free ions is negligible at most salt concentrations of interest. The second prediction is that the energy of Coulombic interactions between fixed charges is constant with respect to density. This emerges from the fact that as density drops, distances between fixed charges increase but charge screening decreases at the same rate, with the two effects cancelling exactly. Despite these conclusions, however, it is important to note that the presence of charges still significantly effects the density equation of state via the contribution of ionic bonds and of ion-dipole associations. Accordingly, discarding the electrostatic term gives for the density equation of state:

$$\tilde{\rho}^2 + \tilde{P} + \tilde{T} \left\{ \ln(1 - \tilde{\rho}) + \tilde{\rho} \left(1 - \frac{1}{\tilde{r}} \right) \right\} = 0, \quad (2.111)$$

which is the same as that for the hydrogen bonding lattice fluid model, albeit with an additional contribution to account for ionic bonding.

Equation (2.106) yields the set of ionic bonding equations of state:

$$v_{lu}^I = \tilde{\rho} v_{l0}^I v_{0u}^I \left(\frac{v_{l0}}{v_d^I} \right)^{d_l^C} \left(\frac{v_{0u}}{v_a^u} \right)^{a_u^A}$$

$$\exp \left\{ -\beta G_{lu}^I - \frac{1}{2\tilde{I}_f} \left[\tilde{\rho}_l^p \left(\frac{\tilde{\rho}_l^p}{\tilde{I}_f} (f_{Cl}^s z_l^{C2} + f_{Au}^s z_u^{A2}) - 2(f_{Cl}^p z_l^C + f_{Au}^p z_u^A) \right) \right. \right. \\ \left. \left. + \frac{\tilde{\kappa}^3}{8\pi} \left(\frac{\tilde{I}_{p\kappa} + \tilde{I}_\kappa - \tilde{I}_{p2\kappa} - \tilde{I}_{2\kappa}}{2\tilde{I}_f} (f_{Cl}^s z_l^{C2} + f_{Au}^s z_u^{A2}) \right) \right. \right. \\ \left. \left. + \frac{z_l^{C2}}{1 + \tilde{\kappa}\sigma_l^C/v^{*1/3}} (1 + f_{Cl}^p) + \frac{z_u^{A2}}{1 + \tilde{\kappa}\sigma_u^A/v^{*1/3}} (1 + f_{Au}^p) \right) \right\}, \quad (2.112)$$

$$-\sum_{i=1}^{m_d} d_i^{lu} \ln \frac{v_{i0}}{v_d^j} - \sum_{j=1}^{m_a} a_j^{lu} \ln \frac{v_{0j}}{v_a^j}$$

where f_{Cy}^s and f_{Az}^s are the fraction of cations of type y and anions of type z , respectively, that are on small molecules:

$$f_{Cy}^s \equiv \sum_{k=t_p+1}^t \frac{\phi_k}{r_k} \frac{C_y^k}{v_C^y} \quad (2.113)$$

and

$$f_{Az}^s \equiv \sum_{k=t_p+1}^t \frac{\phi_k}{r_k} \frac{A_z^k}{v_A^z}. \quad (2.114)$$

Similarly, f_{Cy}^p and f_{Az}^p are the fractions of cations of type y and anions of type z , respectively, found on polymer molecules:

$$f_{Cy}^p \equiv \sum_{k=1}^{t_p} \frac{\phi_k}{r_k} \frac{C_y^k}{v_C^y} \quad (2.115)$$

and

$$f_{Az}^p \equiv \sum_{k=1}^{t_p} \frac{\phi_k}{r_k} \frac{A_z^k}{v_A^z}. \quad (2.116)$$

Note that for most cases, (2.113) through (2.116) will have values of either zero or one as the same type of charged group by definition will generally not be found on both a small and large molecule. Note also that equation (2.112) may be considerably simplified in the limit that long range electrostatics may be neglected.

Chemical potential

As in earlier models, the chemical potential may be separated into contributions from the various partition function factors:

$$\begin{aligned}\mu_k &= \left. \frac{\partial G}{\partial N_k} \right)_{T,P,\{N_{y \neq k}\}, \tilde{v}, \{N_{ij}\}, \{v_{lu}^I\}} \quad . \quad (2.117) \\ &= \mu_{k,P} + \mu_{k,A} + \mu_{k,I} + \mu_{k,E}\end{aligned}$$

The physical contribution to chemical potential is given by equation (2.20) from the lattice fluid model. The associating contribution is:

$$\begin{aligned}\beta \mu_{k,A} &= r_k \sum_{i=1}^{m_d} \sum_{j=1}^{m_a} v_{ij} \\ &+ \sum_{i=1}^{m_d} \left\{ \begin{aligned} &d_i^k + d_i^C \left[\alpha_i^C C_i^k + \frac{1}{2} \sum_{u=1}^{m_A} v_{iu}^I \left(\frac{C_i^k}{v_C^i} - \frac{A_u^k}{v_A^u} \right) \right] \\ &+ \frac{1}{2} \sum_{l=1}^{m_C} \sum_{u=1}^{m_A} v_{lu}^I d_i^{lu} \left(\frac{C_l^k}{v_C^l} + \frac{A_u^k}{v_A^u} \right) \end{aligned} \right\} \ln \frac{v_{i0}}{v_d^i} \quad . \quad (2.118) \\ &+ \sum_{j=1}^{m_a} \left\{ \begin{aligned} &a_j^k + a_j^A \left[\alpha_j^A A_j^k - \frac{1}{2} \sum_{l=1}^{m_C} v_{lj}^I \left(\frac{C_l^k}{v_C^l} - \frac{A_j^k}{v_A^j} \right) \right] \\ &+ \frac{1}{2} \sum_{l=1}^{m_C} \sum_{u=1}^{m_A} v_{lu}^I a_j^{lu} \left(\frac{C_l^k}{v_C^l} + \frac{A_u^k}{v_A^u} \right) \end{aligned} \right\} \ln \frac{v_{0j}}{v_a^j}\end{aligned}$$

The ionic bonding contribution is:

$$\begin{aligned}\mu_{k,I} &= \sum_{l=1}^{m_C} \sum_{u=1}^{m_A} v_{lu}^I \left[r_k + \frac{1}{2} \left(\frac{A_u^k}{v_A^u} + \frac{C_l^k}{v_C^l} \right) \left(\frac{G_{lu}^I}{kT} + \ln \frac{v_{lu}^I}{\tilde{\rho} v_{i0}^I v_{0u}^I} \right) \right] \quad . \quad (2.119) \\ &+ \sum_{l=1}^{m_C} C_l^k \ln \frac{v_{l0}^I}{v_C^l} + \sum_{u=1}^{m_A} A_u^k \ln \frac{v_{0u}^I}{v_A^u}\end{aligned}$$

The electrostatic contribution is:

$$\begin{aligned}
\beta\mu_{k,E} = & \left[\begin{aligned} & \tilde{\rho}_l^p \left[\begin{aligned} & \sum_{l=1}^{m_l} \alpha_l I_l^k z_l \left(2H[t_p - k] - z_l \frac{\tilde{\rho}_l^p}{\tilde{I}_f} H[k - t_p - 1] \right) \\ & - \sum_{l=1}^{m_c} \sum_{u=1}^{m_A} v_{lu}^J \left(\frac{C_l^k}{v_C^J} - \frac{A_u^k}{v_A^u} \right) \left(\frac{\tilde{\rho}_l^p}{2\tilde{I}_f} (z_l^{C2} f_{Cl}^s - z_u^{A2} f_{Au}^s) - (z_l^C f_{Cl}^p - z_u^A f_{Au}^p) \right) \end{aligned} \right] \\ & + \frac{1}{2\tilde{I}_f} \left[\begin{aligned} & \frac{\tilde{I}_{p\kappa} + \tilde{I}_\kappa - \tilde{I}_{p2\kappa} - \tilde{I}_{2\kappa}}{2\tilde{I}_f} \left[\begin{aligned} & \sum_{l=1}^{m_l} \alpha_l I_l^k z_l^2 H[k - t_p - 1] - 2\tilde{I}_f \frac{r_k v_k^*}{\tilde{\rho} v^*} \\ & + \frac{1}{2} \sum_{l=1}^{m_c} \sum_{u=1}^{m_A} v_{lu}^J \left(\frac{C_l^k}{v_C^J} - \frac{A_u^k}{v_A^u} \right) (z_l^{C2} f_{Cl}^s - z_u^{A2} f_{Au}^s) \end{aligned} \right] \end{aligned} \right] \\ & - \frac{\tilde{\kappa}^3}{8\pi} + \sum_{l=1}^{m_l} \frac{\alpha_l I_l^k z_l^2}{1 + \tilde{\kappa} \sigma_l^J / v^{*1/3}} (1 + H[t_p - k]) \\ & + \frac{1}{2} \sum_{l=1}^{m_c} \sum_{u=1}^{m_A} v_{lu}^J \left(\frac{C_l^k}{v_C^J} - \frac{A_u^k}{v_A^u} \right) \left(\begin{aligned} & (1 + f_{Cl}^p) \frac{z_l^{C2}}{1 + \tilde{\kappa} \sigma_l^C / v^{*1/3}} \\ & - (1 + f_{Au}^p) \frac{z_u^{A2}}{1 + \tilde{\kappa} \sigma_u^A / v^{*1/3}} \end{aligned} \right) \end{aligned} \right], \quad (2.120)
\end{aligned}$$

where $H[x]$ is the Heaviside step function, given by

$$H[x] = \begin{cases} 1 & \text{if } x \geq 0 \\ 0 & \text{if } x < 0 \end{cases} \quad (2.121)$$

Note that the relation

$$G = \sum_{k=1}^t N_k \mu_k \quad (2.122)$$

properly recovers the system free energy, as it should. Also note that in the absence of polyelectrolytes, equation (2.120) reduces exactly to equation (2.65) from the prior, polyelectrolyte free, model.

2.2.3. Solution Stability

The above models will entail systems with at least four components (polymer, solvent, cation, and anion), with the electroneutrality condition constraining one of the component mole numbers. It is thus useful to develop in a general way the spinodal of a

multicomponent system under additional constraints. The development will differ depending upon whether the constraint is on composition fractions only, or upon mole numbers and composition fractions, as in the present case. For completeness and comparison, the composition fraction only case is addressed first.

Spinodal with a constraint on the composition fractions

For a t component mixture, in general the system composition will be described by $t-1$ independent composition variables. An appropriate gradient operator with respect to composition may be defined in vector form as

$$\nabla \equiv \left[\left(\frac{\partial}{\partial \phi_1} \right)_{\phi_{j \neq 1}} \quad \left(\frac{\partial}{\partial \phi_2} \right)_{\phi_{j \neq 2}} \quad \dots \quad \left(\frac{\partial}{\partial \phi_{t-1}} \right)_{\phi_{j \neq t-1}} \right]. \quad (2.123)$$

In general, the limit of stability (spinodal) for the system with respect to composition is defined by

$$\det(\nabla \otimes \nabla g) = 0, \quad (2.124)$$

where g is the intensive system free energy and $\nabla \otimes \nabla$ denotes the outer product of the gradient vector with itself. The type of intensive free energy (molar, volumetric, etc.) should be chosen to be conjugate to the composition variable chosen. Several composition variables are of the form

$$\phi_u = \frac{r_u N_u}{\sum_{k=1}^t r_k N_k} = \frac{r_u N_u}{rN}, \quad (2.125)$$

where r_u is some species-specific property of component u on which the composition variable is based. For example, for the mole fraction r_u is identically one, and for the volume fraction r_u is some measure of molecular size.

In many cases, it is convenient to frame the spinodal in terms of chemical potentials rather than in terms of free energy, both because the chemical potential is a commonly calculated quantity and because this form sometimes allows the straightforward use of free energy minimization conditions, such as equations (2.104)

through (2.106), in simplifying the spinodal. The chemical potential is given at constant temperature and pressure in terms of system free energy by

$$\mu_k = \left(\frac{\partial G}{\partial N_k} \right)_{\{N_{j \neq k}\}}. \quad (2.126)$$

In terms of intensive free energy and the composition variable form given by equation (2.125), chemical potential is

$$\mu_k = r_k g + r N \left(\frac{\partial g}{\partial N_k} \right)_{\{N_{j \neq k}\}} \quad (2.127)$$

Applying the chain rule (see appendix A.2.1 for more detail), the general expression for second order derivatives of intensive free energy with respect to composition is then

$$\left(\frac{\partial}{\partial \phi_l} \left(\frac{\partial g}{\partial \phi_k} \right)_{\{\phi_{j \neq k, l}\}} \right)_{\{\phi_{j \neq l, l}\}} = \frac{1}{1 - \phi_k} \left[\begin{array}{c} \frac{1}{r_k} \left(\frac{\partial \mu_k}{\partial \phi_l} \right)_{\{\phi_{j \neq l, l}\}} \\ + \sum_{u \neq k}^{l-1} \phi_u \left(\frac{\partial}{\partial \phi_l} \left(\frac{\partial g}{\partial \phi_u} \right)_{\{\phi_{j \neq u, l}\}} \right)_{\{\phi_{j \neq l, l}\}} \end{array} \right], \quad (2.128)$$

where all composition derivatives are taken with all other composition fractions except the dependent one held constant.

For a two component system equation (2.128) reduces to a single equation and the spinodal is simply

$$\left(\frac{\partial^2 g}{\partial \phi_k^2} \right) = \frac{1}{r_k} \frac{1}{1 - \phi_k} \left(\frac{\partial \mu_k}{\partial \phi_k} \right) = 0. \quad (2.129)$$

However, for a ternary system equation (2.128) yields a set of three equations:

$$g_{11} - \frac{\phi_2}{1 - \phi_1} g_{12} = \frac{1}{1 - \phi_1} \frac{1}{r_1} \left(\frac{\partial \mu_1}{\partial \phi_1} \right)_{\phi_2}; \quad (2.130)$$

$$g_{12} - \frac{\phi_2}{1 - \phi_1} g_{22} = \frac{1}{1 - \phi_1} \frac{1}{r_1} \left(\frac{\partial \mu_1}{\partial \phi_2} \right)_{\phi_1}; \quad (2.131)$$

$$g_{22} - \frac{\phi_1}{1-\phi_2} g_{12} = \frac{1}{1-\phi_2} \frac{1}{r_2} \left(\frac{\partial \mu_2}{\partial \phi_2} \right)_{\phi_1}; \quad (2.132)$$

where

$$g_{kl} \equiv \left(\frac{\partial}{\partial \phi_l} \left(\frac{\partial g}{\partial \phi_k} \right)_{\{\phi_{j \neq k}\}} \right)_{\{\phi_{j \neq l}\}}. \quad (2.133)$$

This set of equations may be solved through straightforward linear algebra, yielding explicit equations for the g_{kl} in terms of composition derivatives of the component chemical potentials. These expressions may then be substituted into equation (2.124) to yield the spinodal in terms of chemical potentials.

Spinodal with a constraint on the mole numbers

A complication in the above approach emerges when the system is also subject to a constraint on the mole numbers, such as the electroneutrality condition in the present models. Such a constraint will always also impose an associated constraint on the composition fractions, and it is at first tempting to simply apply the above development on this basis. However, equation (2.128) becomes incorrect if a mole number constraint is applied to the free energy before the spinodal is calculated. In this case, it is necessary to account for the altered meaning of the chemical potential, as follows.

In general, the free energy is a function of all mole numbers:

$$G = G(\{N_{k \leq t}\}). \quad (2.134)$$

However, when there is a constraint on the mole numbers, the mole number of one of the components (component p) is a dependent function of the other mole numbers such that

$$N_t = N_t(\{N_{k \neq p}\}). \quad (2.135)$$

The free energy can then be expressed as

$$G = G(\{N_{k \neq p}\}, N_t(\{N_{k \neq p}\})). \quad (2.136)$$

Furthermore, via substitution of this constraint into the free energy, a new form \hat{G} may be arrived at for the free energy which is equivalent to the original form but which has no explicit dependence upon N_t :

$$G = \hat{G}(\{N_{k \neq p}\}). \quad (2.137)$$

Throughout this derivation, hats on variables will similarly indicate their form with the substitution of equation (2.135) having already been made. By equating mole number derivatives of equations (2.136) and (2.137), the chemical potential $\hat{\mu}_k$ as determined based on \hat{G} is then related to the fundamental chemical potential μ_k based on G via

$$\hat{\mu}_k = \mu_k + \mu_t \left(\frac{\partial N_t}{\partial N_k} \right)_{\{N_{j \neq k, t}\}}, \quad (2.138)$$

where

$$\hat{\mu}_k \equiv \left(\frac{\partial \hat{G}}{\partial N_k} \right)_{\{N_{j \neq k}\}}. \quad (2.139)$$

As noted above, equation (2.135) will yield a corresponding constraint on the composition fractions:

$$\phi_t = \phi_t(\{\phi_{k \neq p}\}). \quad (2.140)$$

In general, as in the form given by equation (2.125), the composition fractions are a function of all the mole numbers such that

$$\phi_k = \phi_k(\{N_{k \neq p}\}). \quad (2.141)$$

However, as in the free energy applying equation (2.125) yields an alternate form that is not an explicit function of the dependent mole number:

$$\phi_k = \hat{\phi}_k(\{N_{k \neq p}\}). \quad (2.142)$$

Equation (2.125) may be rewritten in this form as

$$\hat{\phi}_k = \frac{r_k N_k}{\hat{r} \hat{N}}. \quad (2.143)$$

In terms of intensive free energy, the substituted form of chemical potential $\hat{\mu}_k$ may now be written as

$$\hat{\mu}_k = \hat{g} \left(\frac{\partial \hat{r}\hat{N}}{\partial N_k} \right)_{\{N_{j \neq k}\}} + rN \left(\frac{\partial \hat{g}}{\partial N_k} \right)_{\{N_{j \neq k}\}}, \quad (2.144)$$

which is comparable to equation (2.127) in the former development. Second derivatives of intensive free energy with respect to composition may then be show via the chain rule to be given by

$$\begin{aligned} & \left(1 - \hat{\phi}_k \frac{1}{r_k} \left(\frac{\partial \hat{r}\hat{N}}{\partial N_k} \right)_{\{N_{j \neq k}\}} \right) \left(\frac{\partial}{\partial \phi_l} \left(\frac{\partial \hat{g}}{\partial \phi_k} \right)_{\{\phi_{j \neq u}\}} \right)_{\{\phi_{j \neq l}\}} \\ & = \frac{1}{r_k} \left(\frac{\partial \hat{\mu}_k}{\partial \phi_l} \right)_{\{\phi_{j \neq l}\}} + \sum_{u \neq k}^{t-1} \hat{\phi}_u \frac{1}{r_k} \left(\frac{\partial \hat{r}\hat{N}}{\partial N_k} \right)_{\{N_{j \neq k}\}} \left(\frac{\partial}{\partial \phi_l} \left(\frac{\partial \hat{g}}{\partial \phi_u} \right)_{\{\phi_{j \neq u}\}} \right)_{\{\phi_{j \neq l}\}} \end{aligned} \quad (2.145)$$

Furthermore, in this case the gradient vector from equation (2.123) will exclude the derivative with respect to N_p . For a quaternary system, equation (2.145) yields the triad of simultaneous equations:

$$g_{11} - \frac{\hat{\phi}_2}{r_1 \left(1 - \hat{\phi}_1 \frac{1}{r_1} \left(\frac{\partial \hat{r}\hat{N}}{\partial N_1} \right)_{N_2} \right)} \left(\frac{\partial \hat{r}\hat{N}}{\partial N_1} \right)_{N_2} g_{12} = \frac{1}{\left(1 - \hat{\phi}_1 \frac{1}{r_1} \left(\frac{\partial \hat{r}\hat{N}}{\partial N_1} \right)_{N_2} \right)} \frac{1}{r_1} \left(\frac{\partial \hat{\mu}_1}{\partial \phi_1} \right)_{\phi_2}; \quad (2.146)$$

$$g_{22} - \frac{1}{\left(1 - \hat{\phi}_2 \frac{1}{r_2} \left(\frac{\partial \hat{r}\hat{N}}{\partial N_2} \right)_{N_1} \right)} \hat{\phi}_1 \frac{1}{r_2} \left(\frac{\partial \hat{r}\hat{N}}{\partial N_2} \right)_{N_1} g_{12} = \frac{1}{\left(1 - \hat{\phi}_2 \frac{1}{r_2} \left(\frac{\partial \hat{r}\hat{N}}{\partial N_2} \right)_{N_1} \right)} \frac{1}{r_2} \left(\frac{\partial \hat{\mu}_2}{\partial \phi_2} \right)_{\phi_1}; \quad (2.147)$$

and

$$g_{12} - \frac{1}{\left(1 - \hat{\phi}_1 \frac{1}{r_1} \left(\frac{\partial \hat{r}\hat{N}}{\partial N_1} \right)_{N_2} \right)} \sum_{u \neq k}^{t-1} \hat{\phi}_u \frac{1}{r_1} \left(\frac{\partial \hat{r}\hat{N}}{\partial N_1} \right)_{N_2} g_{22} = \frac{1}{\left(1 - \hat{\phi}_1 \frac{1}{r_1} \left(\frac{\partial \hat{r}\hat{N}}{\partial N_1} \right)_{N_2} \right)} \frac{1}{r_1} \left(\frac{\partial \hat{\mu}_1}{\partial \phi_2} \right)_{\phi_1}. \quad (2.148)$$

It is important to note that equation (2.138) must be applied in order to obtain equations in terms of standard chemical potentials.

2.3. Applications, Results, and Discussion

Numerical solution of the above models focuses on the base system of polyethylene oxide (PEO) in water. This provides an experimentally relevant model system for which hydrogen-bonding parameters are already available in the literature. Furthermore, it has previously been shown that predictions from the HBLF model provide excellent quantitative agreement with experiment for the pure binary water-PEO system¹³¹. All numerical results shown in the below sections are for PEO molecular weight 6×10^5 grams per mole, with lattice fluid and hydrogen bonding parameters for PEO and water taken from a recent study fitting these parameters to the water-PEO binary system¹³¹. Furthermore, for simplicity, all ions are taken to have a hydration coordination number of six.

2.3.1. Neutral polymer in aqueous salt solution

System definition

Consider a system of polyethylene and water containing a strong monovalent free salt. Water, PEO, cations, and anions will be considered components 1, 2, 3, and 4 respectively. Each molecule of water contains two association donors (the hydrogen atoms) and two association acceptors (free electron pairs on the oxygen atom), corresponding to $d_1^1 = 2$ and $a_1^1 = 2$, respectively. Each polymer chain contains one acceptor site (the oxygen atom) per monomer, so that to a_2^2 is equal to the degree of polymerization of the polymer (from a physical standpoint, it is debatable whether the correct number of acceptors per PEO oxygen is one or two, but one has been used successfully in the literature¹³¹). Each cation has some number of hydration sites which serve as association donors, with this number given by d_2^3 . Similarly each anion has a number of acceptor sites given by a_3^4 . These groups will form five types of association bonds: 1-1 (water-water); 1-2 (water-PEO); 1-3 (water-anion); 2-1 (cation-water); and 2-2 (cation-PEO). Associations between anions and cations are neglected on the basis that

a strong salt will be almost entirely dissociated. Finally, the ratio $s_1/s_2 = 1.3424$ based on a hard sphere model, and $\xi_{12} = 1.0472$ has been shown to provide a good fit with experimental data. All other Berthelot parameters will be taken to have a value of unity and all the other $\{s_k\}$ will be taken to have a value equaling that of water.

One density equation of state and five associating equations of state characterize the system's state. The electroneutrality constraint from equation (2.58) becomes

$$N_3 z_3 + N_4 z_4 = 0, \quad (2.149)$$

and the volume fractions are likewise constrained:

$$\frac{\phi_3}{r_3} z_3 + \frac{\phi_4}{r_4} z_4 = 0. \quad (2.150)$$

It then follows from section 2.2.3 that the spinodal condition is given by the determinant of a two-by-two matrix, and equations (2.146) through (2.148) may be applied to write the condition in terms of chemical potentials rather than free energies.

The above system is solved for the spinodal in the following way. The system of equations of state is first solved over a grid of temperature, polymer volume fraction, and anion volume fraction. The resulting data is then interpolated and numerically differentiated to yield necessary equation of state derivatives with respect to compositions. The locus of points satisfying the spinodal condition is then determined numerically. Further details of this approach, including Mathematica code, may be found in appendix A.3.1.

Results

As shown by Figure 9, predicted phase behavior is characterized by an LCST-type spinodal curve which at higher temperatures curves back over into a UCST type spinodal to form a closed immiscibility loop. With the addition of free salt, the LCST shifts either upward or downward in temperature, corresponding to salting-in or salting-out, depending on salt properties. This shift of the spinodal curve can also be understood

as corresponding to an isothermal ionic strength-triggered transition, as shown by Figure 10. Figure 10 is essentially a parallelogram-shaped cutout of the overall water-PEO-salt ternary phase diagram, as shown by Figure 11.

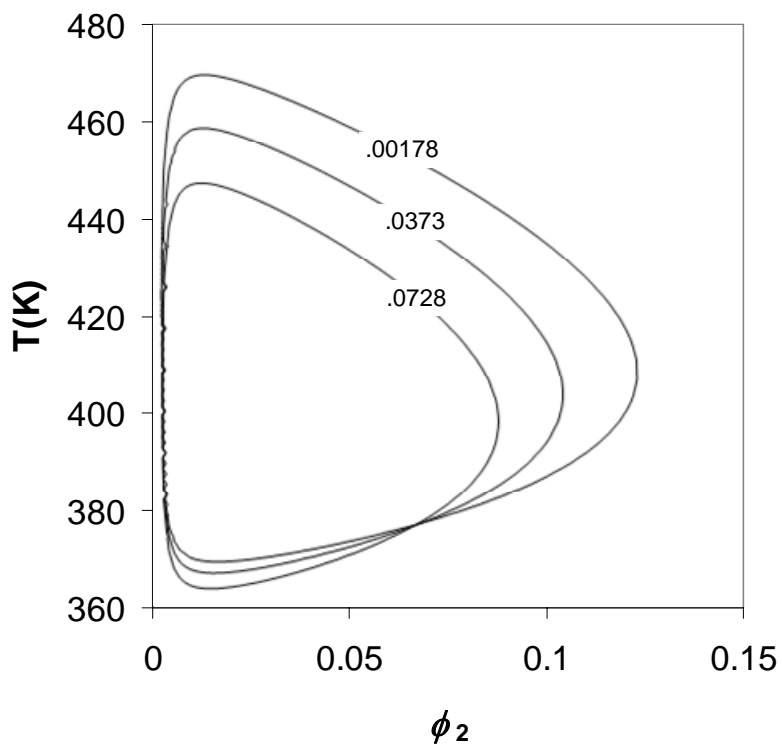


Figure 9: Spinodal curves for aqueous PEO in the presence of salt at various concentrations. Salt properties have been manually adjusted to approximate experimental results for the LCST of PEO with KI. Numbers on curves are salt occupied volume fraction corresponding to that curve. Note that the apparent meeting point of the three curves is not truly a single point upon closer inspection.

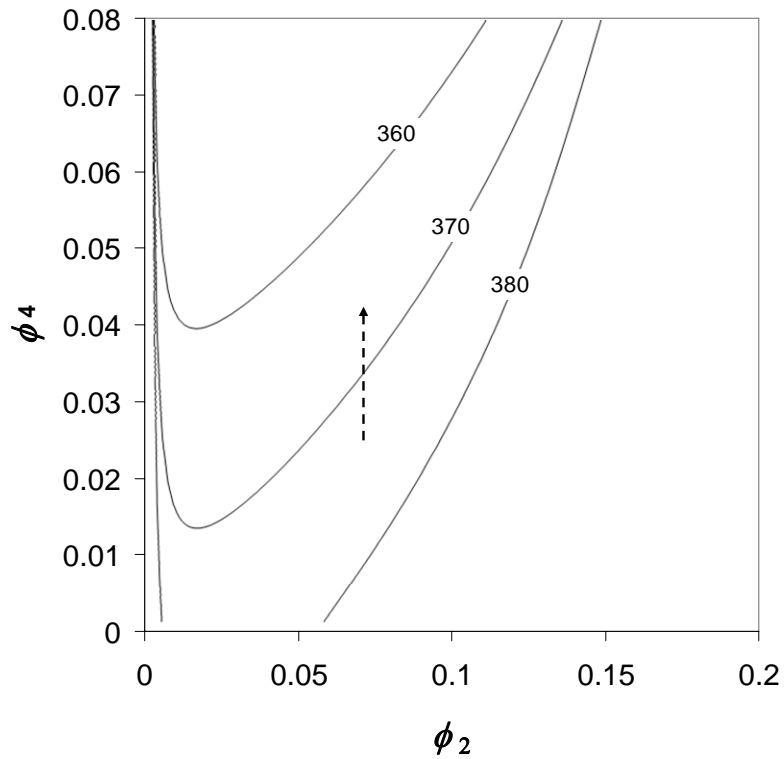


Figure 10: Cutout of isothermal ternary phase diagram for water-PEO-salt system, shown in Figure 11. Curves denote spinodals at indicated temperatures. The vertical axis corresponds to anion occupied volume fraction while the horizontal axis corresponds to polymer occupied volume fraction. Salt properties have been manually adjusted to approximate experimental results for the LCST of PEO with KBr. Numbers on curves denote the system temperature for that curve. Dashed line denotes an isothermal salt-induced LCST transition at 370 K.

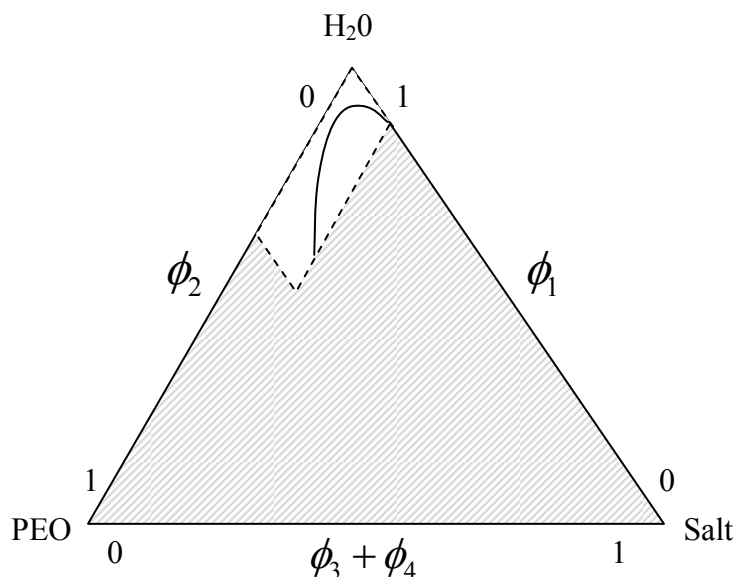


Figure 11: The ternary phase diagram for the present system. The white region corresponds to the region shown in Figure 10. Results have not been obtained for the grey region, and the present model would likely be inappropriate for treatment of the region corresponding to higher salt concentration due to breakdown of the Debye-Huckel model.

There are three mechanisms in this model by which the addition of salt alters solution stability, corresponding to electrostatic, physical and associating contributions. As suggested in the theory development, for these modest charge concentrations the electrostatic effect is quite small and plays little role in affecting stability. In contrast, the effect of salt physical interactions on phase stability is typically one of pronounced destabilization. For normal Berthelot parameters (near one) it is a good rule of thumb for the lattice fluid model that the addition of a third component is energetically unfavorable and tends to lead to destabilize a mixture.

The effect of salt associating interactions is somewhat more complicated and can consist of either stabilization or destabilization of the solution, depending on salt properties. As shown by Figure 12, the central associative interaction that compatibilizes the mixture is the PEO-water hydrogen bond. Cation-PEO and anion-water ion-dipole

interactions compete with this interaction and thus tend to destabilize the mixture. In contrast, the cation-water interaction competes only with the solution-destabilizing water-water hydrogen bond, thereby stabilizing the mixture. The balance of these effects determines the associating contribution to system stability: when cation-PEO and anion-water interactions dominate, they tend to destabilize the solution; when cation-water interactions dominate, it tends to stabilize the solution. The predicted salting-in effect can thus actually be understood as a ‘salting-out’ of water from water.

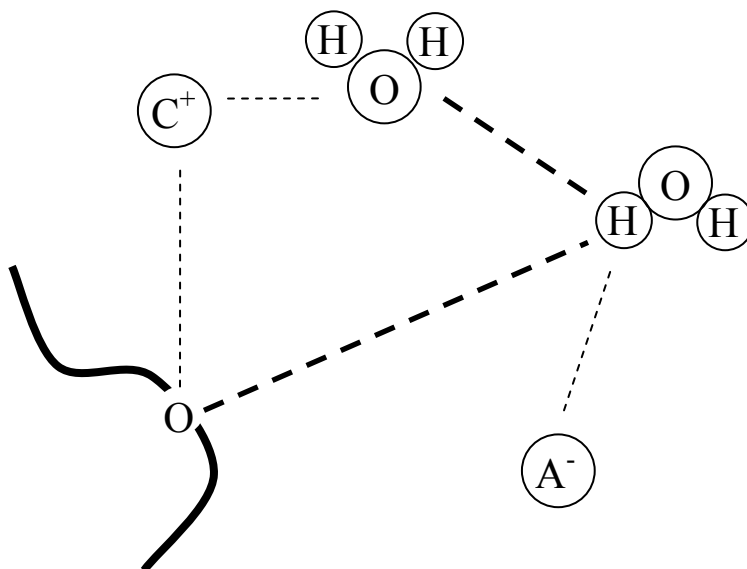


Figure 12: Schematic of possible associations in PEO-water-free salt system. Heavy dashed lined denote hydrogen bond types, which are present in the absence of free ions. Light dashed lines denote ion-dipole bond types. Bonds that share a locus compete with one another for use of that type of site. The heavy curve denotes a PEO chain, with a particular oxygen site note. C^+ and A^- denote free cation and anion, respectively.

The above physics permit the model to reproduce aspects of the lyotropic series of salts. By tuning the above balance of ion-binding interactions towards stabilization or destabilization, it is possible to obtain theoretical salts along a spectrum of salting in and salting out behavior. As shown in Figure 13 for aqueous PEO, the model is capable of at

least semi-quantitative matches with experiment for a variety of salts. Note that since experimental data in this figure is from cloud-point experiments and predictions are for the LCST, an exact quantitative match is not expected. Furthermore, predicted curves are produced by a manual ‘best-fit’ of salt parameters, and numerically optimized best fits presently underway are expected to yield improved agreement. However, interaction parameters for each ion are allowed to differ depending on their counterion; an important future test of the model will be whether a fit comparable to that shown in Figure 13 is possible while using consistent ion parameters for each system.

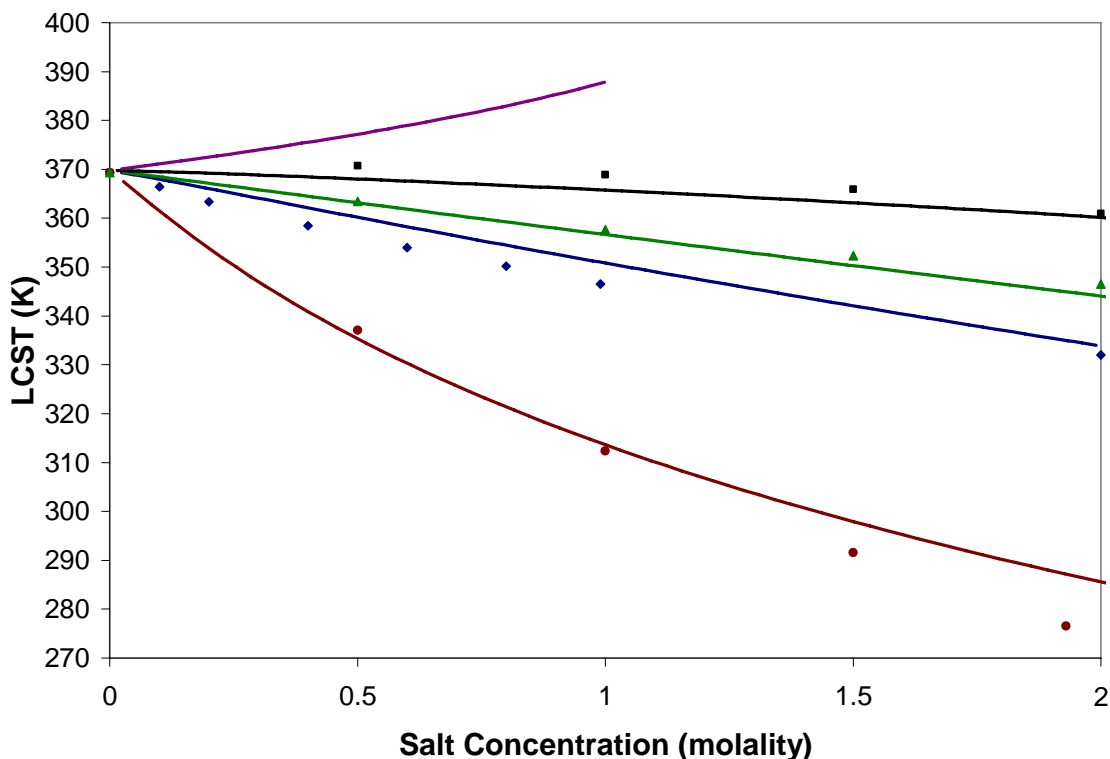


Figure 13: Experimental cloud points⁸⁰ (points) and manual LCST fits (curves) based on the above theory, for aqueous PEO as a function of salt concentration for various salts. Black curve and points correspond to the LCST in the presence of KI, green to KBr, blue to NaCl, and red to KF. The purple line demonstrates a typical salting-in case as predicted by this model for a hypothetical salt characterized by a strong favorable cation-water hydration interaction and weak anion-water and cation-polymer interactions.

As expected, due to the neglect of ternary interactions, the present model does not capture the more extreme lyotropic behavior that is characterized by pronounced salting-in at low salt concentrations followed by salting out at higher. Furthermore, it is not clear that the model is consistent with the observation that salt's anion controls its behavior. Despite these expected shortcomings, it is notable that the model is able to reproduce much of the range of the lyotropic series with binary interactions only. This result bolsters the contention, for example by Park and Hoffman⁸¹, that binary ion-dipole interactions play a significant role in the Lyotropic series. Furthermore, a framework for extension of the present model to incorporate ternary hydration interactions has been described in section 2.2.2, and such an extension would be expected to address these shortcomings.

2.3.2. Polyelectrolyte

System definition

In order to study a polyelectrolytic system, the above PEO-water-salt system is modified by replacing the hydrogen bonding site on a small fraction f_i of PEO monomers with a negatively charged group. The counterion of this charged group is taken to be the same species as the cation of the free salt. As described in the theory section above, this system requires more complex variable sets and indexing conventions than the neutral polymer case. Furthermore, polyelectrolytes of the low charge density sort addressed here are in reality copolymers of charged and uncharged monomers of different types. However, for low polymer charge fractions the effect of differences in the van der Waals interactions of the substituted monomers should be small enough to be neglected, as they are here. Finally, in order to establish the basic behavior of this model with the minimum number of interaction parameters, interactions involving ion pairs will be neglected (i.e. d_i^{lu} and a_j^{lu} will be treated as zero for all ion pairs).

For this model, PEO, water, cations, and anions will be considered components 1, 2, 3, and 4 respectively (note the reversal of PEO and water with respect to the above

system). Each chain of PEO will contain a number of anionic groups A_1^1 equal to f_I times the degree of polymerization of the chain. Each such anionic group will have a_1^A hydration sites that function as association acceptors. The polymer chain will furthermore contain a_4^1 acceptor sites (oxygen atoms) equal to $1 - f_I$ times the degree of polymerization. Each free anion molecule will correspond to one anion group, such that $A_2^A = 1$. Each group will present a_2^A hydration sites that serve as association acceptors. Similarly, each free cation molecule will correspond to one cation group, such that $C_1^C = 1$, and each such group will present d_1^C association donors. Finally, as in the prior model each water molecule will contain two donors and two acceptors, such that $d_2^2 = 2$ and $a_3^2 = 2$. The ionic groups will form one type of ion bond: 1-1, which corresponds to a polyelectrolyte-cation bond. The associating groups will form six types of association bonds: 1-3 (cation-water); 1-4 (cation-PEO oxygen); 2-1 (water-polyelectrolyte anion); 2-2 (water-free anion); 2-3 (water-water); and 2-4 (water-PEO oxygen). Values of s_k and the Berthelot parameters shall be as in the neutral PEO model.

In this case, one density equation of state and six hydrogen bonding equations of state characterize the system's state. The electroneutrality constraint from equation (2.75) becomes

$$\frac{\phi_3}{r_3} C_1^3 z_1^C + \frac{\phi_1}{r_1} A_1^1 z_1^A + \frac{\phi_4}{r_4} A_2^A z_2^A = 0 \quad (2.151)$$

As in the neutral polymer case, the spinodal condition is given by the determinant of a two-by-two matrix, and the necessary relations to write this condition in terms of chemical potentials are given by equations (2.146) through (2.148). Numerical solution methodology for this system is essentially the same as that for the neutral polymer case, albeit with the necessary alterations to parameter and variable definitions.

Finally, for any particular combination of associating and ion-binding parameters, the polymer dissociable groups may be characterized by a pC which is the negative base

ten logarithm of the counterion concentration and is the same as pH when the counterion is hydrogen.

For simplicity, the salt used in generating the below results has lattice fluid parameters based upon NaCl, and all ion-dipole interactions are taken to have energies of formation E_{ij}^0 equal to about two thirds that for the water-water hydrogen bond while entropies of ion-dipole bond formation S_{ij}^0 are taken to be about the same as that for water-water hydrogen bond formation.

Results

The addition of charges to the polymer chain stabilizes the system, increasing the LCST temperature, as shown by Figure 14 for polymers with up to 1% substitution of electrolytic groups. The electrostatic interactions are calculated to play only a small role in such cases, and stabilization is instead driven by enhanced chain hydration. This is consistent with the scaling observation made in the above theoretical development to the effect that the electrostatic term in the free energy is quite small relative to other contributions at small to modest charge concentrations.

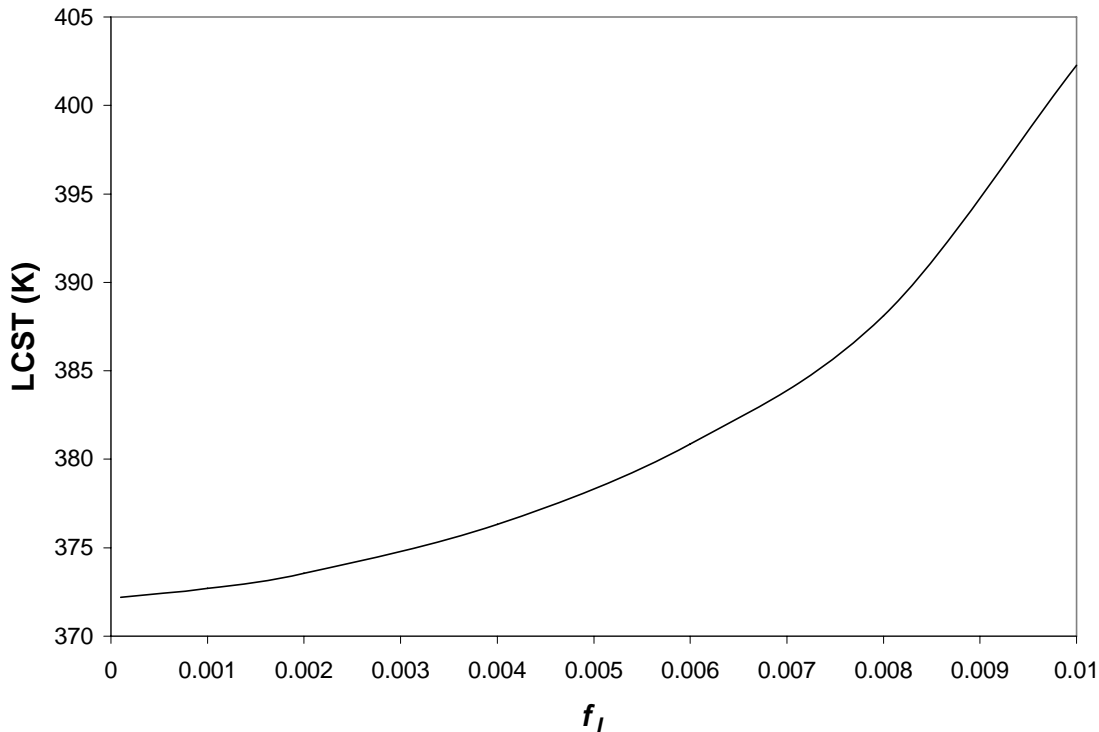


Figure 14: Effect of fraction of electrolytic monomers on PEO LCST, for monomers with a very low pK_0 corresponding to a strong electrolyte, in 0.05 molar aqueous salt solution. The properties of the salt do not correspond exactly to any real salt but fall within the range of lyotropic salting-out behavior.

The addition of free salt to the solution counters this effect, destabilizing the solution and lowering the LCST. Two mechanisms drive this trend. The first is ionic bonding of counterions to the polymer charged groups, which reduces the ionization fraction of the polymer. Figure 15 demonstrates this mechanism for a PEO chain with 1% of its monomers replaced with dissociable ionic groups. As the pK_0 of the dissociable groups is increased through the solution pC at fixed salt concentration, there is a steplike reduction in LCST temperature that is driven by the reduction in unbound ions on the polymer. Note that for high pK_0 the solution is destabilized with respect to the neutral solution, in qualitative agreement with experimental results.

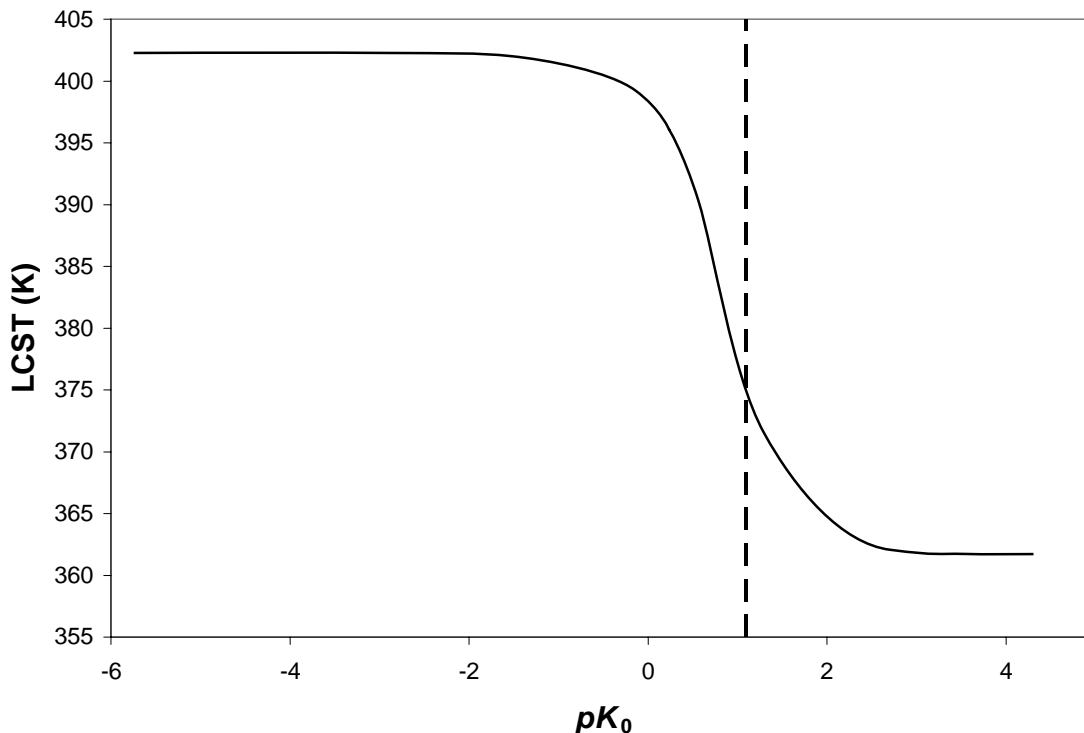


Figure 15: LCST of aqueous PEO with electrolytic subunits substituted for 0.1% of its monomers, as a function of the pK_0 of the electrolyte subunits. The vertical dashed line indicates the pC of the solution (the negative base ten logarithm of the counterion concentration) in solution. The free ions do not correspond to any real salt, but are hypothetical ions constructed to fall into the typical range of salting out behavior described above.

In the present results, the drop in LCST with bonding of counterions at high pK_0 results simply from the reduction in potential hydration sites on the chain. Because ternary interactions between ion pairs and dipoles are not considered, these sites effectively ‘disappear’ upon ion binding. At the molecular level, this mechanism differs from that proposed for experimental systems, namely, favorable interactions between bound ion pairs on the chain with each other and with other sites on the chain. However, at a thermodynamic level the two mechanisms are comparable: as ion pairs form,

favorable interactions with water become dominated by favorable self-interactions, and the system is destabilized.

A second mechanism for reversal of the polyelectrolyte stabilization effect is that of lyotropic salting out, discussed in section 1.3.1 and for the neutral chain model in section 2.3.1. This effect is not strictly related to the charges on the chain; rather it represents a ‘swamping out’ of the polyelectrolyte stabilization by lyotropic destabilization. In other words, whereas the addition of charges to the chain enhances hydration by adding ion hydration sites, the lyotropic effect in this model diminishes hydration by occupying hydrogen-bonding hydration sites. This effect can be isolated from the counterion effect for charged PEO chains with a very low pK_0 , as such chains do not become significantly de-ionized as the free charge concentration increases. Results for such a system can be seen in Figure 16. Despite the unaltered presence of charges on the chain, there is a pronounced salting out with increased system charge that is comparable to that demonstrated for neutral chains in section 2.3.1.

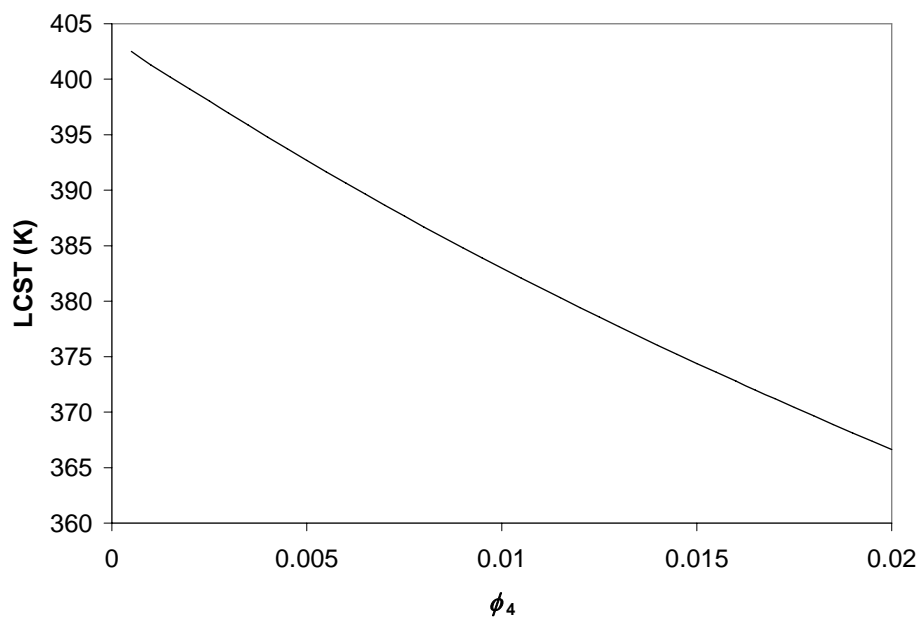


Figure 16: LCST of PEO with strong electrolytic subunits substituted for 0.1% of its monomers, as a function of anion volume fraction. The equivalent range of salt molarity is zero to about 0.7.

2.4. Conclusions

The LCST transition of uncharged aqueous polymers in the presence of salt is shown to be amenable to a two part approach that combines a mean field lattice fluid model with a combinatorial method for strong pair interactions. This approach is an extension of the earlier hydrogen bonding lattice fluid model¹²⁸, and its key addition is the treatment of ion-dipole interactions in the same manner as hydrogen bonding. A competition results between ion hydration and hydrogen bonding hydration, through which salting-in and salting-out effects emerge. Solution destabilization results from dominance of ion dipole-interactions that are in competition with water-polymer hydrogen bonding. Conversely, stabilization emerges from dominance of ion-dipole interactions that compete with water-water hydrogen bonding.

Via manual tuning of ion-dipole interaction parameters, this model is shown to produce results in semi-quantitative agreement with experimental cloud point data for PEO in various salts. Results preliminarily suggest that it is possible to reproduce important experimental aspects of the lyotropic series by considering only binary interactions. However, further work is necessary in order to demonstrate that this result is possible while retaining identical parameters for each ion in differing systems. Furthermore, the apparent inability of this binary-only approach to reproduce more extreme lyotropic behavior, characterized by both salting in and salting out at different salt concentrations, bolsters that argument that ternary or higher interactions are central in producing the full lyotropic series. By explicitly incorporating such ternary interactions into this model, it seems probable a more complete theory for lyotropic behavior could be produced. A method of doing so is offered as part of the development of a model for polyelectrolytes. Application of this extended approach to the lyotropic series would likely be a fruitful avenue of future research. Beyond potentially offering a quantitative model for the lyotropic series, it could help resolve the question of whether salt effects on hydrophobic hydration or hydrogen-bonding hydration are dominant in modulating solution stability.

An extension of this model is employed in order to model lightly charged polyelectrolytes. In addition to the combinatorial approach to hydrogen bonding and ion-dipole interactions, a second, parallel combinatorial network is established to treat ionic bonding. The model predicts that addition of charges to a chain stabilizes the solution (raises the LCST) as a result of enhanced chain hydration, consistent with qualitative experimental observation. It further predicts that there is a step-like reduction in the LCST as the polyelectrolyte pK_0 becomes greater than the pH of the solution, in qualitative agreement with experiment.

In both of the above models, future work should include optimization of charge interaction parameters with respect to various experimental results. Ideally, experimental properties such as heats of mixing and ion dissociation constants could be used to avoid fitting directly to phase behavior. Such an approach would broaden the number of systems for which parameters could be rapidly obtained and would establish a greater predictive (rather than merely interpolative) capacity of the model.

Chapter 3. Single Chain Conformational Behavior

In highly dilute solution, the analogue of the thermally induced phase separation addressed above is expected to be a thermally induced chain collapse. This mechanism is believed to drive the functionality of many biopolymers⁶⁶ and is relevant to the design of synthetic polymer systems in a variety of applications. However, prior to this work no model was available in the literature with a broad ability to semi-quantitatively predict this transition.

In addition to the physics present in models for the lower critical solution temperature (LCST) transition, the treatment of the single chain conformation mainly requires the addition of intrachain excluded volume interactions. From a statistical thermodynamic standpoint, this amounts to counting the number of non-self intersecting chain conformations rather than simply all conformations. As demonstrated by a successful model²⁷ for the coil-globule transition (CGT) that is associated with the upper critical solution temperature (UCST), the Widom insertion parameter approach to the chemical potential provides a far simpler calculation of this quantity than that possible by calculation of the system partition function. The present work follows this approach within both lattice fluid and scaled particle theory frameworks. The lattice fluid approach offers the advantage of greater simplicity. However, unpublished results by Sanchez¹³² suggest that pure component parameters for the SPT model have a much closer link to component molecular characteristics, offering a stronger link to underlying physics and potentially greater predictive power.

3.1. Theory

3.1.1. General model

Consider a polymer-solvent system at infinite dilution. In such a system, the polymer chains do not interact, and each will independently pervade a volume characterized by a gyration radius R . Within this domain the polymer chain will occupy a volume fraction η_p , which scales as

$$\eta_p \sim \frac{r_p \sigma^3}{R^3}, \quad (3.1)$$

where r_p is a measure of chain length and σ^3 is a measure of chain occupied volume per length. Furthermore, within the pervaded volume N_s solvent molecules will occupy volume fraction η_s . Accounting for vacant space, the total occupied volume fraction within this domain, given by $\tilde{\rho} = \eta_p + \eta_s$, will in general be less than one. At any given thermodynamic state, two equilibrium conditions will describe the chain and its immediate surroundings. The first is an equilibrium condition on the gyration radius or occupied volume fraction of the chain. The second is an equilibrium condition on the occupied volume fraction of the solvent within the pervaded volume

The equilibrium gyration radius corresponds to the mean value of the partition function with respect to R . In the thermodynamic limit such a condition is typically determined by simply finding the minimum of the free energy (or maximum of the partition function) with respect to the variable of interest. However, the partition function Q of an ideal chain is known to be skewed with respect to gyration radius. On this basis the equilibrium chain gyration radius for the above system is given in terms of free energy G by the Hermans-Overbeek approximation²⁷:

$$\left(\frac{\partial (\ln R + \beta G / N_p)}{\partial R} \right)_{T, P, N_s, \{v_j\}} = 0, \quad (3.2)$$

where N_p is the number of such isolated polymer chains in the system.

The second equilibrium condition is that the solvent occupied volume fraction must satisfy equality of chemical potential with respect to the bulk solvent:

$$\mu_s = \mu_s^B, \quad (3.3)$$

where μ_s is the chemical potential of the solvent in the pervaded volume and μ_s^B is the chemical potential of the solvent in the bulk. This constraint may be used to simplify the minimization in equation (3.2), as follows.

The system free energy may be written in terms of chemical potentials as

$$G = N_p \mu_p + N_p N_s (\mu_s - \mu_s^B) + N_s^T \mu_s^B, \quad (3.4)$$

where μ_p is the polymer chemical potential, N_p is the total number of polymer chains in the system, and N_s^T is the total number of solvent molecules in the system. Since the system is at infinite dilution, μ_s^B must be constant with respect to all properties of the chain and thus equation (3.2) reduces to

$$\frac{1}{R} + \beta \left(\frac{\partial \mu_p}{\partial R} \right)_{T,P,\eta_s} = 0. \quad (3.5)$$

The polymer chemical potential may be calculated via the calculated via the Widom insertion parameter:

$$\beta \mu_p = \ln \left(\frac{\rho_p \lambda^3}{\mathbf{B}_p P_0(R)} \right), \quad (3.6)$$

where ρ_p is the number density of polymer in the entire system volume and λ is the thermal wavelength, both of which are constant with respect to chain gyration radius and may be neglected for the purposes of this model. $P_0(R)$ is the ideal chain gyration radius distribution function and \mathbf{B}_p is the insertion parameter for the polymer chain. The ideal chain gyration radius is well approximated by the modified Flory-Fisk distribution:

$$P_0(R) dR \sim R^6 \exp\left(-\frac{7}{2} \frac{a}{r_p^{1/3} \eta_p^{2/3}}\right), \quad (3.7)$$

where r_p is a measure of chain length.

It follows from equations (3.5) and (3.6) that the condition for the equilibrium chain gyration radius is

$$\frac{1}{R} - \beta \left(\frac{\partial \ln(\mathbf{B}_p P_0(R) dR)}{\partial R} \right)_{T,P,\eta_s} = 0. \quad (3.8)$$

Since the CGT is defined as the point at which the chain is in its ideal state, the contributions to equation (3.8) that apply to the ideal state are zero at the CGT by definition. This leaves simply

$$-\left(\frac{\partial \ln \mathbf{B}_p |_{\alpha=1}}{\partial R} \right)_{T,P,\eta_s} = 0 \quad (3.9)$$

as the condition for the CGT, where α^2 is known as the expansion factor and is a dimensionless square gyration radius defined with respect to the ideal chain state:

$$\alpha^2 \equiv R^2 / \langle R^2 \rangle_0, \quad (3.10)$$

where $\langle R^2 \rangle_0$ is the mean square gyration radius of an ideal chain. For such a chain, $\langle R^2 \rangle_0 \sim r_p \sigma^2$, and combining equations (3.10) and (3.1) yields a relationship between the expansion factor and polymer occupied volume fraction within the pervaded volume:

$$\alpha^2 = \frac{a}{r_p^{1/3} \eta_p^{2/3}}, \quad (3.11)$$

where a is some dimensionless constant. Most importantly, by definition of the CGT,

$$\alpha^2 = \begin{cases} \ll 1 & \text{collapsed globule} \\ 1 & \text{CGT (ideal coil)} \\ \gg 1 & \text{expanded coil} \end{cases}. \quad (3.12)$$

Thus at the CGT itself,

$$\eta_p = \frac{a^{3/2}}{r_p^{1/2}}. \quad (3.13)$$

It is important to note that the chain occupied volume fraction is thus zero in the limit of an infinite chain at the CGT.

The insertion parameter, required by equations (3.8) and (3.9), is given by

$$\mathbf{B}_k = \mathbf{P}_k \exp[-\beta\langle\psi_k\rangle], \quad (3.14)$$

where \mathbf{P}_k is the hard-core insertion probability of a molecule of species k and $\langle\psi_k\rangle$ is the average interaction energy of the molecule upon insertion. In general, the hard core insertion probability of the chain may be related to the insertion probability $\mathbf{P}_{p,j}$ of a chain subunit by taking the product of $\mathbf{P}_{p,j}$ over all subunits, accounting for the increasing occupied volume fraction as the chain is inserted:

$$\mathbf{P}_p = \prod_{j=0}^{r_p-1} \mathbf{P}_{p,j}, \quad (3.15)$$

where r_p is the number of subunits and where short range chain correlations have been neglected.

Up until this point, no particular model for the chain or fluid have been required. Furthermore, no explicit definition has been provided for “the number of chain subunits”. Thus, two alternate models for the mixture will be applied in order to obtain $\mathbf{P}_{p,j}$ and $\langle\psi_p\rangle$, as well as the bulk solvent properties. These models will also provide explicit definitions for the number of chain subunits. The first model is the lattice fluid model, and the second is a scaled particle model.

3.1.2. Lattice model

Within a lattice-fluid framework, each molecule of species k occupies r_k lattice sites, each of volume v^* . In these variables the polymer occupied volume fraction is related to the gyration radius by

$$\eta_p = \frac{r_p v^*}{R^3}. \quad (3.16)$$

Furthermore, $\mathbf{P}_{p,j}$ is simply the fraction of unoccupied sites:

$$\mathbf{P}_{p,j} = 1 - \eta_s - \frac{j}{r_p} \eta_p, \quad (3.17)$$

where j is the number of previously inserted chain subunits. Adjacent sites occupied by molecules of species i and j interact with a characteristic energy of ε_{ij} . Simply by summing over the average number of interactions per site, the chain interaction energy is then given by

$$\begin{aligned} \langle \psi_p \rangle &= -z \left(r_p \varepsilon_{sp} \eta_s + \sum_{j=1}^{r_p-1} \frac{j}{r_p} \varepsilon_{pp} \eta_p \right), \\ &= -r_p \left(2\varepsilon_{sp}^* \eta_s + \varepsilon_{pp}^* \eta_p \right) \end{aligned} \quad (3.18)$$

where

$$\varepsilon_{ij}^* = \frac{z \varepsilon_{ij}}{2} \quad (3.19)$$

is a characteristic interaction energy between species i and species j and where z is the coordination number of the lattice. Substitution of the insertion probability and energy above into equation (3.14) yields

$$\mathbf{B}_p = e^{-r_p} \frac{(1-\eta_s)^{\frac{1-\eta_s r_p}{\eta_p}}}{(1-\eta_s - \eta_p)^{\frac{1-\eta_s - \eta_p r_p}{\eta_p}}} \exp \left[\beta r_p \left(\varepsilon_{pp}^* \eta_p + 2\varepsilon_{sp}^* \eta_s \right) \right]. \quad (3.20)$$

Equation (3.6) then yields the polymer chemical potential:

$$\beta \mu_p = r_p \left[\begin{aligned} &1 + \frac{1-\eta_s}{\eta_p} \ln \left(1 - \frac{\eta_p}{1-\eta_s} \right) - \ln(1-\eta_s - \eta_p) \\ &- \beta \left(\varepsilon_{pp}^* \eta_p + 2\varepsilon_{sp}^* \eta_s \right) - \frac{2}{r_p} \ln \left(\frac{r_p v^*}{\eta_p} \right) + \frac{7}{2} \frac{a}{r_p^{4/3} \eta_p^{2/3}} \end{aligned} \right]. \quad (3.21)$$

The equilibrium gyration radius may now be obtained from equation (3.8):

$$\frac{7}{3} (\alpha^2 - 1) = -r_p \left\{ \beta \varepsilon_{pp}^* \eta_p + [\ln(1-\varphi) + \varphi] / \varphi \right\}, \quad (3.22)$$

where

$$\varphi \equiv \frac{\eta_p}{1-\eta_s} < 1. \quad (3.23)$$

As noted above, η_s is determined by equating solvent chemical potential in the pervaded volume and the bulk. The solvent chemical potentials are obtained in a similar fashion to that of the polymer, through the insertion parameter, albeit without an ideal chain gyration radius contribution. Within the pervaded volume, the insertion parameter for the solvent is given by

$$\mathbf{B}_s = (1-\eta_p - \eta_s)^{r_s} \exp\left[\beta r_s (\varepsilon_{ss}^* \eta_s + 2\varepsilon_{sp}^* \eta_p)\right]. \quad (3.24)$$

In the bulk, it is given by

$$\mathbf{B}_s^B = (1-\eta_s^B)^{r_s} \exp\left[\beta r_s \varepsilon_{ss}^* \eta_s^B\right]. \quad (3.25)$$

where η_s^B is the bulk solvent density. Equations (3.24) and (3.25) yield the chemical potential equality constraint on the solvent density in the pervaded volume:

$$\eta_s = \tilde{\rho}^B \left(\frac{1-\eta_p - \eta_s}{1-\eta_s^B}\right)^{r_s} \exp\left[\beta r_s (\varepsilon_{ss}^* (\eta_s - \eta_s^B) + 2\varepsilon_{sp}^* \eta_p)\right]. \quad (3.26)$$

At the CGT itself, equation (3.22) is simplified in accordance with equation (3.9) to yield the condition for the CGT:

$$\frac{\varepsilon_{pp}^*}{k\Theta} \eta_{p,0} + [\ln(1-\varphi_0) + \varphi_0] / \varphi_0 = 0, \quad (3.27)$$

where ‘0’ subscripts denote values at the CGT, where $\langle \alpha^2 \rangle = 1$. Also, it has been previously shown²⁷ that for this model $a = (19/27)^{1/3}$, which is needed to determine $\eta_{p,0}$ via equation (3.13) at the CGT. Expanding the logarithmic term in equation (3.27) gives

$$\frac{T_p^*}{\Theta} \eta_{p,0} - \left[\frac{\varphi_0}{2} + \frac{\varphi_0^2}{3} + \dots\right] = \eta_p \left[\frac{T_p^*}{\Theta} - \frac{1}{2(1-\eta_s)} - \frac{\eta_{p,0}}{3(1-\eta_s)^2} - \dots\right] = 0, \quad (3.28)$$

where $T_p^* = \varepsilon_{pp}^*/k$ is a characteristic temperature of the polymer and Θ is the CGT temperature. In the limit of infinite molecular weight, $r \rightarrow \infty$, $\langle \phi \rangle_0 \rightarrow 0$, $\tilde{\rho} \rightarrow \tilde{\rho}^B$, and from eq. (3.28), the coil-globule transition temperature is given by the simple equation:

$$\Theta = 2T_p^* \left[1 - \eta_s^B(\Theta) \right]. \quad (3.29)$$

The first order correction $\delta\Theta$ to this transition temperature for a chain of finite length is obtained from eq. (3.28) and yields

$$\frac{|\delta\Theta|}{T_p^*} = \frac{4}{3} \phi_0 \sim r^{-1/2}, \quad (3.30)$$

where $\delta\Theta = \Theta(r) - \Theta(\infty)$. Furthermore, in the infinite chain length limit the polymer volume fraction goes to zero within the pervaded volume. This follows from the fact that at the coil-globule transition the chain is in its ideal state and the gyration radius scales as $R \sim r_p^{1/2}$, and thus $\eta_p \sim r_p^{-1/2}$, which goes to zero as chain length goes to infinity. Thus the solvent in the pervaded volume is effectively in its pure state and equation (3.26) for solvent chemical potential equality reduces to equality of solvent density in the pervaded volume and the bulk.

For the bulk solvent, the most self-consistent approach would be to use an equation of state derived based on the solvent insertion parameter above. However, this is not strictly necessary – all that is required is a relation for solvent density as a function of temperature and pressure. The Sanchez-Lacombe (S-L) equation of state is based up on the same general physical approach as the present one, albeit via the overall partition function as opposed to the Widom Insertion Parameter as described in the introduction. Furthermore, parameters for the S-L model are tabulated for a wide variety of common polymers and solvents. Therefore the S-L EOS will be used to obtain the density of the bulk solvent. This is given by

$$\left(\tilde{\rho}^B \right)^2 + \tilde{P}_s + \tilde{T}_s \left[\ln(1 - \tilde{\rho}^B) + (1 - 1/r_s) \tilde{\rho}^B \right] = 0, \quad (3.31)$$

where \tilde{T} and \tilde{P} are the solvent reduced temperature and pressure T/T_s^* and P/P_s^* . The appropriate equation of state parameters (T_s^* , P_s^* , r_s) for many solvents have been tabulated¹⁵. The reduced solvent density $\tilde{\rho}^B$ is also related to equation of state parameters by $\tilde{\rho}^B = \rho / \rho^*$ with $\rho^* = (M / r_s) P_s^* / kT_s^*$.

By combining equation (3.29) for the CGT and equation (3.31) for bulk solvent density, it is possible to obtain an equation directly relating the temperature and pressure of the CGT:

$$-\tilde{P}_s = (1 - \tilde{\Theta})^2 + 2\zeta\tilde{\Theta} \left[\ln \tilde{\Theta} + (1 - 1/r_s)(1 - \tilde{\Theta}) \right], \quad (3.32)$$

where $\tilde{\Theta} \equiv \Theta / 2T_p^*$ and the parameter $\zeta \equiv T_p^* / T_s^*$ is the ratio of characteristic temperatures of the polymer and solvent and characterizes the relative strength of their self-interactions. Alternatively, for the case of a finite chain, a numerical result for the P - T behavior of the CGT may be obtained via simultaneous solution of equations (3.26), (3.27), and (3.31). An additional value of interest is the slope of the P - T curve at zero pressure. From equation (3.32), the slope $\partial\Theta / \partial P|_{P=0}$ of the CGT for an infinite chain is given by

$$\left. \frac{\partial\Theta}{\partial P} \right|_{P=0} = \frac{T_p^*}{2P_s^*} \left\{ 1 + \tilde{\Theta}_0 \left[2\zeta \left(1 - \frac{1}{r_s} \right) - 1 \right] - \zeta \left(2 - \frac{1}{r_s} + \ln \tilde{\Theta}_0 \right) \right\}^{-1}, \quad (3.33)$$

where $\tilde{\Theta}_0 = \tilde{\Theta}|_{P=0}$. Obtaining a numerical result for equation (3.33) requires solving equation (3.32) for temperature at zero pressure and substituting the result into equation (3.33). For a finite chain $\partial\Theta / \partial P|_{P=0}$ may be obtained numerical via simultaneous solution of equations (3.26), (3.27), and (3.31) followed by numerical determination of the slope at $P = 0$. An equation for the temperature of P_{max} of an infinite chain can be established through a similar approach. From equation (3.32), this maximum must satisfy the condition

$$\frac{\partial \tilde{P}_s}{\partial \tilde{\Theta}} = 0 = 2 \left\{ 1 + \tilde{\Theta} \left[2\zeta \left(1 - \frac{1}{r_s} \right) - 1 \right] - \zeta \left[2 - \frac{1}{r_s} + \ln \tilde{\Theta} \right] \right\}. \quad (3.34)$$

3.1.3. Scaled particle theory

Consider the more general case in which the system may, in addition to the polymer chain of interest, contain multiple solvent species. Let molecules of each species k in such a solution be represented by a hard sphere or chain of r_k hard spheres, each of diameter σ_k . The volume fraction η_k occupied by a species k is then given by

$$\eta_k = \frac{\pi r_k N_k \sigma_k^3}{6V}. \quad (3.35)$$

It follows that the total occupied volume fraction is

$$\tilde{\rho} = \sum_k \eta_k = \frac{\pi \sum_k r_k N_k \sigma_k^3}{6V}. \quad (3.36)$$

In the general case of multiple solvent species, this can be separated into two contributions, one accounting only for the polymer chain and the other accounting for all solvent species:

$$\tilde{\rho} = \eta_p + \eta_s, \quad (3.37)$$

where the solvent occupied volume fraction is

$$\eta_s = \frac{\pi \sum_{k \neq p} r_k N_k \sigma_k^3}{6V} = \sum_{k \neq p} \eta_k, \quad (3.38)$$

and the polymer occupied volume fraction is

$$\eta_p = \frac{\pi r_p N_p \sigma_p^3}{6V}. \quad (3.39)$$

Once the entire chain is inserted, it will occupy a volume fraction within the pervaded volume of

$$\eta_p = \frac{r_p \sigma_p^3}{8R^3}. \quad (3.40)$$

Upon insertion of the j th monomer the polymer occupied volume fraction will be

$$\eta_{p,j} = \eta_p \frac{j}{r_p}, \quad (3.41)$$

which is of the same form as that for the lattice model. It follows that the total occupied volume fraction upon insertion of the j th monomer will be

$$\tilde{\rho}_j = \eta_p \frac{j}{r_p} + \eta_s. \quad (3.42)$$

For the purpose of calculating the insertion probability of any one hard sphere into such a solution, the connectivity of the hard spheres constituting the solution may be neglected. The insertion probability of a single such sphere has then been shown to be^{132, 133.}

$$-\ln \mathbf{P}_{k,1} = \ln(1+y) + y \left[\frac{(3\sigma_{-1}\sigma_k + 3\sigma_{-2}\sigma_k^2 + \sigma_{-3}\sigma_k^3)}{+(9\sigma_{-1}^2\sigma_k^2/2 + 3\sigma_{-1}\sigma_{-2}\sigma_k^3)y + 3\sigma_{-1}^3\sigma_k^3y^2} \right], \quad (3.43)$$

where $y = \tilde{\rho}/(1-\tilde{\rho})$, and where

$$\sigma_{-l} \equiv \sum_i \frac{\eta_i}{\tilde{\rho}} \sigma_i^{-l}. \quad (3.44)$$

Equation (3.43) may then be cast in a form that is explicitly dependent upon j and combined with equation (3.15) to yield the insertion probability for the entire chain (see appendix A.2.2 for more details).

The interaction energy of a sphere of type i with surrounding spheres of type j is given by¹³²

$$\begin{aligned} \psi_{ij} &= -4\pi\epsilon_{ij}\rho_j \int_{\sigma_{ij}}^{\infty} x^2 \left(\frac{\sigma_{ij}}{x} \right)^6 dx, \\ &= -2\epsilon_{ij}^* \eta_j \end{aligned} \quad (3.45)$$

where

$$\varepsilon_{ij}^* \equiv \frac{2\pi}{3} \left(\frac{\sigma_{ij}}{\sigma_{jj}} \right)^3 \varepsilon_{ij}. \quad (3.46)$$

Equation (3.45) is of the same form as that for the lattice fluid model. Thus the average insertion energy of the chain is of the same form as that for the lattice fluid model:

$$-\beta \langle \psi_p \rangle = \beta r_p \left(\varepsilon_{pp}^* \eta_p + \sum_{i \neq p} \varepsilon_{ip}^* \eta_i \right), \quad (3.47)$$

noting that equation (3.46) rather than (3.19) now applies and the Berthelot rule thus gives

$$\varepsilon_{ij}^* = \left(\frac{\sigma_{ij}}{\sigma_j} \right)^3 \xi_{ij} (\varepsilon_i^* \varepsilon_j^*)^{1/2}, \quad (3.48)$$

where $\varepsilon_i^* \equiv \varepsilon_{ii}^*$.

Applying equations (3.43) and (3.47) for a sufficiently long chain, equation (3.8) for the equilibrium gyration radius now yields the condition

$$\begin{aligned} & -\beta(1-\eta_s) \varphi \varepsilon_{pp}^* - \frac{\varphi + \ln[(1-\varphi)]}{\varphi} + \frac{1}{\varphi} (\varphi_{1,1} + \ln(1-\varphi)) \left(1 + \frac{\zeta_3}{1-\eta_s} \right) \\ & + \varphi_{1,1} \left(3 - \frac{7}{r_p} \right) + \varphi_{2,2} \left(3 - \frac{22}{r_p} \right) - \varphi_{3,3} \frac{24}{r_p} - \varphi_{4,4} \frac{9}{r_p} \\ & + \varphi_{1,2} \left[-\frac{15\zeta_1 + 6\zeta_2 + \zeta_3}{r_p(1-\eta_s)} + 3 \frac{\frac{5}{2}\zeta_1 + \zeta_2}{1-\eta_s} + \frac{3\zeta_1^3}{2(1-\eta_s)^3} + 3 \frac{3\zeta_1^2 + \zeta_1\zeta_2}{(1-\eta_s)^2} \right] \\ & + 3\varphi_{1,3} \left(-\frac{3\zeta_1^2 + 2\zeta_1\zeta_2}{r_p(1-\eta_s)^2} + \frac{\zeta_1^3}{(1-\eta_s)^3} - 3 \frac{\zeta_1^2}{r_p(1-\eta_s)^2} \right) \\ & 3\varphi_{2,3} \left[-\frac{14\zeta_1 + 2\zeta_2}{r_p(1-\eta_s)} + 1 + 3 \frac{\zeta_1}{(1-\eta_s)} + 3 \frac{\zeta_1^2}{(1-\eta_s)^2} \right] \\ & - 9\varphi_{1,4} \frac{\zeta_1^3}{r_p(1-\eta_s)^3} - 27\varphi_{2,4} - 27\varphi_{3,4} \frac{\zeta_1}{r_p(1-\eta_s)} - \frac{7}{3r_p} (1-\alpha^2) = 0 \end{aligned}, \quad (3.49)$$

where

$$\varphi \equiv \frac{\eta_p}{1-\eta_s}, \quad (3.50)$$

$$\varphi_{i,j} = \frac{\varphi^i}{(1-\varphi)^j}, \quad (3.51)$$

and

$$\zeta_k \equiv \sum_{i \neq p} \eta_i \left(\frac{\sigma_p}{\sigma_i} \right)^k. \quad (3.52)$$

Similarly, equation (3.9) for the CGT yields

$$\begin{aligned} & -\beta(1-\eta_s)\varphi\varepsilon_{pp}^* - \frac{\varphi + \ln[(1-\varphi)]}{\varphi} + \frac{1}{\varphi}(\varphi_{1,1} + \ln(1-\varphi)) \left(1 + \frac{\zeta_3}{1-\eta_s} \right) \\ & + \varphi_{1,1} \left(3 - \frac{7}{r_p} \right) + \varphi_{2,2} \left(3 - \frac{22}{r_p} \right) - \varphi_{3,3} \frac{24}{r_p} - \varphi_{4,4} \frac{9}{r_p} \\ & + \varphi_{1,2} \left[-\frac{15\zeta_1 + 6\zeta_2 + \zeta_3}{r_p(1-\eta_s)} + 3\frac{5}{2}\frac{\zeta_1 + \zeta_2}{1-\eta_s} + \frac{3\zeta_1^3}{2(1-\eta_s)^3} + 3\frac{3\zeta_1^2 + \zeta_1\zeta_2}{(1-\eta_s)^2} \right] \\ & + 3\varphi_{1,3} \left(-\frac{3\zeta_1^2 + 2\zeta_1\zeta_2}{r_p(1-\eta_s)^2} + \frac{\zeta_1^3}{(1-\eta_s)^3} - 3\frac{\zeta_1^2}{r_p(1-\eta_s)^2} \right) \\ & 3\varphi_{2,3} \left[-\frac{14\zeta_1 + 2\zeta_2}{r_p(1-\eta_s)} + 1 + 3\frac{\zeta_1}{(1-\eta_s)} + 3\frac{\zeta_1^2}{(1-\eta_s)^2} \right] \\ & - 9\varphi_{1,4} \frac{\zeta_1^3}{r_p(1-\eta_s)^3} - 27\varphi_{2,4} - 27\varphi_{3,4} \frac{\zeta_1}{r_p(1-\eta_s)} = 0 \end{aligned} \quad (3.53)$$

However, in the infinite chain length limit, this reduces to the much simpler expression:

$$\frac{\Theta}{T_p^*} = \frac{(1-\eta_s)^4}{4(1-\eta_s)^3 + \left(\frac{15\zeta_1 + 6\zeta_2 + \zeta_3}{2} \right) (1-\eta_s)^2 + (9\zeta_1^2 + 3\zeta_1\zeta_2)(1-\eta_s) + \frac{9\zeta_1^3}{2}}. \quad (3.54)$$

If all molecular diameters are the same, it further reduces to

$$\frac{\Theta}{T_p^*} = \frac{(1-\eta_s)^4}{4 - \eta_s + 2\eta_s^2 - \eta_s^3/2}. \quad (3.55)$$

As in the lattice fluid case, an equation of state for the solvent is necessary. In this case, the insertion parameter approach yields an equation of state consistent with the above model, for which parameters are available in a limited range of polymer and solvents. An equation of state can be directly derived from the insertion parameter via

$$z = \beta \frac{P}{\rho} = 1 - \ln \mathbf{B} + \frac{1}{\rho} \int_0^\rho \ln \mathbf{B} d\rho, \quad (3.56)$$

where for a multicomponent mixture in which self-interactions are not explicitly considered as they are for the CGT:

$$\ln \mathbf{B} = \sum_k x_k \ln \mathbf{B}_k^{r_k}. \quad (3.57)$$

This has been shown¹³² to give for the equation of state:

$$Pv^*/kT = y(\sigma_{-3} + 3\sigma_{-1}\sigma_{-2}y + 3\sigma_{-1}^3y^2)/\sigma_{-3} - \eta_s(1 - 1/r_s) - \eta_s^2\beta P^*v^*. \quad (3.58)$$

Furthermore, for a finite length chain, it is necessary to obtain equations for the chemical potential of the solvent in the pervaded volume and in the bulk in order to implement chemical potential equality. The chemical potential of any component for which self interaction need not be explicitly considered may be calculated simply by scaling equation (3.43) appropriately with the number of beads comprising a molecule of the component.. The chemical potential has thereby been shown¹³² to be given by

$$\beta\mu_k = \frac{\eta_k}{r_k v_k^*} + r_k \left[\ln(1+y) + (3\sigma_{-1}\sigma_k + 3\sigma_{-2}\sigma_k^2 + \sigma_{-3}\sigma_k^3)y \right. \\ \left. + \left(\frac{9}{2}\sigma_{-1}^2\sigma_k^2 + 3\sigma_{-1}\sigma_{-2}\sigma_k^3 \right) y^2 + 3\sigma_{-1}^3\sigma_k^3 y^3 \right], \quad (3.59) \\ -2\beta r_k v_k^* \sum_l \eta_l P_{kl}^*$$

where

$$v_k^* = \pi\sigma_i^3/6, \quad (3.60)$$

and

$$P_{ij}^* = 4\varepsilon_{ij}^* \left(\frac{\sigma_{ij}}{\sigma_i\sigma_j} \right)^3. \quad (3.61)$$

For a pure bulk solvent, equation (3.59) reduces to

$$\beta\mu_s^B = \frac{\eta_s^B}{r_s v_s^*} + r_s \left[\ln(1 + y^B) + 7y^B + \frac{15}{2}y^{B2} + 3y^{B3} \right] - 2\beta r_s \eta_s^B \varepsilon_s^*, \quad (3.62)$$

where $y^B = \tilde{\rho}^B / (1 - \tilde{\rho}^B)$. Within the pervaded volume, equation (3.59) is not subject to simplification.

3.2. Results

3.2.1. Overall pressure-temperature behavior

Typical conformational behavior as predicted by equation (3.32) for the lattice fluid approach is consistent with the high temperature behavior predicted in the literature as shown in Figure 6. As shown in Figure 17, it is characterized by an HCGT that smoothly passes into negative pressure at low temperatures and curves over into a maximum and a CCGT at high temperatures. Furthermore, for an infinite chain the pressure of the CCGT approaches zero as the system approaches the theoretical vapor/liquid critical temperature of the chain ($2T_p^*$). As shown in Figure 18 for the CGT behavior of polyisobutylene in n-pentane, the SPT model likewise qualitatively conforms to the behavior predicted by Figure 6. One additional interesting, if experimentally unpractical, observation is that as the solvent size goes to infinity, the CGT pressure actually reaches a minimum at $\tilde{\Theta} = 1$ so that this point represents a theoretical hypercritical point rather than a CCGT.

The SPT and LF models are in reasonable agreement with each other and with experiment at temperatures well below the high pressure hypercritical point. As shown in Figure 19, the P-T behavior of the CGT in this region as predicted by the LF model is in good quantitative agreement with experimental results for several systems for which such data are available. The SPT model is in somewhat weaker but still reasonable quantitative agreement with the same experimental results. However, the LF and SPT models quantitatively diverge as the high pressure hypercritical point is approached. In

particular, the SPT model typically predicts the hypercritical point to be at much higher pressure and temperature than the LF model. Given the fact that equation of state parameters for both models are by necessity fit to the extant data in the lower temperature region, it is unsurprising that they differ in the higher temperature region where behavior is purely extrapolated. Due to the lack of experimental data for polymers in this higher temperature domain, it is presently difficult to establish whether the difference emerges simply from a poor fit of the parameters to this region or from some more fundamental weakness in one or both of the models. As additional data for the CGT or LCST in very high pressure high temperature systems become available in the literature, it may become possible to better resolve this discrepancy.

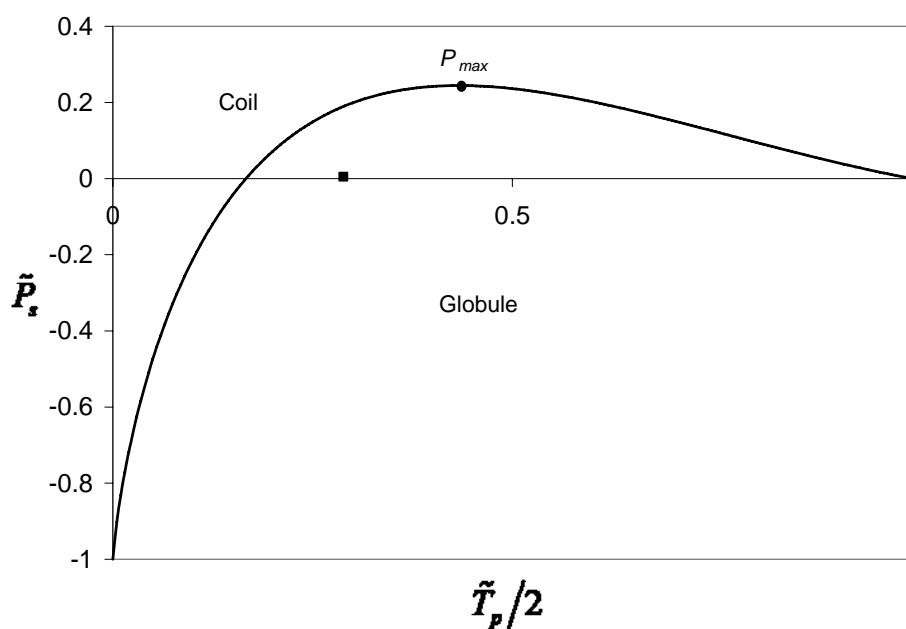


Figure 17: Plot of dimensionless CGT pressure versus temperature as predicted by equation (3.32) for an infinite chain in solution with $r_s = 10$ and $\zeta = \tilde{T}_p^*/\tilde{T}_s^* = 2.0$.

Because $\tilde{\Theta} \equiv \Theta/2T_p^* = (\tilde{T}_p/2)|_{\alpha=1}$, the scaling of the temperature axis is such that the temperature value given for any point on the curve corresponds to the value of $\tilde{\Theta}$ at that pressure. The solid square denotes the critical point of the solvent. Values to the left of

the hypercritical point P_{\max} correspond to an HCGT while values to the right correspond to a CCGT.

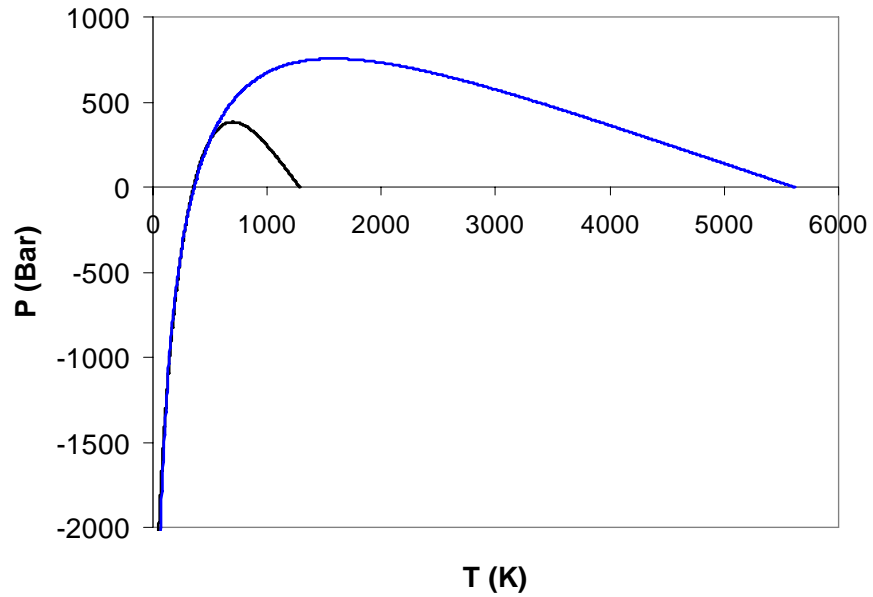


Figure 18: Plot of CGT of polyisobutylene in n-pentane. The solid line is the lattice fluid prediction, while the blue line is the scaled particle theory prediction.

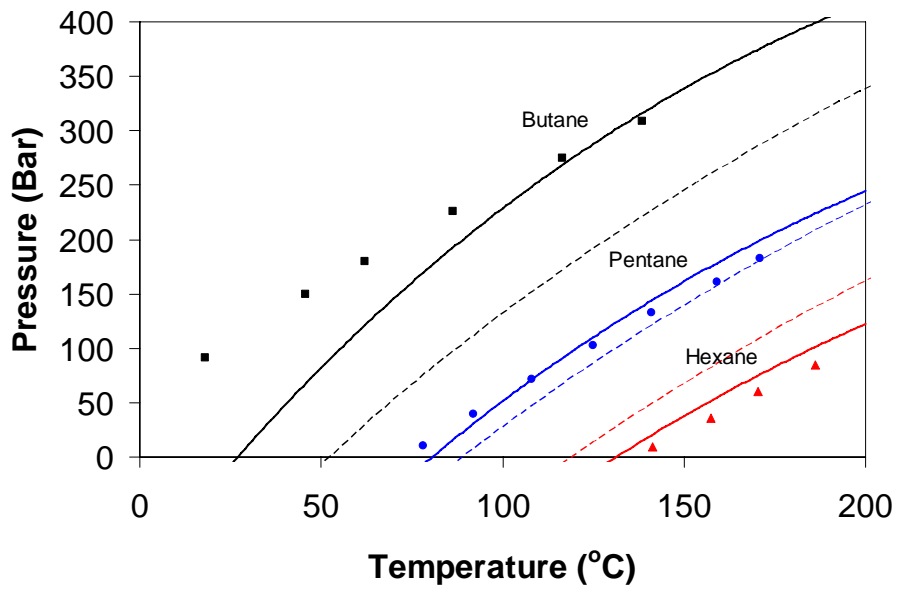


Figure 19: P - T plot of the HCGT of polyisobutylene ($M_w = 1.66 \times 10^6$ g/mol) in various solvents. Solid lines correspond to predictions based upon equation (3.32) for the lattice fluid model for an infinite chain. Dashed lines correspond to predictions based upon equation (3.54) for the SPT model for an infinite chain. Points correspond to experimental data¹¹.

3.2.2. Physics of the transition

The predicted transitions can best be understood physically by examining equation (3.22), which has a straightforward interpretation. The LHS is the chain elastic force that is balanced at equilibrium by the thermodynamic driving forces on the RHS. The RHS is the sum of 2 terms: a negative term corresponding to the attractive energy of the chain with itself and a positive term corresponding to the excluded volume interaction of the chain with itself and with solvent. The self interaction energy term always favors chain collapse, while the excluded volume term always favors chain expansion. Equivalently, a positive net driving force corresponds to an expanded coil, a negative net driving force to a collapsed globule, and a zero net driving force to a coil-globule transition. The qualitative contributions of these two thermodynamic forces are shown in Figure 20. As can be seen there, the derivative of the net driving force with temperature will be positive at a CCGT and negative at a HCGT; this provides an additional mathematical means of distinguishing between the two. By rearranging equation (3.54), it can be shown that these same physical arguments apply to the SPT model.

The collapsed states associated with both transitions are characterized by dominance of self interaction energy over excluded volume. Since the polymer self-interaction effect is the only thermodynamic driving force that favors the globule state, this model predicts that a chain with no attractive self interactions will have no equilibrium globule state. This represents a limitation of this model that is also characteristic of the S-L model, which does not predict an LCST in the absence of attractive interactions. In contrast, simulation studies have predicted a CGT in the absence of attractive interactions^{60, 61}.

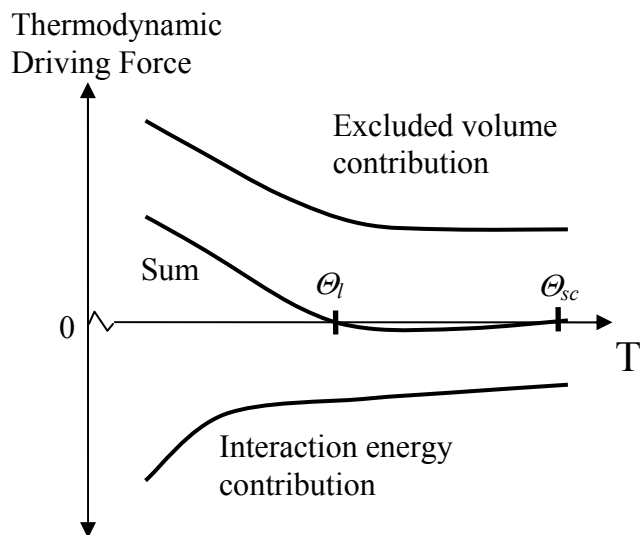


Figure 20: Qualitative contributions by excluded volume and polymer self-interaction energy to the RHS of equation (3.22) as a function of temperature for a system in which the polymer S-L characteristic temperature is greater than the solvent S-L characteristic temperature. Coil-globule transitions occur when the sum of these contributions is zero.

Both the LF and SPT models make the qualitative prediction that for similar interaction energies (and thus similar characteristic temperatures), higher bulk solvent occupied volume fractions will yield warmer HCGTs and cooler CCGTs. For the lattice fluid model, this can be seen by noting the series expansion of equation (3.22) shown in equation (3.28). Since all contributions to the excluded volume scale as $(1-\eta_s)^{-x}$, where x is an integer, the excluded volume always increases with increased solvent occupied volume fraction. By rearranging equation (3.54), it can be straightforwardly shown that the same holds true for the SPT model. Since, as argued above, the excluded volume interaction always contributes to the expanded coil state, such an increase in the excluded volume will tend to expand the temperature range of the globule state, increasing the HCGT temperature and lowering the CCGT temperature.

Since the characteristic density of each solvent is different, this trend cannot be expected to be exactly true in terms of dimensional density. Nevertheless, as most solvent characteristic densities fall within a reasonably narrow range, it is expected to be a good rule of thumb that increased solvent density will typically correlate with an elevated HCGT temperature. As shown in Figure 21 for polyisobutylene in various solvent, this prediction is reasonably born out both in numerical results of these two theories as well as in experimental LCST results, with some aberrations where interaction energies greatly differ. As will be shown later in Table 1, this trend is even more apparent when solvents are grouped by carbon number.

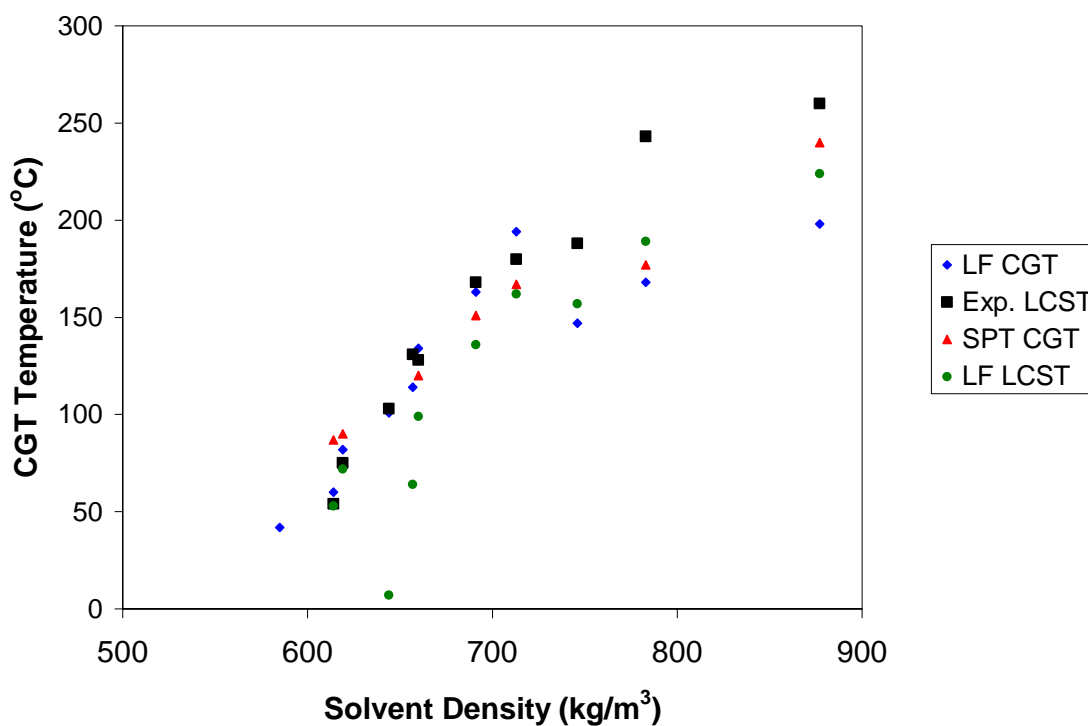


Figure 21: LCST and CGT data for polyisobutylene in various solvents as a function of solvent density.

3.2.3. The high pressure hypercritical point

Via numerical solution, equation (3.34) yields an estimate for the dimensionless temperature $\tilde{\Theta}_{P_{max}}$ of the high pressure hypercritical point for the LF model (the SPT model cannot be reduced to two parameters and thus it is not possible to make a comparably universal two dimensional plot for this model). This is of particular interest because systems with relatively low values of $\tilde{\Theta}_{P_{max}}$ are expected to be most likely to exhibit and experimentally accessible high temperature UCST. As shown in Figure 22 for long chains, $\tilde{\Theta}_{P_{max}}$ generally decreases with increasing ζ and r_s . Solvents associated with the lowest values of $\tilde{\Theta}_{P_{max}}$ tend to be small, symmetric molecules with relatively weak self interactions; for example, as shown in Figure 22, carbon dioxide, nitrogen, and methane (as well as oxygen and ethylene, not shown) yield values of $\tilde{\Theta}_{P_{max}}$ considerably below the more typical range offered by larger organic solvents such as propane, benzene, and hexanes. However, as shown in Figure 17, P_{max} is typically well into the solvent supercritical region, which can present additional experimental challenges. Since solutions of polymer in supercritical carbon dioxide in particular are presently an area of active study, they might provide a convenient system in which to begin a search for a high temperature UCST. The CO₂ – polystyrene system in particular has a particularly low value of $\tilde{\Theta}_{P_{max}}$ for this solvent and could be of particular interest for this purpose.

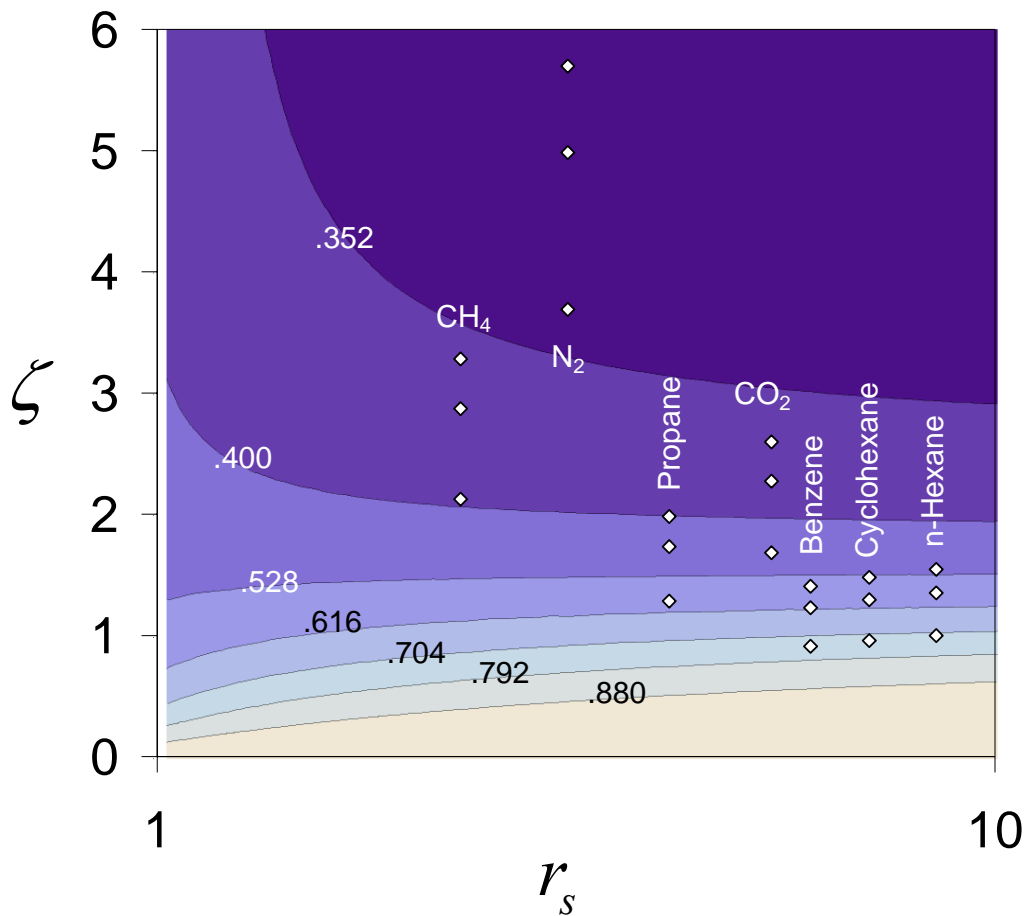


Figure 22: Contour plot of temperature $\tilde{\Theta}_{p_{max}}$ at the high pressure hypercritical point as a function of interaction ratio ζ and solvent size r_s , for the LF model in the limit of infinite chain length. The numbered lines indicate the value of $\tilde{\Theta}_{p_{max}}$ along that contour. White points indicate the position of various polymer / solvent systems. Each vertical triplet of points corresponds, from top to bottom, to polystyrene, polyisobutylene, and PDMS in the labeled solvent.

3.2.4. The CGT near the solvent vapor pressure

As suggested above, a point of particular interest that is the focus of Table 1 is the CGT at or near the vapor pressure of the solvent, which is nearly at zero pressure. In general, such a CGT may theoretically occur either in the gas phase or the liquid phase.

This behavior may be elucidated in the following way. By combining equation (3.29) with the S-L equation of state, it is possible to arrive for the LF model at a form of the dimensionless CGT temperature Θ/T_s^* that for an infinite chain is dependent only upon r_s and the ratio of the polymer and solvent characteristic temperatures defined as $\zeta \equiv T_p^*/T_s^*$. As noted above, it is not possible to obtain a similar two parameter reduction of the SPT model, and this investigation will therefore focus on the LF model alone.

The behavior of the transition temperature as a function of these LF parameters is shown in Figure 23. These plots can be understood in the following way. Within a P-T plot such as Figure 17, follow the vapor pressure curve of the solvent to its critical point, and then follow an isobaric line to higher temperature. The curves in Figure 23 denote the CGT transitions that are encountered while travelling this path, as a function of ζ as a given r_s . As shown in these plots, for any given r_s there will be a critical value ζ_c at which the transition will occur at the liquid-vapor critical point of the solvent. Based on the S-L equations for critical temperature and density of the solvent this value can be shown to be $\zeta_c = \sqrt{r_s}/(1 + \sqrt{r_s})$ for an infinite chain, so that it goes to unity as r_s goes to infinity and one half as r_s approaches unity. Furthermore, the temperature of this unique point will be also given by $\tilde{\Theta}_{c,CGT} = \sqrt{r_s}/(1 + \sqrt{r_s})$. For $\zeta > \zeta_c$, there will be an HCGT in the solvent liquid state and a CCGT in the solvent supercritical state at higher temperature. For ζ significantly less than ζ_c , there will be only a CCGT in the solvent gas phase. However, from a practical standpoint, there is no polymer in the solvent gas phase, and as such ζ_c represents an effective minimum condition at which a CGT will occur.

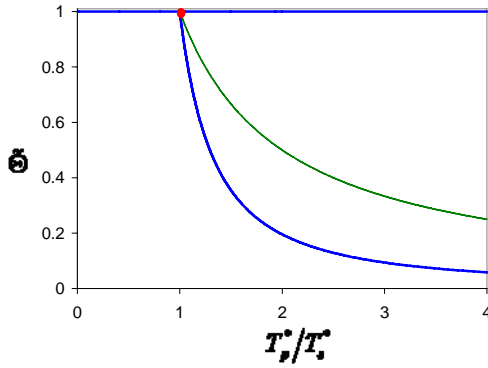


Figure 23a

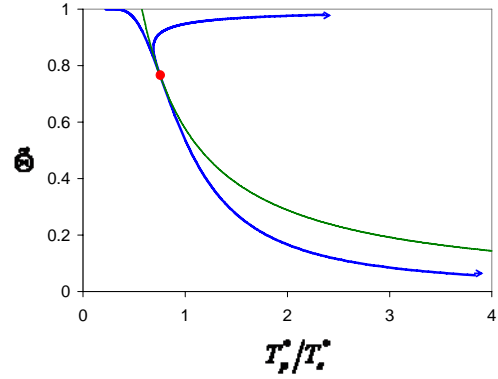


Figure 23b

Figure 23: Quantitative plot of dimensionless transition temperature vs. the ratio of the S-L characteristic temperatures of the polymer and solvent for infinite chain length. The vertical axis is the dimensionless transition temperature $\tilde{\Theta}$. Figure 23a is for infinite r_s while Figure 23a is for r_s equal to 10. The point marked in red on each plot is the liquid-vapor critical point of the solvent. The green curve denotes the critical point of the solvent as a function of ζ . Each branch from the critical point corresponds to a coil globule transition for a chain in a different solvent phase, as labeled on the plots. Note that in the limit of infinite r_s (Figure 23b) both the gas and supercritical phases are at zero solvent density. Sub-critical data is at the solvent saturated vapor pressure while supercritical data is at the solvent critical pressure.

Numerical solutions of equation (3.29) for the lattice fluid model and equation (3.54) for the SPT model yield good correspondence between predicted HCGT temperatures and experimental and S-L LCST temperatures, as shown in Table 1. Furthermore, theoretical predictions of $\partial T/\partial P|_{P=0}$, as shown in Table 2 for a variety of systems, exhibit a generally good match with experimental results, albeit with a moderate bias towards under-prediction, as shown in Figure 24.

Table 1: Comparison of theoretical HCGT temperatures at solvent vapor pressure with experimental and theoretical LCSTs for polyisobutylene in various solvents. Solvents are grouped by carbon number. SPT results are unavailable for some solutions due to present limitations on parameter availability for this model.

Polyisobutylene/ <i>Pentanes</i>	Density ρ , 25 °C (kg/m ³)	Reduced Density ρ/ρ^* , 25 °C	LCST, °C		HCGT, °C	
			Exp.	Theory	LF	SPT
Immiscible at 25 °C						
Neopentane	585	0.786		-40	42	-
Isopentane	614	0.802	54	53	60	87
n-Pentane	619	0.82	75	72	82	90
Cyclopentane	746	0.86	188	157	147	
<i>Hexanes</i>						
2,2-Dimethylbutane	644	0.833	103	7	101	-
2,3-Dimethylbutane	657	0.841	131	64	114	-
n-Hexane	660	0.852	128	99	134	120
Cyclohexane	783	0.868	243	189	168	177
<i>Other</i>						
n-Heptane	691	0.864	168	136	163	151
n-Octane	713	0.875	180	162	194	167
Benzene	877	0.882	260	224	198	240

Table 2: Comparison of theoretical and experimental results for $\partial\Theta/\partial P|_{P=0}$ for various systems. For the LF model, theoretical calculations are based on polymer molecular weights chosen to match those associated with each experimental result. For the SPT model, calculations are at infinite molecular weight, which is expected to cause little error due to the large size of the chain. SPT results are unavailable for some solutions due to present limitations on parameter availability for this model.

Polymer	Solvent	$\partial\Theta/\partial P _{P=0}$ ($^{\circ}\text{C} / \text{bar}$)		
		Experiment	LF Theory	SPT Theory
Polystyrene	Tert-butyl acetate ¹³⁴	0.68	0.50	-
	Methyl cyclohexane ¹³⁵	0.80	0.65	-
	Methyl acetate ¹³⁶	0.47	0.22	-
Polyisobutylene ¹¹	Propane	0.33	0.23	.27
	n-Butane	0.37	0.27	.32
	n-Pentane	0.45	0.36	.37
	n-Hexane	0.61	0.47	.42

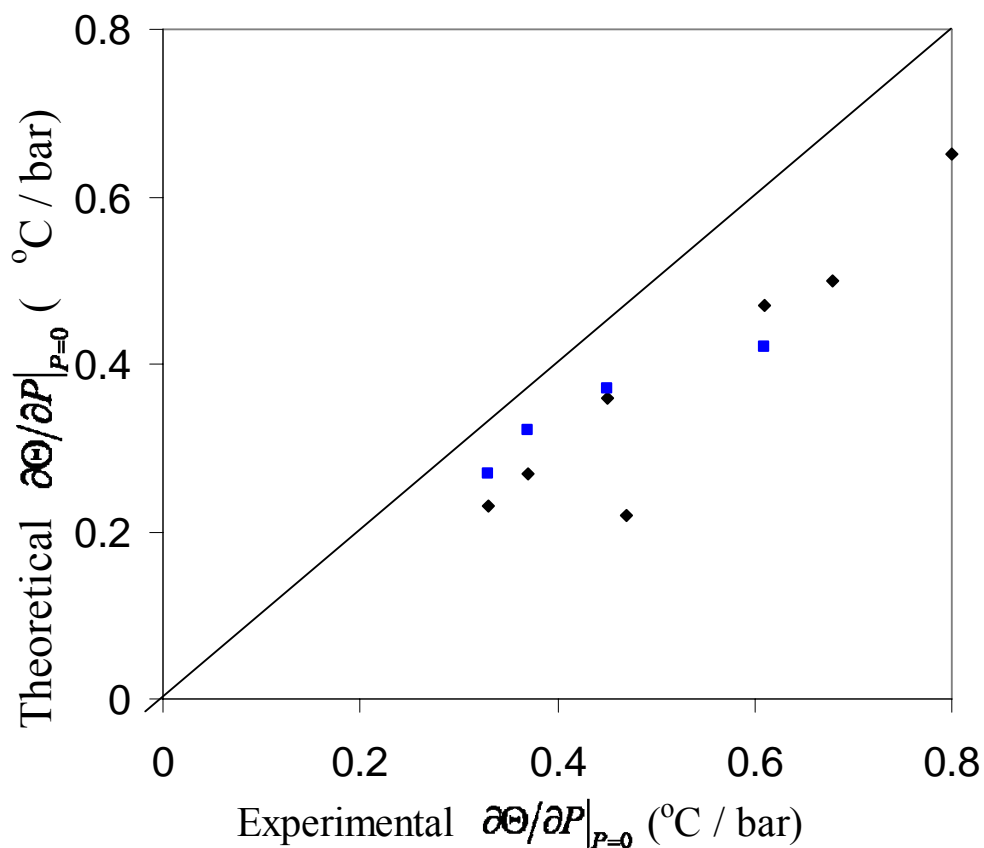


Figure 24: Plot of theoretical vs experimental values of $\partial\Theta/\partial P|_{P=0}$ for systems shown in Table 2. Black diamonds denote LF-CGT results while blue squares denote SPT-CGT results. The 45 degree line indicates the locus of points along which theoretical and experimental values would agree.

3.2.5. Chain conformation through the CGT

Chain collapse or expansion will occur any time the system crosses the CGT curve in Figure 6 (or equivalently Figure 17) through any combination of pressure and temperature changes. The two CGT transitions of particular interest are the cases of an isobaric thermally triggered CGT and an isothermal pressure triggered CGT. The

isobaric CGT will typically be nearly the same as a third case of interest, which is a CGT triggered along the vapor pressure curve of the solvent.

Equation (3.22) can be used to solve for the Lattice-Fluid gyration radius and chain mer density around an isobaric HCGT transition, yielding results such as those shown in Figure 25 and Figure 26 for a polyisobutylene / n-pentane system. As expected, the coil state is predicted at temperatures below the transition while the globular state is predicted at temperatures above the transition. Numerical fitting of results shows that $R \sim r_p^{1/3}$ in the globule state and $R \sim r_p^{3/5}$ in the coil state, consistent with Flory's predicted scaling. In addition, the chain occupied volume fraction η_p is an appropriate order parameter that is bounded between zero and unity. As shown in Figure 26, as the chain approaches infinite density there is a discontinuity at the transition in the slope of η_p but not in η_p itself. This is consistent with a second order thermodynamic transition.

Figure 27 shows typical results from the LF model for the expansion factor of the chain through isothermal CGTs at temperatures near solvent vapor-liquid equilibrium. The transition is qualitatively similar to experimental results for pressure induced swelling of aqueous polymer networks¹³⁷. As expected, an increase in pressure triggers expansion of the chain. This can be equivalently understood as a pressure induced shift of the CGT temperature upward through the system temperature. In addition, it is apparent that for the small differences in temperature shown in this figure, the P - T relationship is approximately linear, which is consistent with experimental results over small temperature ranges.

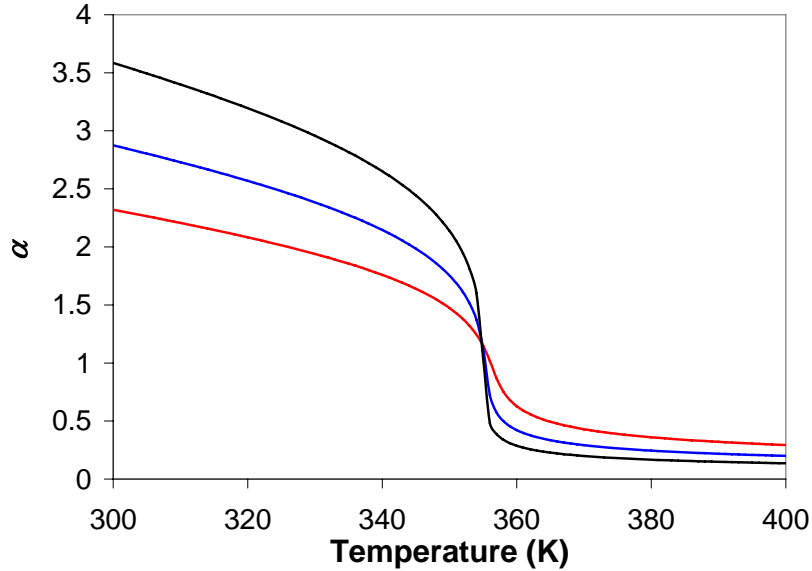


Figure 25: Expansion factor as a function of temperature for various molecular weights of polyisobutylene in n-pentane near the HCGT. The red line corresponds to a molecular weight of 10^6 , the blue to a molecular weight of 10^7 , and the black to a molecular weight of 10^8 .

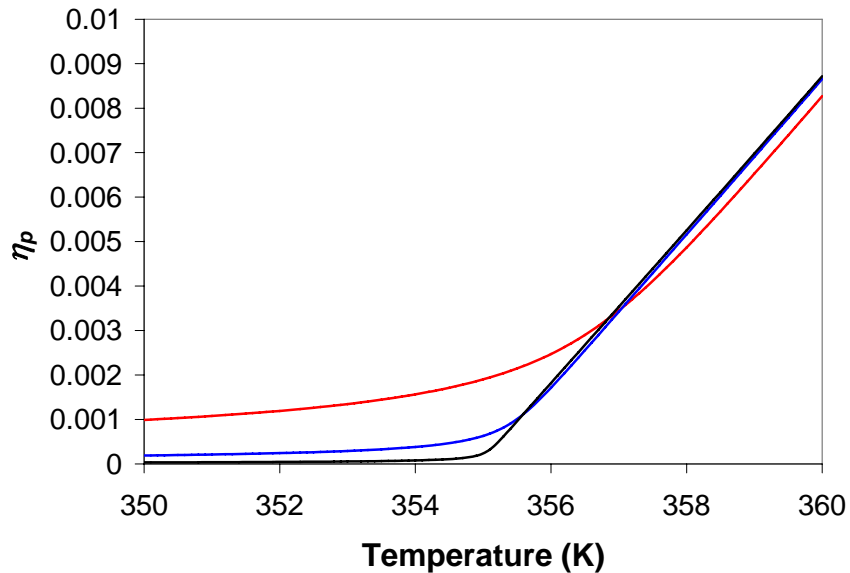


Figure 26: Polymer volume fraction as a function of temperature for various molecular weights of polyisobutylene in n-pentane near the HCGT. The red line corresponds to a molecular weight of 10^6 , the blue to a molecular weight of 10^7 , and the black to a molecular weight of 10^8 .

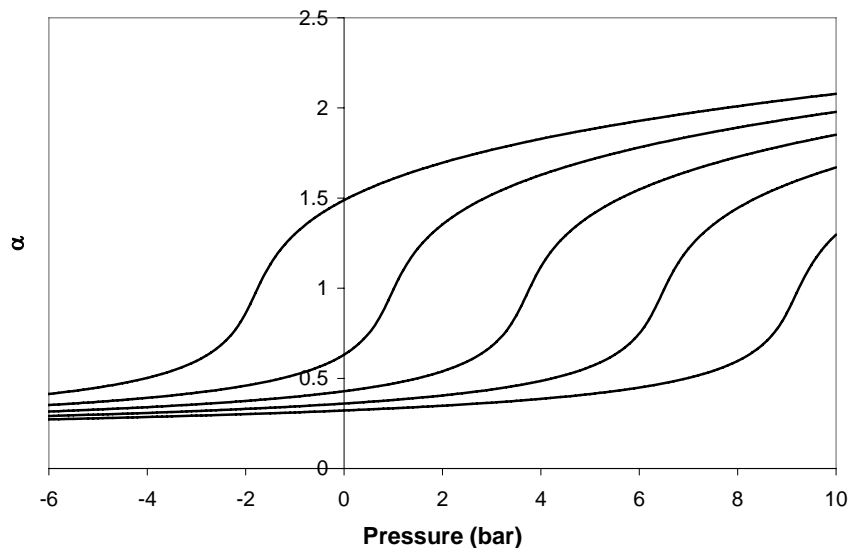


Figure 27: Typical plot of chain expansion factor through the pressure induced globule-to-coil transition as predicted by this model, shown as calculated for the system polyisobutylene / n-pentane. Curves correspond to different temperatures. From leftmost to rightmost curve, corresponding temperatures are 353 K, 354 K, 355 K, 356 K, and 357 K.

3.3. Conclusions

Proposed lattice fluid (LF) and scaled particle theory (SPT) models for single chain conformational behavior with pressure and temperature offer semi-quantitative agreement with experiment without the use of adjustable mixture parameters. Coil-globule transition (CGT) pressures and temperatures are well predicted for a variety of polymer / solvent systems, and important aspects of a proposed³ master phase boundary for weakly interacting polymers are reproduced. Predicted slopes of the CGT with pressure exhibit reasonable agreement with experimental results, albeit with a tendency towards under prediction.

Qualitatively, predicted behavior is characterized by a heating induced coil-to-globule transition (HCGT) that smoothly passes into negative pressure at low

temperatures and curves over into a maximum and a cooling induced coil-to-globule transition (CCGT) at high temperatures. The behavior of the predicted transitions is consistent with a second order thermodynamic transition. The maximum at which the CCGT and HCGT meet corresponds to a high pressure hypercritical point P_{max} in the polymer / solvent phase behavior¹⁰. This behavior is often experimentally inaccessible due to polymer degradation; however, results suggest that solutions of polymer in very small molecule supercritical solvents such as O₂, CO₂, N₂, and CH₄ may exhibit a P_{max} at sufficiently low temperatures to allow observation.

The single chain lattice fluid approach predicts a critical polymer/solvent interaction energy ratio $\zeta_c = \sqrt{r_s} / (1 + \sqrt{r_s})$, significantly below which no experimental CGT will be found for most systems. For systems with $\zeta > \zeta_c$ it predicts two CGTs: an HCGT in the solvent liquid phase and a CCGT in the solvent supercritical phase. Within both models, the collapsed states associated with both the CCGT and HCGT are characterized by dominance of polymer self interaction energy over excluded volume effects. All else being equal, solvents with higher reduced density yield warmer HCGTs and cooler CCGTs due to greater excluded volume effects. Conversely, increasing chain length correlates with cooler HCGTs and warmer CCGTs due to reduction of the excluded volume effect.

Results from the LF model appear to compare to experiment similarly or even slightly better than those for the SPT model. Furthermore, the governing equations for the LF model are far simpler than those for the SPT model. This outcome emphasizes the surprising success of the lattice fluid model in obtaining good quantitative correlation with experiment. However, one outstanding point favors the SPT model. In the LF model, it is very difficult to relate component parameters in any direct way to underlying molecular properties of the substance. In contrast, preliminary results indicate that there is often quantitative or semi-quantitative agreement¹³² between SPT parameters and molecular properties. As a consequence, the SPT model may offer a more direct connection to the underlying physics of the system than the LF model, and

correspondingly may provide prediction of the CGT based upon a narrower range of experimental data.

Chapter 4. Towards a Model for the Aqueous CGT

As suggested in the introduction, the CGT is of particular relevance in an aqueous setting. Many biomolecules are believed to possess a CGT which is relevant to their function, and CGT-driven stimuli-responsive polymers of interest in biological settings must by necessity exhibit their swelling behavior in an aqueous environment. A seemingly ideal theoretical approach to this phenomenon would straight-forwardly combine the combinatoric hydrogen bonding approach of Chapter 2 with the CGT model of Chapter 3. However, such an approach is complicated by the fact that the former results from a system partition function approach while the latter results from an insertion parameter approach. As noted in section 1.4, such combinations may be problematic at best due to sometimes contradictory outcomes of these two approaches. Nevertheless, such an attempt is described below in an attempt to establish groundwork towards the development of a successful model for this phenomenon.

4.1. CGT with Veytsman Statistics

Consider a polymer-solvent system at infinite dilution. In such a system, the polymer chains do not interact, and each will independently pervade a volume characterized by a gyration radius R . Within this domain the polymer chain will occupy a volume fraction η_p and N_s solvent molecules will occupy a cumulative volume fraction η_s . Accounting for vacancies, the total occupied volume fraction $\tilde{\rho} = \eta_p + \eta_s$ within this domain will in general be less than one. Furthermore, hydrogen bonding within the system will be characterized by the set of variables $\{v_{ij}\}$, where v_{ij} is an intrinsic measure of the number of hydrogen bonds between proton donors of type i and proton acceptors of type j .

The partition function Q of an ideal chain is known to be skewed with respect to gyration radius, and on this basis the equilibrium chain gyration radius for the above

system is given in terms of free energy G by the Hermans-Overbeek approximation²⁷, as in the above models:

$$\left(\frac{\partial(\ln R + \beta G)}{\partial R} \right)_{T, P, \hat{\phi}_s, \{v_{ij}\}} = 0 \quad (3.63)$$

The system free energy may be written in terms of chemical potentials as

$$G = N_p \mu_p + N_p N_s (\mu_s - \mu_s^B) + N_s^T \mu_s^B \quad (3.64)$$

where μ_p and μ_s are polymer and solvent chemical potential within the pervaded volume, respectively, μ_s^B is the solvent chemical potential within the bulk, N_p is the total number of polymer chains in the system, and N_s^T is the total number of solvent molecules in the system. Throughout this development, “ B ” superscripts on any variable will denote its bulk value. Furthermore, the solvent within the pervaded volume must satisfy equality of chemical potential with the bulk solvent, such that

$$\mu_s = \mu_s^B \quad (3.65)$$

Making use of the fact that the bulk solvent chemical potential at infinite polymer dilution is not a function of chain gyration radius, equation (3.2) now reduces to

$$\frac{1}{R} + \beta N_p \left(\frac{\partial \mu_p}{\partial R} \right)_{T, P, \hat{\phi}_s, \{v_{ij}\}} = 0 \quad (3.66)$$

As in the hydrogen bonding lattice fluid model (HBLF) described in section 2.1.2, the partition function will taken as factorable into separate contributions from hydrogen bonding (Q_{HB}) and physical interactions, such as excluded volume and van Der Waals forces (Q_P):

$$Q = Q_P Q_{HB} \quad (3.67)$$

The free energy will, as in the HBLF model, likewise be separable into corresponding contributions, such that

$$G = G_P + G_{HB}, \quad (3.68)$$

as will the chemical potential of any component k (k being s for solvent or p for polymer):

$$\mu_k = \mu_{k,P} + \mu_{k,HB} \quad (3.69)$$

4.1.1. Physical contribution

The physical contribution to the chemical potential is given as in the CGT model of Chapter 3. It follows from that development that the physical contribution to polymer chemical potential is given by

$$\beta\mu_{p,P} = r_p \left[\begin{array}{l} 1 + \frac{1-\eta_s}{\eta_p} \ln \left(1 - \frac{\eta_p}{1-\eta_s} \right) - \ln(1-\eta_s-\eta_p) \\ -\beta(\varepsilon_{pp}^* \eta_p + 2\varepsilon_{sp}^* \eta_s) - \frac{2}{r_p} \ln \left(\frac{r_p v^*}{\eta_p} \right) + \frac{7}{2} \frac{a}{r_p^{4/3} \eta_p^{2/3}} \end{array} \right]. \quad (3.70)$$

The physical contribution to the solvent chemical potential is similarly calculated via the Widom insertion parameter:

$$\mu_{s,P} = kT \ln \left(\frac{\rho_s \lambda^3}{\mathbf{B}_s} \right). \quad (3.71)$$

Within the pervaded volume, this is given by

$$\beta\mu_{s,P} \cong \ln \rho_s - \ln \left[(1-\eta_p-\eta_s)^{r_s} \exp \left[\beta r_s (\varepsilon_{ss}^* \eta_s + 2\varepsilon_{sp}^* \eta_p) \right] \right]. \quad (3.72)$$

Within the bulk, it is

$$\beta\mu_{s,P}^B = \ln \rho_s^B - \ln \left[(1-\tilde{\rho}^B)^{r_s} \exp \left[\beta r_s \varepsilon_{ss}^* \tilde{\rho}^B \right] \right]. \quad (3.73)$$

4.1.2. Hydrogen bonding contribution

Based on the HBLF model, the contribution to free energy from hydrogen bonding, within the pervaded volume is

$$\beta G_{HB}^{PV} = rN \left[\sum_{i=1}^{m_d} \sum_{j=1}^{m_a} v_{ij} \left(1 + \beta G_{ij}^0 + \ln \frac{v_{ij}}{\tilde{\rho} v_{i0} v_{0j}} \right) + \sum_{i=1}^{m_d} v_d^i \ln \frac{v_{i0}}{v_d^i} + \sum_{j=1}^{m_a} v_a^j \ln \frac{v_{0j}}{v_a^j} \right], \quad (3.74)$$

where $G_{ij}^0 = E_{ij}^0 - TS_{ij}^0 + PV_{ij}^0$, and $v_d^i = \frac{N_d^i}{rN}$, $v_{i0} = \frac{N_{i0}}{rN}$, $v_{ij} = \frac{N_{ij}}{rN}$, and so on. Similarly for the bulk solvent:

$$\beta G_{HB}^B = r_s N_s^B \left[\sum_{i=1}^{m_d} \sum_{j=1}^{m_a} v_{ij}^B \left(1 + \beta G_{ij}^0 + \ln \frac{v_{ij}^B}{\tilde{\rho}^B v_{i0}^B v_{0j}^B} \right) + \sum_{i=1}^{m_d} v_d^{Bi} \ln \frac{v_{i0}^B}{v_d^{Bi}} + \sum_{j=1}^{m_a} v_a^j \ln \frac{v_{0j}^B}{v_a^{Bj}} \right]. \quad (3.75)$$

The contribution to the overall system free energy from hydrogen bonding is then given by

$$\beta G_{HB} = \beta G_{HB}^B + N_p \beta G_{HB}^{PV}. \quad (3.76)$$

It follows that the hydrogen bonding contribution to the polymer chemical potential is

$$\begin{aligned} \beta \mu_{p,HB} = & -\frac{r_p n_s}{\eta_p} \left[\sum_{i=1}^{m_d} \sum_{j=1}^{m_a} v_{ij}^B \left(1 + \beta G_{ij}^0 + \ln \frac{v_{ij}^B}{\tilde{\rho}^B v_{i0}^B v_{0j}^B} \right) + \sum_{i=1}^{m_d} v_d^{Bi} \ln \frac{v_{i0}^B}{v_d^{Bi}} + \sum_{j=1}^{m_a} v_a^j \ln \frac{v_{0j}^B}{v_a^{Bj}} \right] \\ & + rN \left[\sum_{i=1}^{m_d} \sum_{j=1}^{m_a} v_{ij} \left(1 + \beta G_{ij}^0 + \ln \frac{v_{ij}}{\tilde{\rho} v_{i0} v_{0j}} \right) + \sum_{i=1}^{m_d} v_d^i \ln \frac{v_{i0}}{v_d^i} + \sum_{j=1}^{m_a} v_a^j \ln \frac{v_{0j}}{v_a^j} \right]. \end{aligned} \quad (3.77)$$

The hydrogen bonding contribution to solvent chemical potential in the pervaded volume is

$$\beta \mu_{s,HB} = r_s \sum_{i=1}^n \sum_{j=1}^m v_{ij} + \sum_{i=1}^n d_i^s \ln \frac{v_{i0}}{v_d^i} + \sum_{j=1}^m a_j^s \ln \frac{v_{0j}}{v_a^j} \quad (3.78)$$

and in the bulk is

$$\beta \mu_{s,HB}^B = r_s \sum_{i=1}^n \sum_{j=1}^m v_{ij}^B + \sum_{i=1}^n d_i^s \ln \frac{v_{i0}^B}{v_d^{B,i}} + \sum_{j=1}^m a_j^s \ln \frac{v_{0j}^B}{v_a^{B,j}}. \quad (3.79)$$

4.1.3. Chain gyration radius and coil-globule transition

Substitution of equations (3.70) and (3.77) into equation (3.66) yields as a condition for the equilibrium gyration radius:

$$\begin{aligned}
& \frac{\eta_s}{\eta_p} \left[\sum_{i=1}^{m_d} \sum_{j=1}^{m_a} \left(v_{ij} \left(1 + \frac{\eta_p}{\eta_s} \right) - v_{ij}^B \right) \right. \\
& \left. + \sum_{i=1}^{m_d} \left(v_d^i \left(1 + \frac{\eta_p}{\eta_s} \right) \ln \frac{v_{i0}}{v_d^i} - v_d^{Bi} \ln \frac{v_{i0}^B}{v_d^{Bi}} \right) + \sum_{j=1}^{m_a} \left(v_a^j \left(1 + \frac{\eta_p}{\eta_s} \right) \ln \frac{v_{0j}}{v_a^j} - v_a^j \ln \frac{v_{0j}^B}{v_a^{Bj}} \right) \right] \quad (3.80) \\
& - \sum_{i=1}^{m_d} \frac{d_i^p}{r_p} \ln \frac{v_d^i}{v_{i0}} - \sum_{j=1}^{m_a} \frac{a_j^p}{r_p} \ln \frac{v_a^j}{v_{0j}} + \frac{1-\eta_s}{\eta_p} \ln \left(1 - \frac{\eta_p}{1-\eta_s} \right) + 1 + \beta \varepsilon_{pp}^* \eta_p = \frac{7}{3} \frac{1}{r_p} (1-\alpha^2)
\end{aligned}$$

The chain coil-globule transition is defined as the condition at which the chain gyration radius is equal to that of an ideal chain, such that

$$\alpha|_{CGT} = 1. \quad (3.81)$$

Thus at the CGT equation (3.80) reduces to the condition

$$\begin{aligned}
& \frac{\hat{\phi}_s}{\hat{\phi}_p} \left[\sum_{i=1}^{m_d} \sum_{j=1}^{m_a} \left(v_{ij} \left(1 + \frac{\hat{\phi}_p}{\hat{\phi}_s} \right) - v_{ij}^B \right) \right. \\
& \left. + \sum_{i=1}^{m_d} \left(v_d^i \left(1 + \frac{\hat{\phi}_p}{\hat{\phi}_s} \right) \ln \frac{v_{i0}}{v_d^i} - v_d^{Bi} \ln \frac{v_{i0}^B}{v_d^{Bi}} \right) + \sum_{j=1}^{m_a} \left(v_a^j \left(1 + \frac{\hat{\phi}_p}{\hat{\phi}_s} \right) \ln \frac{v_{0j}}{v_a^j} - v_a^j \ln \frac{v_{0j}^B}{v_a^{Bj}} \right) \right], \quad (3.82) \\
& - \sum_{i=1}^{m_d} \frac{d_i^p}{r_p} \ln \frac{v_d^i}{v_{i0}} - \sum_{j=1}^{m_a} \frac{a_j^p}{r_p} \ln \frac{v_a^j}{v_{0j}} + \frac{1-\hat{\phi}_s}{\hat{\phi}_p} \ln \left(1 - \frac{\hat{\phi}_p}{1-\hat{\phi}_s} \right) + 1 + \frac{T_p^*}{\Theta} \hat{\phi}_p = 0
\end{aligned}$$

where Θ is the CGT temperature. Note that in the absence of hydrogen bonding, equation and for an infinite chain, equation (3.82) reduces to

$$\Theta = 2T_p^* (1-\eta_s) \quad (3.83)$$

which is the same result as that given by the lattice fluid CGT model.

However, a crucial problem arises in the presence of hydrogen bonding interactions within this model. As the chain length goes to infinity, the physical terms in equations (3.80) and (3.82) go to zero faster than the hydrogen bonding terms. Thus, this model indicates that in the infinite chain length limit hydrogen bonding alone determines the chain conformation. This is a clearly aphysical result that likely results from discrepancies between the system partition function and insertion parameter approaches. In this case, the contribution of physical interactions (including excluded volume) has

been calculated via the insertion parameter, whereas the contribution of hydrogen bonding interactions has been calculated from the system partition function. A model for this phenomenon thus appears to require either an insertion parameter model for hydrogen bonding or a computation of the system partition function that accounted explicitly for polymer intramolecular interactions.

4.2. Basis for a Consistent Approach

A self-consistent insertion parameter approach that would satisfy this requirement could be developed in the following way. Begin with equation (1.19) for the insertion parameter, in which insertions resulting in a repulsive interaction (corresponding to overlapping bodies in the hard sphere case) have already been separated out in the form of an insertion probability:

$$\mathbf{B}_i = \mathbf{P}_i \langle \exp(-\beta\psi_i) \rangle. \quad (3.84)$$

Now note that the interaction energy of insertion can be separated into physical and hydrogen bonding contributions:

$$\mathbf{B}_i = \mathbf{P}_i \langle \exp(-\beta(\psi_{i,P} + \psi_{i,HB})) \rangle, \quad (3.85)$$

or equivalently

$$\mathbf{B}_i = \mathbf{P}_i \langle \exp(-\beta\psi_{i,P}) \exp(-\beta\psi_{i,HB}) \rangle. \quad (3.86)$$

Recall that in the hydrogen bonding lattice fluid model, the partition function was taken to be separable into explicitly independent factors: one accounting for physical interactions and ignoring hydrogen bonding, and one accounting for hydrogen bonding and ignoring physical interactions. An equivalent separation may be implemented in the insertion parameter by separating the average over a product of Boltzmann factors in equations (3.86) into the product of two averages, one including only hydrogen bonding interactions and the other including only physical interactions.

$$\mathbf{B}_i = \mathbf{P}_i \langle \exp(-\beta\psi_{i,P}) \rangle \langle \exp(-\beta\psi_{i,HB}) \rangle. \quad (3.87)$$

Without approximation, this is equivalent to

$$\mathbf{B}_i = \left[\mathbf{P}_i \exp(-\beta \langle \psi_{i,P} \rangle) \exp(-\beta \langle \psi_{i,HB} \rangle) \right. \\ \left. \langle \exp(-\beta(\psi_{i,P} - \langle \psi_{i,P} \rangle)) \rangle \langle \exp(-\beta(\psi_{i,HB} - \langle \psi_{i,HB} \rangle)) \rangle \right]. \quad (3.88)$$

Under a mean field approximation, the latter two factors are neglected, yielding

$$\mathbf{B}_i = \mathbf{P}_i \exp(-\beta \langle \psi_{i,P} \rangle) \exp(-\beta \langle \psi_{i,HB} \rangle) \\ = \mathbf{B}_{i,P} \mathbf{B}_{i,HB}. \quad (3.89)$$

The physical contribution to the insertion parameter $\mathbf{B}_{i,P} = \mathbf{P}_i \exp(-\beta \langle \psi_{i,P} \rangle)$ is then given in exactly the same way as in section 4.1.1.

The hydrogen bonding contribution to the insertion parameter $\mathbf{B}_{i,HB} = \exp(-\beta \langle \psi_{i,HB} \rangle)$ requires a new treatment recasting Veysman statistics in a single molecule basis. A framework for such an approach is as follows. As in the hydrogen bonding lattice fluid model, consider a system containing m_d types of proton donors and m_a types of proton acceptors. Each molecule of species k contains d_i^k such donor sites of type i and a_j^k such acceptor sites of type j . Such a molecule may in general participate in both intramolecular bonds and in inter-molecular bonds as both donor and receiver. The number of bonds between a donor i on the molecule and an acceptor j on a different molecule will be denoted d_{ij}^k . Likewise, the number of bonds between an acceptor j on the molecule and a donor i on a different molecule will be denoted a_{ij}^k . The number of intramolecular bonds participated in by the molecule will be denoted as b_{ij}^k . If the energy of formation of a hydrogen bond between a donor of type i and an acceptor of type j is given by E_{ij}^0 , the hydrogen bonding interaction energy of the molecule in any particular state is given by

$$\psi_{i,HB} = \frac{1}{2} \sum_{i=1}^n \sum_{j=1}^m E_{ij}^0 (d_{ij}^k + a_{ij}^k + 2b_{ij}^k). \quad (3.90)$$

The hydrogen bonding contribution to the insertion parameter is then, trivially

$$\mathbf{B}_{i,HB} = \exp\left(-\beta \left\langle \frac{1}{2} \sum_{i=1}^n \sum_{j=1}^m E_{ij}^0 (d_{ij}^k + a_{ij}^k + 2b_{ij}^k) \right\rangle\right). \quad (3.91)$$

Physically, the average over insertion energies is typically taken to be over all possible particle positions for which the interaction energy is negative. However, for the hydrogen bonding insertion energy, it is appropriate to treat this average as being over all possible hydrogen bond states of the system.

Chapter 5. Conclusions

The novel theoretical approaches presented herein have the potential to extend understanding and prediction of behavior of LCST-driven stimuli responsive polymers. The approaches address the LCST phenomenon on two scales: the macroscopic scale, at which overlapping chains in semi-dilute solution experience a phase transition at the LCST; and the nano-scale, at which isolated chains in dilute solution exhibit a coil-globule transition (CGT) near the LCST. With modest further development, the models have great potential to guide development of stimuli responsive polymers for a variety of applications. For example, the lattice fluid model for polyelectrolytes could be quantitatively fit to Poly(*N*-isopropylacrylamide) in order to allow targeted design of PNIPAAm copolymers via inclusion of charged groups in order to control the LCST. Such a model would facilitate design of PNIPAAm based drug delivery systems, among other applications.

Of additional interest would be the development of a model for the single chain LCST-driven CGT of aqueous polymers and low charge polyelectrolytes. However, a straightforward combination of the single chain lattice fluid model with the hydrogen bonding model described above has been shown to fail due to inconsistencies between insertion parameter and system partition function approaches. A framework has thus been described for the development of a self-consistent model via calculation of the hydrogen bonding contribution to the Widom insertion parameter. Such a model could be further extended to address the behavior of aqueous polyelectrolytes, including swelling transitions of smart synthetic polymers, elements of protein cold denaturation, and aspects of DNA conformational behavior. Finally, by incorporating crosslinks, the models could be generalized to quantitatively treat network polymers.

Appendix 1. Nomenclature

A_u^k	number of anionic sites of type u on a molecule of species k
a	intensive Helmholtz free energy
a_j^A	in the polyelectrolyte model, the number of association acceptors of type j on an anion of type j
a_j^k	number of association acceptors of type j on a molecule of species k ; in the model for polyelectrolytes this excludes ion hydration sites
a_j^{lu}	number of association acceptors of type j on an ion pair consisting of a cationic group of type l and an anionic group of type u
\mathbf{B}_k	insertion parameter of a molecule of species k
C_l^k	number of cationic sites of type l on a molecule of species k
d_i^C	in the polyelectrolyte model, the number of association donors of type i on a cation of type i
d_i^k	number of association donors of type i on a molecule of species k ; in the model for polyelectrolytes this excludes ion hydration sites
d_i^{lu}	number of association donor sites of type i on an ion pair consisting of a cationic group of type l and an anionic group of type u
E_{ij}^0	energy of formation of association bond between donor of type i and acceptor of type j
E_{lu}^l	energy of formation of ionic bond between cation of type l and anion of type u
$E_{L,i}$	ionic lattice energy of salt i
F_{ij}^0	Helmholtz free energy of formation of association bond between donor of type i and acceptor of type j
F_{lu}^l	Helmholtz free energy of formation of ionic bond between cation of type l and anion of type u
f_l	fraction of dissociable subunits in a polyelectrolyte chain

f_{Au}^p	fraction of anions of type u that are on polymeric molecules
f_{Cl}^p	fraction of cations of type l that are on polymeric molecules
f_{Au}^s	fraction of anions of type u that are on small molecules
f_{Cl}^s	fraction of cations of type l that are on small molecules
G	extensive free energy
g	intensive free energy
G_A	associating contribution to extensive free energy
G_E	electrostatic contribution to extensive free energy
G_{HB}	hydrogen bonding contribution to extensive free energy
G_I	ion-binding contribution to extensive free energy
G_P	physical contribution to extensive free energy
G_{ij}^0	Gibbs free energy of formation of association bond between donor of type i and acceptor of type j
G_{lu}^l	Gibbs free energy of formation of ionic bond between cation of type l and anion of type u
$H[x]$	Heaviside step function
I	ionic strength
\tilde{I}	dimensionless ionic strength
\tilde{I}_f	dimensionless contribution to ionic strength from free ions
$\tilde{I}_{p\kappa}$	dimensionless contribution from ions fixed on polymer to screened ionic strength
\tilde{I}_κ	dimensionless screened ionic strength
k_B	Boltzmann's constant
l_B	Bjerrum length
m_A	number of types of anionic sites in system
m_a	number of types of association acceptor sites in system

m_C	number of types of cationic sites in system
m_d	number of types of association donor sites in system
m_I	number of types of ions in system
N	total number of molecules of all species
N_0	unoccupied lattice sites
N_k	molecules of component k
N_C^l	total number of cationic sites of type l
N_A^u	total number of anionic sites of type u
N_{ij}	number of association bonds between donor of type i and acceptor of type j
N_{i0}	number of unbonded association donors of type i
N_{0j}	number of unbonded association acceptors of type j
N_{ij}^I	number of ionic bonds between a cation of type l and an anion of type u
N_{i0}^I	number of unbonded cationic sites of type l
N_{0u}^I	number of unbonded anionic sites of type u
P	pressure
\tilde{P}	reduced pressure
\tilde{P}_k	reduced pressure based on characteristic pressure of species k
\mathbf{P}_k	insertion probability of a molecule of species k
P_k^*	characteristic temperature of species k
Q	system partition function
Q_A	associating contribution to system partition function
Q_E	electrostatic contribution to system partition function
Q_{HB}	hydrogen bonding contribution to system partition function
Q_I	ion-binding contribution to system partition function
Q_P	physical contribution to system partition function
q	elementary charge

R	gyration radius
r	number average molecular size parameter
r_k	molecular size parameter: lattice sites per molecule in lattice theory; hard spheres per molecule in scaled particle theory
S_{ij}^0	entropy of formation of association bond between donor of type i and acceptor of type j
S_{lu}^I	entropy of formation of ionic bond between cation of type l and anion of type u
s	lattice fluid hard core volume fraction mixture average surface to volume ratio parameter; also intensive system entropy
s_k	in lattice fluid model, surface to volume ratio parameter for species k
T	absolute temperature
\tilde{T}	reduced temperature
\tilde{T}_k	reduced temperature based on characteristic temperature of species k
T_k^*	characteristic temperature of species k
t	number of mixture components
t_p	number of polymeric mixture components
t_s	number of small-molecule mixture components
V	extensive volume
V_{ij}^0	volume change of formation of association bond between donor of type i and acceptor of type j
V_{lu}^I	volume change of formation of ionic bond between cation of type l and anion of type u
v	intensive volume
v_{ij}	number of association bonds between a donor of type i and an acceptor of type j per lattice site
v_{ij}^I	number of ionic bonds between a cation of type l and an anion of type u per lattice site
v_{0j}	number of unbonded association acceptors of type j per lattice site
v_{i0}	number of unbonded association donors of type i per lattice site

v_{0u}^I	number of unbonded anionic groups of type u per lattice site
v_{l0}^I	number of unbonded cationic groups of type l per lattice site
v_A^u	number of anionic sites of type u per occupied lattice site
v_C^l	number of cationic sites of type l per occupied lattice site
v^*	mixture average volume per r
v_k^*	pure state volume of component k per r_k .
\tilde{v}	intensive reduced volume
X_{ij}	equivalent to chi-interaction parameter, modified to include surface to volume ratio parameters
x	degree of polymerization
x_k	mole fraction of component k
z_k	in the hydrogen bonding with free salt lattice fluid model, charge valency of component k ; in the polyelectrolyte mode, charge valency of ionic group of type k
α^2	polymer chain expansion factor
α_l	ionization fraction of ionic sites of type l
α_u^A	ionization fraction of anionic sites of type u
α_l^C	ionization fraction of cationic sites of type l
β	inverse of thermal energy
ϵ_0	permittivity of free space
ϵ_r	dielectric constant
ϵ_{ij}	interaction energy between a site of component i and component j
ζ	ratio of polymer to solvent characteristic temperatures
ζ_c	critical ratio of polymer to solvent characteristic temperatures
η_k	occupied volume fraction of component k
Θ	coil-globule transition temperature

$\tilde{\Theta}$	dimensionless coil-globule transition temperature
$\tilde{\Theta}_{P_{\max}}$	dimensionless coil-globule transition temperature at the high pressure hypercritical point
θ_k	surface fraction of component k
Γ_l^k	number of ionic groups of type l on a molecule of type k
κ	Debye-Huckel inverse screening length
$\tilde{\kappa}$	dimensionless Debye-Huckel inverse screening length
κ_T	isothermal compressibility
λ_t	thermal wavelength
μ_k	chemical potential of component k
$\mu_{k,A}$	associating contribution to chemical potential of component k
$\mu_{k,E}$	electrostatic contribution to chemical potential of component k
$\mu_{k,HB}$	hydrogen bonding contribution to chemical potential of component k
$\mu_{k,I}$	ion bonding contribution to chemical potential of component k
$\mu_{k,P}$	physical contribution to chemical potential of component k
$\tilde{\rho}$	reduced density; equivalently, total occupied volume fraction
ρ_k	number density of species k
ρ_k^*	characteristic density of species k
$\tilde{\rho}_I^p$	total dimensionless charge density of polymeric charges
σ_k	in the scaled particle theory, the diameter of a hard sphere of species k
σ_{-n}	hard core volume fraction mixture average of n^{th} order inverse hard sphere diameter
σ_l^A	ionic diameter of a cationic group of type l
σ_u^C	ionic diameter of an anionic group of type u
σ_i^I	in the hydrogen bonding with salt lattice fluid model, ionic diameter of an ion of species i ; in the polyelectrolyte model, ionic diameter of an ionic group of type i

ζ_n	volume fraction mixture average of n^{th} power of polymer sphere diameter to solvent sphere diameter ratio
ν_{lu}^I	intrinsic measure of extent of ionic bonding between cationic groups of type l and anionic groups of type u
Φ	ratio of polymer occupied volume fraction to total unoccupied volume fraction
φ	ratio of polymer occupied volume fraction to volume fraction that is not occupied by solvent
ϕ_k	hard-core occupied volume fraction of component k
Ψ	Gibbs partition function
$\langle \psi_k \rangle$	position-average insertion energy of a molecule of component k , for successful insertions

Appendix 2. Extended Derivations

A.2.1. Solution Stability

In section 2.2.3, equation (2.128) is stated to follow from equation (2.127) via the chain rule. An extended development of this statement follows. In general,

$$G = G(\{N_k\}). \quad (\text{A2.1})$$

Equivalently,

$$G = G\left(\left\{\phi_{k \neq t}(\{N_k\})\right\}, \phi_t\left(\left\{\phi_{k \neq t}(\{N_k\})\right\}\right)\right), \quad (\text{A2.2})$$

where the t^{th} composition fraction has been separated out. Composition fractions are in general constrained by the condition that

$$\sum_{k=1}^t \phi_k = 1, \quad (\text{A2.3})$$

so that the t^{th} composition fraction can be written as a function of the other $t-1$ fractions.

The free energy may then be written with this substitution having been made:

$$g = \hat{g}\left(\left\{\phi_{k \neq t}(\{N_k\})\right\}\right), \quad (\text{A2.4})$$

where the hat denotes the form of g in which the constraint (A2.3) has been applied to explicitly eliminate the t^{th} composition fraction. Hence

$$\left(\frac{\partial \hat{g}}{\partial \phi_k}\right)_{\{\phi_{l \neq k}\}} = \left(\frac{\partial g}{\partial \phi_k}\right)_{\{\phi_{l \neq k, t}\}}, \quad (\text{A2.5})$$

which yields

$$\left(\frac{\partial g}{\partial N_k}\right)_{\{N_{j \neq k}\}} = \left(\frac{\partial \hat{g}\left(\left\{\phi_{k \neq t}(\{N_k\})\right\}\right)}{\partial N_k}\right)_{\{N_{j \neq k}\}} = \sum_{u=1}^{t-1} \left(\frac{\partial g}{\partial \phi_u}\right)_{\{\phi_{j \neq u, t}\}} \left(\frac{\partial \phi_u}{\partial N_k}\right)_{\{N_{j \neq k}\}}. \quad (\text{A2.6})$$

Then pulling the k^{th} term out of the summation in equation (A2.6) gives

$$\left(\frac{\partial g}{\partial N_k}\right)_{\{N_{j \neq k}\}} = \left(\frac{\partial g}{\partial \phi_k}\right)_{\{\phi_{j \neq u, t}\}} \left(\frac{\partial \phi_k}{\partial N_k}\right)_{\{N_{j \neq k}\}} + \sum_{u \neq k}^{t-1} \left(\frac{\partial g}{\partial \phi_u}\right)_{\{\phi_{j \neq u, t}\}} \left(\frac{\partial \phi_u}{\partial N_k}\right)_{\{N_{j \neq k}\}}. \quad (\text{A2.7})$$

Recalling the form of the composition variable given by equation (2.125),

$$\left(\frac{\partial \phi_k}{\partial N_k} \right)_{\{N_{j \neq k}\}} = \frac{r_k}{rN} (1 - \phi_k), \quad (\text{A2.8})$$

and

$$\left(\frac{\partial \phi_{u \neq k}}{\partial N_k} \right)_{\{N_{j \neq k}\}} = -\frac{r_k}{rN} \phi_u. \quad (\text{A2.9})$$

Combining equations (A2.7) through (A2.9) then yields

$$\left(\frac{\partial g}{\partial N_k} \right)_{\{N_{j \neq k}\}} = \frac{r_k}{rN} (1 - \phi_k) \left(\frac{\partial g}{\partial \phi_k} \right)_{\{\phi_{j \neq u, l}\}} - \sum_{u \neq k}^{t-1} \frac{r_k}{rN} \phi_u \left(\frac{\partial g}{\partial \phi_u} \right)_{\{\phi_{j \neq u, l}\}}, \quad (\text{A2.10})$$

and substitution of equation (A2.10) into equation (2.127) gives

$$\left(\frac{\partial g}{\partial \phi_k} \right)_{\{\phi_{j \neq k, l}\}} = \frac{1}{r_k (1 - \phi_k)} \left[\mu_k - r_k g + r_k \sum_{u \neq k}^{t-1} \phi_u \left(\frac{\partial g}{\partial \phi_u} \right)_{\{\phi_{j \neq u, l}\}} \right]. \quad (\text{A2.11})$$

Differentiating equation (A2.11) with respect to a second composition variable ϕ_l then yields equation (2.128).

A.2.2. Scaled Particle Theory Coil-Globule Transition

As given by equation (3.43) the general SPT insertion probability for a single sphere is given by

$$-\ln \mathbf{P}_k = \ln(1 + y) + y \left[\frac{(3\sigma_{-1}\sigma_k + 3\sigma_{-2}\sigma_k^2 + \sigma_{-3}\sigma_k^3)}{+(9\sigma_{-1}^2\sigma_k^2/2 + 3\sigma_{-1}\sigma_{-2}\sigma_k^3)y + 3\sigma_{-1}^3\sigma_k^3y^2} \right]. \quad (\text{A2.12})$$

As given by equation (3.15), the overall insertion probability of the chain is given by

$$\mathbf{P}_p = \prod_{j=0}^{r_p-1} \mathbf{P}_j, \quad (\text{A2.13})$$

where \mathbf{P}_j is the insertion probability of segment j of the chain and is a function of the number of previously inserted segments. Combining equations (A2.12) and (A2.13) yields

$$\begin{aligned}
-\ln \mathbf{P}_p &= \ln \left[\prod_{j=0}^{r_p-1} \mathbf{P}_{p,j} \right] = \sum_{j=0}^{r_p-1} \ln(\mathbf{P}_{p,j}) \\
&= \sum_{j=0}^{r_p-1} \left[\ln(1+y_j) + y_j \left[\frac{(3\sigma_{-1}\sigma_p + 3\sigma_{-2}\sigma_p^2 + \sigma_{-3}\sigma_p^3)}{(9\sigma_{-1}^2\sigma_p^2/2 + 3\sigma_{-1}\sigma_{-2}\sigma_p^3)y_j + 3\sigma_{-1}^3\sigma_p^3 y_j^2} \right] \right].
\end{aligned}
\tag{A2.14}$$

In order to implement the summation in equation (A2.14), it is useful to split all variables into contributions that are and are not functions of j .

$$\begin{aligned}
-\ln \mathbf{P}_p &= -\ln \prod_{j=0}^{r_p-1} \left(1 - \eta_s - \frac{j}{r_p} \eta_p \right) \\
&+ \sum_{j=0}^{r_p-1} \left[\frac{1}{1 - \tilde{\rho}_j} \left[\frac{(3(\tilde{\rho}\sigma_{s,-1}\sigma_p + \eta_{p,j}) + 3(\tilde{\rho}\sigma_{s,-2}\sigma_p^2 + \eta_{p,j}) + (\tilde{\rho}\sigma_{s,-3}\sigma_p^3 + \eta_{p,j}))}{(9(\tilde{\rho}\sigma_{s,-1}\sigma_p + \eta_{p,j})^2/2 + 3(\tilde{\rho}\sigma_{s,-1}\sigma_p + \eta_{p,j})(\tilde{\rho}\sigma_{s,-2}\sigma_p^2 + \eta_{p,j})) \frac{1}{1 - \tilde{\rho}_j}} \right. \right. \\
&\quad \left. \left. + 3(\tilde{\rho}\sigma_{s,-1}\sigma_p + \eta_{p,j})^3 \left(\frac{1}{1 - \tilde{\rho}_j} \right)^2 \right] \right],
\end{aligned}
\tag{A2.15}$$

where

$$\eta_{p,j} = \eta_p \frac{j}{r_p}, \tag{A2.16}$$

$$\tilde{\rho}_j = \eta_{p,j} + \eta_s, \tag{A2.17}$$

$$y_j = \frac{\tilde{\rho}_j}{1 - \tilde{\rho}_j}, \tag{A2.18}$$

and

$$\sigma_{s,-k} = \sum_{i \neq p} \frac{\eta_i}{\eta_s} \sigma_i^{-k}, \tag{A2.19}$$

so that

$$\sigma_{-k,j} = \frac{1}{\tilde{\rho}_j} \left[\eta_s \sigma_{s,-k} + \eta_{p,j} \sigma_p^{-k} \right]. \quad (\text{A2.20})$$

The only factors in equation (A2.15) that are a function of j are now $\frac{1}{1-\tilde{\rho}_j}$, $\eta_{p,j}$, and j

itself. Equation (A2.15) can thus be rewritten as

$$\begin{aligned} -\ln \mathbf{P}_p = & -\ln \left[(1-\eta_s) \left(\frac{\eta_p}{r_p} \right)^{r_p} \left(\frac{r_p}{\eta_p} \right)^{r_p-1} \prod_{j=1}^{r_p-1} \left[\frac{r_p}{\eta_p} (1-\eta_s) - j \right] \right] \\ & + (3\zeta_1 + 3\zeta_2 + \zeta_3) \frac{r_p}{\eta_p} \left(\sum_{j=0}^{r_p} \frac{1}{r_p/\varphi - j} - \frac{\Phi}{r_p} \right) + 7 \left(\sum_{j=0}^{r_p} \frac{j}{r_p/\varphi - j} - \Phi \right) \\ & + \left(\frac{9}{2} \zeta_1^2 + 3\zeta_1 \zeta_2 \right) \left(\frac{r_p}{\eta_p} \right)^2 \left(\sum_{j=0}^{r_p} \frac{1}{(r_p/\varphi - j)^2} - \frac{\Phi^2}{r_p^2} \right) \\ & + (12\zeta_1 + 3\zeta_2) \frac{r_p}{\eta_p} \left(\sum_{j=0}^{r_p} \frac{j}{(r_p/\varphi - j)^2} - \frac{\Phi^2}{r_p} \right) + \frac{15}{2} \left(\sum_{j=0}^{r_p} \left(\frac{j}{r_p/\varphi - j} \right)^2 - \Phi^2 \right) \\ & + 3\zeta_1^3 \left(\frac{r_p}{\eta_p} \right)^3 \left(\sum_{j=0}^{r_p} \frac{1}{(r_p/\varphi - j)^3} - \frac{\Phi^3}{r_p^3} \right) + 9\zeta_1^2 \left(\frac{r_p}{\eta_p} \right)^2 \left(\sum_{j=0}^{r_p} \frac{j}{(r_p/\varphi - j)^3} - \frac{\Phi^3}{r_p^2} \right) \\ & + 9\zeta_1 \frac{r_p}{\eta_p} \left(\sum_{j=0}^{r_p} \frac{j^2}{(r_p/\varphi - j)^3} - \frac{\Phi^3}{r_p} \right) + 3 \left(\sum_{j=0}^{r_p} \left(\frac{j}{r_p/\varphi - j} \right)^3 - \Phi^3 \right) \end{aligned} \quad (\text{A2.21})$$

where

$$\varphi \equiv \frac{\eta_p}{1-\eta_s}, \quad (\text{A2.22})$$

$$\zeta_k \equiv \sum_{i \neq p} \eta_i \left(\frac{\sigma_p}{\sigma_i} \right)^k, \quad (\text{A2.23})$$

and

$$\Phi \equiv \frac{\eta_p}{1-\tilde{\rho}} = \frac{\varphi}{1-\varphi}. \quad (\text{A2.24})$$

For a sufficiently long chain, the summations in equation (A2.21) can be approximated as integrals:

$$\begin{aligned}
-\ln \mathbf{P}_p = & -\ln \left[(1-\eta_s) \left(\frac{\eta_p}{r_p} \right)^{r_p} \left(\frac{r_p}{\eta_p} \right)^{r_p-1} \prod_{j=1}^{r_p-1} \left[\frac{r_p}{\eta_p} (1-\eta_s) - j \right] \right] \\
& + (3\zeta_1 + 3\zeta_2 + \zeta_3) \frac{r_p}{\eta_p} \left(\int_0^{r_p} \frac{1}{r_p/\varphi - j} dj - \frac{\Phi}{r_p} \right) + 7 \left(\int_0^{r_p} \frac{j}{r_p/\varphi - j} dj - \Phi \right) \\
& + \left(\frac{9}{2} \zeta_1^2 + 3\zeta_1 \zeta_2 \right) \left(\frac{r_p}{\eta_p} \right)^2 \left(\int_0^{r_p} \frac{1}{(r_p/\varphi - j)^2} dj - \frac{\Phi^2}{r_p^2} \right) \\
& + (12\zeta_1 + 3\zeta_2) \frac{r_p}{\eta_p} \left(\int_0^{r_p} \frac{j}{(r_p/\varphi - j)^2} dj - \frac{\Phi^2}{r_p} \right) + \frac{15}{2} \left(\int_0^{r_p} \left(\frac{j}{r_p/\varphi - j} \right)^2 dj - \Phi^2 \right) \\
& + 3\zeta_1^3 \left(\frac{r_p}{\eta_p} \right)^3 \left(\int_0^{r_p} \frac{1}{(r_p/\varphi - j)^3} dj - \frac{\Phi^3}{r_p^3} \right) + 9s_1^2 \left(\frac{r_p}{\eta_p} \right)^2 \left(\int_0^{r_p} \frac{j}{(r_p/\varphi - j)^3} dj - \frac{\Phi^3}{r_p^2} \right) \\
& + 9\zeta_1 \frac{r_p}{\eta_p} \left(\int_0^{r_p} \frac{j^2}{(r_p/\varphi - j)^3} dj - \frac{\Phi^3}{r_p} \right) + 3 \left(\int_0^{r_p} \left(\frac{j}{r_p/\varphi - j} \right)^3 dj - \Phi^3 \right) \quad , (A2.25)
\end{aligned}$$

Equation (A2.25) then becomes

$$\begin{aligned}
-\ln \mathbf{P}_p = & -r_p \left[-1 - \left(\frac{1}{\varphi} - 1 \right) \ln(1-\varphi) + \ln(1-\eta_s) \right] \\
& - \frac{r_p}{\varphi} \ln(1-\varphi) \left[1 + \frac{\zeta_3}{(1-\eta_s)} \right] - 9 \frac{\zeta_1}{(1-\eta_s)} \frac{\varphi^2}{(1-\varphi)^3} - 3 \left(\frac{\varphi}{1-\varphi} \right)^3 + \frac{1}{2} r_p \\
& + \frac{1}{1-\varphi} \left[-\frac{3\zeta_1 + 3\zeta_2 + \zeta_3}{(1-\eta_s)} + r_p \left(\frac{3\zeta_1^3}{2(1-\eta_s)^3} + \frac{9}{2} \frac{\zeta_1^2 + 3\zeta_1 \zeta_2}{(1-\eta_s)^2} + \frac{3\zeta_1 + 3\zeta_2}{1-\eta_s} - \frac{3}{2} \right) \right] \\
& + \frac{\varphi}{1-\varphi} \left[-7 + 3r_p \right] + \left(\frac{1}{1-\varphi} \right)^2 \left(-\frac{9}{2} \frac{\zeta_1^2 + 3\zeta_1 \zeta_2}{(1-\eta_s)^2} + \frac{3}{2} r_p \frac{\zeta_1^3}{(1-\eta_s)^3} \right) \\
& + 3 \frac{\varphi}{(1-\varphi)^2} \left(-(4s_1 + 1s_2) \frac{1}{(1-\eta_s)} + \frac{1}{2} r_p \left(3 \frac{\zeta_1^2}{(1-\eta_s)^2} + 3 \frac{\zeta_1}{(1-\eta_s)} + 1 \right) \right) \\
& + -\frac{15}{2} \left(\frac{\varphi}{1-\varphi} \right)^2 - 3 \frac{\zeta_1^3}{(1-\eta_s)^3} \left(\frac{1}{1-\varphi} \right)^3 - 9 \frac{\zeta_1^2}{(1-\eta_s)^2} \frac{\varphi}{(1-\varphi)^3} \quad , (A2.26)
\end{aligned}$$

The chain interaction energy is given by (3.47) as explained in that section. Applying this along with (A2.26) to yield the insertion parameter and then applying equation (3.8) for the gyration radius and equation (3.9) for the CGT yields equations (3.49) and (3.53), respectively.

Appendix 3. Mathematica code

A.3.1. LCST in Aqueous Solution with Salt

The numerical method for calculation of the LCST of uncharged polymers in salt solutions is as follows. The solution density and hydrogen bond counts are first calculated from the equations of state as a function of polymer and anion volume fractions over a range of temperature. The equations of state are often very sensitive to guess values, and several tactics are thus employed to obtain correct results. Firstly, as EOS calculation proceeds over the grid of compositions and temperatures, previous EOS results are used as guesses via finite-difference-like extrapolation methods. During this process, any gridpoint for which a numerical problem is encountered is flagged. Once this initial solving process is complete, a series of smart algorithms then attempt to find a correct solution to the equations of state at these gridpoints by attempting better guesses based upon interpolation or extrapolation of nearby successful gridpoints. Three dimensional plots are then produced of EOS results in order to enable the user to visually determine whether any points are still flagged as incorrect and repeat the above correction process as necessary.

Once the equations of state are solved over composition and temperature grids, the results are interpolated in isothermal planes using Mathematica's built-in interpolation function. Numerical derivatives of these data sets are then taken with respect to polymer and anion volume fractions. These interpolation objects are fed into the governing spinodal equation for the solution, yielding an interpolated spinodal curve at each temperature. Spinodal data is then re-interpolated in the temperature-polymer volume fraction plane in order to be consistent with the usual T-x phase diagram plane. The LCST itself is then determined as a function of salt concentration by finding the minimum of the spinodal with temperature over a range of salt concentration.

Representative Mathematica code employing this approach follows:

Constants

`FILENAME = "Salt 014" (*Data file save name*)`

`Salt 014`

■ Physical Constants

`kB = 1.3806503 10-23; (*Boltzmann's Constant*)`

`nA = 6.022 1023; (*Avogadro's number*)`

`q = 1.60217646 10-19; (*elementary charge*)`

`ε0 = 8.854187817 10-12; (*electric permittivity of vacuum*)`

■ Trivial berthelot self interaction parameters

`ξ1,1 = 1;`

`ξ2,2 = 1;`

`ξ3,3 = 1;`

`ξ4,4 = 1;`

Input parameters

■ Mixture

`t = 4 (*number of components, in psuedocomponent form*)`

`4`

■ Lattice

`ξ1,2 = 1.0472; (*Berthelot prefactor 12*)`

`ξ1,3 = 1; (*Berthelot prefactor 13*)`

`ξ1,4 = 1; (*Berthelot prefactor 14*)`

`ξ2,4 = 1; (*Berthelot prefactor 23*)`

`ξ2,3 = 1; (*Berthelot prefactor 24*)`

`ξ3,4 = 1; (*Berthelot prefactor 34*)`

sr_{1,2} = 1.3424; (*water-polymer surface area ratio*)

sr_{1,3} = 1; (*water-cation surface area ratio*)

sr_{1,4} = 1; (*water-anion surface area ratio*)

■ Hydrogen Bonding

n = 2; (*Number of types of hydrogen bond donors*)

m = 3; (*Number of types of hydrogen bond acceptors*)

E0 = {{-1.55 10⁴, -1.1 10⁴}, {-1.42 10⁴, -1 10⁴}, {-1 10⁴, 0}}/nA
(*Hydrogen bond energies of formation*)

{{-2.5739 × 10⁻²⁰, -1.82664 × 10⁻²⁰},
{-2.35802 × 10⁻²⁰, -1.66058 × 10⁻²⁰}, {-1.66058 × 10⁻²⁰, 0}}

S0 = {{-16.6, -16}, {-16.0, -16}, {-16, -16}}/nA
(*Hydrogen bond entropies of formation*)

{{-2.75656 × 10⁻²³, -2.65692 × 10⁻²³},
{-2.65692 × 10⁻²³, -2.65692 × 10⁻²³}, {-2.65692 × 10⁻²³, -2.65692 × 10⁻²³}}

V0 = {{-4.2 10⁻⁶, 0}, {-8.5 10⁻⁷, 0}, {0, 0}}/nA
(*Hydrogen bond volumes of formation*)

{{-6.97443 × 10⁻³⁰, 0}, {-1.41149 × 10⁻³⁰, 0}, {0, 0}}

■ Component 1 (Solvent)

z₁ = 0; (*valency*)

■ Lattice

Ts₁ = 518; (*Characteristic temperature*)

Ps₁ = 4.75 10⁸; (*Characteristic pressure*)

ρs₁ = 853; (*Characteristic density*)

Mw₁ = 18 10⁻³ / nA (*Molecular weight*)

2.98904 × 10⁻²⁶

■ Hydrogen Bonding

d1₁ = 2;

$d1_2 = 0;$

$a1_1 = 2;$

$a1_2 = 0;$

$a1_3 = 0;$

■ Component 2 (Polymer)

$z_2 = 0;$ (*valency*)

■ Lattice

$Ts_2 = 541;$ (*Characteristic temperature*)

$Ps_2 = 6.05 \cdot 10^8;$ (*Characteristic pressure*)

$\rho s_2 = 1172;$ (*Characteristic density*)

$Mw_2 = 6 \cdot 10^5 \cdot 10^{-3} / nA$ (*Molecular Weight*)

9.96347×10^{-22}

$monMw_2 = 44 \cdot 10^{-3} / nA$ (*monomer residue molecular weight*)

7.30654×10^{-26}

■ Hydrogen Bonding

$d2_1 = 0;$

$d2_2 = 0;$

$a2_1 = 0;$

$a2_2 = DOP;$

$a2_3 = 0;$

■ Component 3 (Cation)

$Ts_3 = 400;$ (*Characteristic temperature*)

$Ps_3 = 1.92 \cdot 10^9;$ (*Characteristic pressure*)

$\rho s_3 = 3468;$ (*Characteristic density*)

$Mw_3 = 23 \cdot 10^{-3} / nA$ (*Molecular Weight*)

3.81933×10^{-26}

$z_3 = 1$; (*cation charge*)

$a_3 = v s_3^{1/3}$;

■ Hydrogen Bonding

$d_{31} = 0$;

$d_{32} = 6$;

$a_{31} = 0$;

$a_{32} = 0$;

$a_{33} = 0$;

■ Component 4 (Anion)

$Ts_4 = 104$; (*Characteristic temperature*)

$Ps_4 = 2.48 \cdot 10^8$; (*Characteristic pressure*)

$\rho s_4 = 1870$; (*Characteristic density*)

$Mw_4 = 18 \cdot 10^{-3} / n_A$ (*Molecular Weight*)

2.98904×10^{-26}

$monMw_4 = 35 \cdot 10^{-3} / n_A$ (*monomer residue molecular weight*)

5.81202×10^{-26}

$z_4 = -1$; (*anion charge*)

$a_4 = v s_4^{1/3}$;

■ Hydrogen Bonding

$d_{41} = 0$;

$d_{42} = 0$;

$a_{41} = 0$;

$a_{42} = 0$;

$a_{43} = 6$;

Calculated parameters

$$DOP = Mw_2 / monMw_2$$

$$13\,636.4$$

■ Inverse Berthelot indices

$$\xi_{2,1} = \xi_{1,2};$$

$$\xi_{3,1} = \xi_{1,3};$$

$$\xi_{4,1} = \xi_{1,4};$$

$$\xi_{3,2} = \xi_{2,3};$$

$$\xi_{4,2} = \xi_{2,4};$$

$$\xi_{4,3} = \xi_{3,4};$$

■ Derivatives ratios

$$SF_{2,3} = \frac{SF_{1,3}}{SF_{1,2}};$$

$$SF_{2,4} = \frac{SF_{1,4}}{SF_{1,2}};$$

$$SF_{3,4} = \frac{SF_{1,4}}{SF_{1,3}};$$

$$SF_{2,1} = \frac{1}{SF_{1,2}};$$

$$SF_{3,1} = \frac{1}{SF_{1,3}};$$

$$SF_{4,1} = \frac{1}{SF_{1,4}};$$

$$SF_{3,2} = \frac{1}{SF_{2,3}};$$

$$SF_{4,2} = \frac{1}{SF_{2,4}};$$

$$SF_{4,3} = \frac{1}{SF_{3,4}};$$

$$s_{1,1} = 1;$$

$$s_{2,2} = 1;$$

$$s_{3,3} = 1;$$

$$s_{4,4} = 1;$$

- **Dummy s values**

$$s_1 = 1;$$

$$s_2 = s_1 s_{2,1};$$

$$s_3 = s_1 s_{3,1};$$

$$s_4 = s_1 s_{4,1};$$

- **Characteristic volume, self interaction energy, and characteristic size**

- **Solvent and Polymer**

$$\text{For } [k = 1, k < t + 1, k++, v_{s_k} = \frac{T s_k k B}{P s_k}; \epsilon_{s_k} = k B T s_k; r_k = \frac{M w_k}{\rho s_k v_{s_k}}]$$

- **Mixture**

$$\text{For } [k = 1, k < t + 1, k++,$$

$$\text{For } [l = k + 1, l < t + 1, l++,$$

$$\epsilon_{s_{k,l}} = \xi_{k,l} (\epsilon_{s_k} \epsilon_{s_l})^{1/2}]]$$

(*Berthelot rule for cross-interactions*)

Variable parameters

- **Dielectric constant**

$$\epsilon_r = 236.99865609725444 - 0.7064317817094816 T + 0.0005877578200716843 T^2;$$

(*Dielectric constant of water based on data from internet

w/ temp dependence*)

- **Volume fractions**

$$\phi_1 = 1 - \phi_2 - \phi_3 - \phi_4$$

$$1 - \phi_2 - \phi_3 - \phi_4$$

$$\phi_3 = -\phi_4 \frac{r_3}{r_4} \frac{z_4}{z_3}$$

$$1.38689 \phi_4$$

■ Surface Fractions

$$\text{For } [k = 1, k < t + 1, k++, \theta_k = \frac{\phi_k}{\sum_{i=1}^t (sr_{i,k} \phi_i)}]$$

■ Mixture averaged properties

$$\text{rov} = \left(\sum_{k=1}^t \frac{\phi_k}{r_k} \right)^{-1} \quad (*\text{Mixture characteristic size}*)$$

$$\frac{1}{0.0000145225 \phi_2 + 0.429672 (1 - \phi_2 - 2.38689 \phi_4) + 0.724445 \phi_4}$$

$$\text{vov} = \text{Simplify} \left[\sum_{k=1}^t \phi_k v_{s_k} \right] \quad (*\text{Mixture characteristic volume}*)$$

$$1.50564 \times 10^{-29} - 2.71037 \times 10^{-30} \phi_2 - 2.61588 \times 10^{-29} \phi_4$$

$$\text{sov} = \text{Simplify} \left[\sum_{k=1}^t \phi_k s_k \right] \quad (*\text{Dummy value of overall } s, *$$

actually scales with s_1 but since only ratios matter it will cancel out*)

$$1 - 0.255066 \phi_2 + 2.22045 \times 10^{-16} \phi_4$$

$$\text{For } [k = 1, k < t + 1, k++,$$

$$\text{For } [l = k + 1, l < t + 1, l++,$$

$$X_{k,l} = \frac{1}{k_B T} (\epsilon s_k + sr_{k,l} \epsilon s_l - 2 sr_{k,l}^{1/2} \epsilon s_{k,l})]$$

$$\epsilon = \sum_{k=1}^t \sum_{l=1}^t \theta_k \theta_l \xi_{k,l} (\epsilon s_k \epsilon s_l)^{1/2} \sum_{i=1}^t \phi_i (sr_{i,k} sr_{i,l})^{1/2};$$

$$\text{Tred} = T k_B / \epsilon; \quad (*\text{System reduced temperature}*)$$

$$\text{Pred} = P \text{vov} / \epsilon; \quad (*\text{System reduced pressure}*)$$

■ Mole Fractions

■ Component properties

$$\text{For } [k = 1, k < t + 1, k++, \text{Tr}_k = T / T_{s_k}; \text{Pr}_k = P / P_{s_k}]$$

■ Hydrogen bonding

$$vH = \sum_{i=1}^n \sum_{j=1}^m v_{i,j} \text{ (*So-called hydrogen bonding fraction*)}$$

$$v_{1,1} + v_{1,2} + v_{1,3} + v_{2,1} + v_{2,2} + v_{2,3}$$

$$rbar = \frac{1}{1 / rov - vH}$$

$$1 / (0.0000145225 \phi_2 + 0.429672 (1 - \phi_2 - 2.38689 \phi_4) + 0.724445 \phi_4 - v_{1,1} - v_{1,2} - v_{1,3} - v_{2,1} - v_{2,2} - v_{2,3})$$

$$\text{For [} i = 1, i < n + 1, i++, vd_i = \frac{d1_i \phi_1}{r_1} + \frac{d2_i \phi_2}{r_2} + \frac{d3_i \phi_3}{r_3} + \frac{d4_i \phi_4}{r_4} ;]$$

(*donor bond fractions*)

$$\text{For [} j = 1, j < m + 1, j++, va_j = \frac{a1_j \phi_1}{r_1} + \frac{a2_j \phi_2}{r_2} + \frac{a3_j \phi_3}{r_3} + \frac{a4_j \phi_4}{r_4} ;]$$

(*acceptor bond fractions*)

$$\text{For [} i = 1, i < n + 1, i++, v_{i,0} = vd_i - \sum_{j=1}^m v_{i,j} ;]$$

(*unbonded donor fractions*)

$$\text{For [} j = 1, j < m + 1, j++, v_{0,j} = va_j - \sum_{i=1}^n v_{i,j} ;]$$

(*unbonded acceptor fractions*)

For [$i = 1, i < n + 1, i++,$

$$\text{For [} j = 1, j < m + 1, j++, G0_{i,j} = E0[[j, i]] + P V0[[j, i]] - T S0[[j, i]]]]$$

(*Hydrogen bond free energy of formation*)

■ Coulombic properties

$$IB = \frac{q^2}{4 \pi \epsilon_0 \epsilon r k_B T} ;$$

$$IS = \frac{1}{2} \rho \left(\frac{\phi_3}{r_3} z_3^2 + \frac{\phi_4}{r_4} z_4^2 \right) ;$$

$$xred = \left((8 \pi IS)^{3/2} \left(\frac{IB^3}{vov} \right)^{1/2} \right)^{1/3} ;$$

$$IS\kappa = \frac{1}{2} \rho \left(\frac{\phi_3}{r_3} \frac{z_3^2}{1 + \frac{\kappa red a_3}{vov^{1/3}}} + \frac{\phi_4}{r_4} \frac{z_4^2}{1 + \frac{\kappa red a_4}{vov^{1/3}}} \right);$$

$$IS2\kappa = \frac{1}{2} \rho \left(\frac{\phi_3}{r_3} \frac{\kappa red a_3}{vov^{1/3}} \frac{z_3^2}{\left(1 + \frac{\kappa red a_3}{vov^{1/3}}\right)^2} + \frac{\phi_4}{r_4} \frac{\kappa red a_4}{vov^{1/3}} \frac{z_4^2}{\left(1 + \frac{\kappa red a_4}{vov^{1/3}}\right)^2} \right);$$

$$E0Scoul = Tred \frac{\kappa red^3 (IS\kappa - IS2\kappa)}{32 \pi IS};$$

Governing equations

■ Free Energy and Chemical Potential

■ Component 2 chemical potential

$$\beta\mu_{2LF} = \text{Log}[\phi_2] + 1 - \frac{r_2}{rov} + r_2 \left(\frac{-\rho + \frac{Pr_2}{\rho}}{Tr_2} + \left(\frac{1}{\rho} - 1\right) \text{Log}[1 - \rho] + \frac{1}{r_2} \text{Log}[\rho] \right) +$$

$$r_2 \rho (\theta_1 sr_{2,1} X_{1,2} + \theta_3 X_{2,3} + \theta_4 X_{2,4} - \theta_1 \theta_2 sr_{2,1} X_{1,2} - \theta_1 \theta_3 sr_{2,1} X_{1,3} -$$

$$\theta_1 \theta_4 sr_{2,1} X_{1,4} - \theta_2 \theta_3 X_{2,3} - \theta_2 \theta_4 X_{2,4} - \theta_3 \theta_4 sr_{2,3} X_{3,4});$$

(«Lattice Fluid Contribution»)

$$\beta\mu_{2A} = r_2 vH - \sum_{i=1}^n \left(d_{2,i} \text{Log} \left[\frac{vd_i}{v_{i,0}} \right] \right) - \sum_{j=1}^m \left(a_{2,j} \text{Log} \left[\frac{va_j}{v_{0,j}} \right] \right);$$

(«Associationg Contribution»)

$$\beta\mu_{2E} = - \frac{\kappa red^3}{16 \pi IS} \left((IS\kappa - IS2\kappa) \left(\frac{z_2^2}{2 IS} - \frac{vs_2 r_2}{vov \rho} \right) + \frac{z_2^2}{1 + \kappa red \frac{a_2}{vov^{1/3}}} \right);$$

(«Electrosatic Contribution»)

$$\beta\mu_2 = \beta\mu_{2LF} + \beta\mu_{2A} + \beta\mu_{2E};$$

■ Component 3 chemical potential

$$\beta\mu_{3LF} = \text{Log}[\phi_3] + 1 - \frac{r_3}{rov} + r_3 \left(\frac{-\rho + \frac{Pr_3}{\rho}}{Tr_3} + \left(\frac{1}{\rho} - 1\right) \text{Log}[1 - \rho] + \frac{1}{r_3} \text{Log}[\rho] \right) +$$

$$r_3 \rho (\theta_1 sr_{3,1} X_{1,3} + \theta_2 sr_{3,2} X_{2,3} + \theta_4 X_{3,4} - \theta_1 \theta_2 sr_{3,1} X_{1,2} - \theta_1 \theta_3 sr_{3,1} X_{1,3} -$$

$$\theta_1 \theta_4 sr_{3,1} X_{1,4} - \theta_2 \theta_3 sr_{3,2} X_{2,3} - \theta_2 \theta_4 sr_{3,2} X_{2,4} - \theta_3 \theta_4 X_{3,4});$$

(«Lattice Fluid Contribution»)

$$\beta\mu_{3A} = r_3 vH - \sum_{i=1}^n \left(d_{3i} \text{Log} \left[\frac{vd_i}{v_{i,0}} \right] \right) - \sum_{j=1}^m \left(a_{3j} \text{Log} \left[\frac{va_j}{v_{0,j}} \right] \right);$$

(*Associating Contribution*)

$$\beta\mu_{3E} = -\frac{\kappa red^3}{16 \pi IS} \left((IS\kappa - IS2\kappa) \left(\frac{z_3^2}{2 IS} - \frac{vs_3 r_3}{vov \rho} \right) + \frac{z_3^2}{1 + \kappa red \frac{a_3}{vov^{1/3}}} \right);$$

(*Electrostatic Contribution*)

$$\beta\mu_3 = \beta\mu_{3LF} + \beta\mu_{3A} + \beta\mu_{3E};$$

■ Component 4 chemical potential

$$\beta\mu_{4LF} = \text{Log}[\phi_4] + 1 - \frac{r_4}{rov} + r_4 \left(\frac{-\rho + \frac{Pr_4}{\rho}}{Tr_4} + \left(\frac{1}{\rho} - 1 \right) \text{Log}[1 - \rho] + \frac{1}{r_4} \text{Log}[\rho] \right) +$$

$$r_4 \rho (\theta_1 sr_{4,1} X_{1,4} + \theta_2 sr_{4,2} X_{2,4} + \theta_3 sr_{4,3} X_{3,4} - \theta_1 \theta_2 sr_{4,1} X_{1,2} - \theta_1 \theta_3 sr_{4,1} X_{1,3} - \theta_1 \theta_4 sr_{4,1} X_{1,4} - \theta_2 \theta_3 sr_{4,2} X_{2,3} - \theta_2 \theta_4 sr_{4,2} X_{2,4} - \theta_3 \theta_4 sr_{4,3} X_{3,4});$$

(*Lattice fluid Contribution*)

$$\beta\mu_{4A} = r_4 vH - \sum_{i=1}^n \left(d_{4i} \text{Log} \left[\frac{vd_i}{v_{i,0}} \right] \right) - \sum_{j=1}^m \left(a_{4j} \text{Log} \left[\frac{va_j}{v_{0,j}} \right] \right);$$

(*Associating Contribution*)

$$\beta\mu_{4E} = -\frac{\kappa red^3}{16 \pi IS} \left((IS\kappa - IS2\kappa) \left(\frac{z_4^2}{2 IS} - \frac{vs_4 r_4}{vov \rho} \right) + \frac{z_4^2}{1 + \kappa red \frac{a_4}{vov^{1/3}}} \right);$$

(*Electrostatic Contribution*)

$$\beta\mu_4 = \beta\mu_{4LF} + \beta\mu_{4A} + \beta\mu_{4E};$$

■ Free energy

$$\beta g_{LF} = -\frac{\rho}{Tred} + \frac{Pred}{\rho Tred} + \left(\frac{1}{\rho} - 1 \right) \text{Log}[1 - \rho] + \frac{1}{rov} \text{Log}[\rho] + \left(\sum_{k=1}^c \frac{\phi_k}{r_k} \text{Log}[\phi_k] \right);$$

(*Lattice Fluid Contribution*)

$$\beta g_A = vH + \left(\sum_{i=1}^n vd_i \text{Log} \left[\frac{v_{i,0}}{vd_i} \right] \right) + \left(\sum_{j=1}^m va_j \text{Log} \left[\frac{v_{0,j}}{va_j} \right] \right);$$

(*Associating Contribution*)

$$\beta g_E = -\frac{\kappa red^3 IS\kappa}{16 \pi IS};$$

(*Electrostatic Contribution*)

$$\beta g = \beta g_{LF} + \beta g_A + \beta g_E;$$

- Spinodal Equations

- Set up spinodal matrix

$$\text{SpinMat} = \{ \{ \text{dg}_{2,2}, \text{dg}_{2,4} \}, \{ \text{dg}_{4,2}, \text{dg}_{4,4} \} \};$$

$$\text{MatrixForm}[\text{SpinMat}]$$

$$\begin{pmatrix} \text{dg}_{2,2} & \text{dg}_{2,4} \\ \text{dg}_{4,2} & \text{dg}_{4,4} \end{pmatrix}$$

$$\text{Spinodal} = \text{Det}[\text{SpinMat}]$$

$$-\text{dg}_{2,4} \text{dg}_{4,2} + \text{dg}_{2,2} \text{dg}_{4,4}$$

$$g_{\mu C M} = \begin{pmatrix} 1 & -\frac{\phi_4}{1-\phi_2} & 0 \\ 0 & 1 & -\frac{\phi_4}{1-\phi_2} \\ 0 & -\frac{\phi_2 \left(1 - \frac{x_3}{x_4} \frac{s_4}{s_3}\right)}{1-\phi_4 \left(1 - \frac{x_3}{x_4} \frac{s_4}{s_3}\right)} & 1 \end{pmatrix};$$

$$g_{\mu C B} = \begin{pmatrix} \frac{1}{1-\phi_2} \frac{1}{x_2} \text{d}\mu_2 \text{d}\phi_2 \\ \frac{1}{1-\phi_2} \frac{1}{x_2} \text{d}\mu_2 \text{d}\phi_4 \\ \frac{1}{1-\phi_4 \left(1 - \frac{x_3}{x_4} \frac{s_4}{s_3}\right)} \frac{1}{x_4} \text{d}\mu_4 \text{d}\phi_4 \end{pmatrix};$$

- Convert from free energy to chemical potential form

$$g_{\mu \text{conversion}} = \text{LinearSolve}[g_{\mu C M}, g_{\mu C B}];$$

$$\text{dg}_{2,2} = \text{First}[\text{First}[g_{\mu \text{conversion}}]]$$

$$-1. \left(\frac{0.0000145225 \text{d}\mu_2 \text{d}\phi_2}{1. - 1. \phi_2} - \frac{1. \phi_4 \left(\frac{0.0000145225 \text{d}\mu_2 \text{d}\phi_4}{1. - 1. \phi_2} + \frac{1. \left(\frac{0.362222 \text{d}\mu_4 \text{d}\phi_4}{1. - 2.38689 \phi_4} + \frac{0.0000346637 \text{d}\mu_2 \text{d}\phi_4 \phi_2}{(1. - 1. \phi_2)(1. - 2.38689 \phi_4)} \right) \phi_4}{(1. - 1. \phi_2) \left(1. - \frac{2.38689 \phi_2 \phi_4}{(1. - 1. \phi_2)(1. - 2.38689 \phi_4)} \right)} \right)$$

$$dg_{2,4} = g\mu conversion[[2]][[1]]$$

$$-1. \left(\frac{0.0000145225 d\mu_2 d\phi_4}{1. - 1. \phi_2} - \frac{1. \left(\frac{0.262222 d\mu_4 d\phi_4}{1. - 2.38689 \phi_4} + \frac{0.0000346637 d\mu_2 d\phi_4 \phi_2}{(1. - 1. \phi_2)(1. - 2.38689 \phi_4)} \right) \phi_4}{(1. - 1. \phi_2) \left(1. - \frac{2.38689 \phi_2 \phi_4}{(1. - 1. \phi_2)(1. - 2.38689 \phi_4)} \right)} \right)$$

$$dg_{4,4} = g\mu conversion[[3]][[1]]$$

$$\frac{1. \left(\frac{0.262222 d\mu_4 d\phi_4}{1. - 2.38689 \phi_4} + \frac{0.0000346637 d\mu_2 d\phi_4 \phi_2}{(1. - 1. \phi_2)(1. - 2.38689 \phi_4)} \right)}{1. - \frac{2.38689 \phi_2 \phi_4}{(1. - 1. \phi_2)(1. - 2.38689 \phi_4)}}$$

$$dg_{4,2} = dg_{2,4};$$

■ Chemical potential 'total' derivatives

$$\beta\mu_{hat}_4 = \beta\mu_4 - \frac{Z_4}{Z_3} \beta\mu_3;$$

$$\beta\mu_{hat}_2 = \beta\mu_2;$$

$$\frac{\beta\mu_{4LF} + \beta\mu_{3LF}}{r_4} /. \{\phi_2 \rightarrow .1, \phi_4 \rightarrow .001, \rho \rightarrow .88, v_{1,1} \rightarrow .6, v_{1,2} \rightarrow .001, v_{1,3} \rightarrow .001, v_{2,1} \rightarrow .0001, v_{2,2} \rightarrow .0001\};$$

$$\frac{\beta\mu_{4A} + \beta\mu_{3A}}{r_4} /. \{\phi_2 \rightarrow .1, \phi_4 \rightarrow .001, \rho \rightarrow .88, v_{1,1} \rightarrow .6, v_{1,2} \rightarrow .001, v_{1,3} \rightarrow .001, v_{2,1} \rightarrow .0001, v_{2,2} \rightarrow .0001\};$$

$$d\mu_4 d\phi_4 = \delta\mu_4 \delta\phi_4 + \delta\mu_4 \delta\rho d\rho d\phi_4 + \sum_{i=1}^n \sum_{j=1}^m \delta\mu_4 \delta v_{i,j} dv d\phi_{i,j};$$

$$d\mu_2 d\phi_2 = \delta\mu_2 \delta\phi_2 + \delta\mu_2 \delta\rho d\rho d\phi_2 + \sum_{i=1}^n \sum_{j=1}^m \delta\mu_2 \delta v_{i,j} dv d\phi_{i,j};$$

$$d\mu_2 d\phi_4 = \delta\mu_2 \delta\phi_4 + \delta\mu_2 \delta\rho d\rho d\phi_4 + \sum_{i=1}^n \sum_{j=1}^m \delta\mu_2 \delta v_{i,j} dv d\phi_{i,j};$$

■ Analytic partial derivatives

$$\delta\mu_4 \delta\phi_4 = D[\beta\mu_{hat}_4, \phi_4];$$

$$\delta\mu_4 \delta\rho = D[\beta\mu_{hat}_4, \rho];$$

For [i = 1, i < n + 1, i++,

For [j = 1, j < m + 1, j++,

$$\delta\mu_4 \delta v_{i,j} = D[\beta\mu_{hat}_4, v_{i,j}]]]$$

(*H-bond partial derivatives*)

$$\delta\mu_2\delta\phi_2 = D[\beta\mu\text{hat}_2, \phi_2];$$

$$\delta\mu_2\delta\phi_4 = D[\beta\mu\text{hat}_2, \phi_4];$$

$$\delta\mu_2\delta\rho = D[\beta\mu\text{hat}_2, \rho];$$

For [i = 1, i < n + 1, i++,

For [j = 1, j < m + 1, j++,

$$\delta\mu_2\delta v_{i,j} = D[\beta\mu\text{hat}_2, v_{i,j}]]]$$

(*H-bond partial derivatives*)

■ Volumetric equation of state

$$\text{EOS} = 1 - \text{Exp}\left[-\left(\frac{\rho^2 + \text{Pred}}{\text{Tred}} + \left(1 - \frac{1}{\text{rbar}}\right)\rho\right) + \frac{\text{xred}^3 (\text{IS}\kappa - \text{IS}2\kappa)}{16 \pi \text{IS}}\right];$$

■ Hydrogen bond equations of state

For [i = 1, i < n + 1, i++,

For [j = 1, j < m + 1, j++,

$$\text{hbondEOS}_{i,j} = v_{i,0} v_{0,j} \rho \text{Exp}\left[-\frac{G_{i,j}}{\text{KB T}}\right]]] \quad (*\text{One for each } i,$$

j pair*)

■ Set Ion Binding to zero

$$v_{2,3} = 0;$$

$$\delta\mu_2\delta v_{2,3} = 0;$$

$$\delta\mu_4\delta v_{2,3} = 0;$$

$$v_{2,0}$$

$$2.17333 \phi_4 - v_{\ell,1} - v_{\ell,\ell}$$

Solving EOS

- Setup

- Thermodynamic conditions

```
P = 107;
```

```
Tmin = 320; (*temperature grid minimum*)
```

```
Tmax = 380; (*temperature grid maximum*)
```

```
Tint = 5; (*temperature grid interval*)
```

```
Tpts = (Tmax - Tmin) / Tint + 1; (*temperature grid size*)
```

```
Tlist = Table[Tmin + i Tint, {i, 1, Tpts}]; (*temperature grid*)
```

- Define grids in ϕ_2 and ϕ_4

```
 $\phi_{2int}$  = .001;
```

```
 $\phi_{2min}$  =  $\phi_{2int}$ ;
```

```
 $\phi_{2max}$  = .2;
```

```
 $\phi_{2pts}$  = ( $\phi_{2max}$  -  $\phi_{2min}$ ) /  $\phi_{2int}$  + 1;
```

```
 $\phi_{2list}$  = Table[ $\phi_{2min}$  + (i - 1)  $\phi_{2int}$ , {i, 1,  $\phi_{2pts}$ }];
```

```
 $\phi_{4max}$  = .04;
```

```
 $\phi_{4int}$  = .0005;
```

```
 $\phi_{4min}$  =  $\phi_{4int}$ ;
```

```
 $\phi_{4pts}$  = ( $\phi_{4max}$  -  $\phi_{4min}$ ) /  $\phi_{4int}$  + 1;
```

```
 $\phi_{4list}$  = Table[ $\phi_{4min}$  + (j - 1)  $\phi_{4int}$ , {j, 1,  $\phi_{4pts}$ }];
```

- Define result arrays

```
 $\rho_{data}$  = Table[0, {Tpts}, { $\phi_{2pts}$ }, { $\phi_{4pts}$ }];
```

```
vdata11 = Table[0, {Tpts}, { $\phi_{2pts}$ }, { $\phi_{4pts}$ }];
```

```
vdata12 = Table[0, {Tpts}, { $\phi_{2pts}$ }, { $\phi_{4pts}$ }];
```

```
vdata13 = Table[0, {Tpts}, { $\phi_{2pts}$ }, { $\phi_{4pts}$ }];
```

```
vdata21 = Table[0, {Tpts}, { $\phi_{2pts}$ }, { $\phi_{4pts}$ }];
```

```
vdata22 = Table[0, {Tpts}, { $\phi_{2pts}$ }, { $\phi_{4pts}$ }];
```

- Initially Solve EOS

- Define function to find EOS root

```

EOSroot = Function[{iT, i, j},
  Check[
    FindRoot[
      { $\rho$  == EOS /. { $\phi_2 \rightarrow \phi_2list[[i]]$ ,  $\phi_4 \rightarrow \phi_4list[[j]]$ , T  $\rightarrow$  Tlist[[iT]]},
      v1,1 == hbondEOS1,1 /. { $\phi_2 \rightarrow \phi_2list[[i]]$ ,  $\phi_4 \rightarrow \phi_4list[[j]]$ ,
      T  $\rightarrow$  Tlist[[iT]]}, v1,2 == hbondEOS1,2 /.
      { $\phi_2 \rightarrow \phi_2list[[i]]$ ,  $\phi_4 \rightarrow \phi_4list[[j]]$ , T  $\rightarrow$  Tlist[[iT]]},
      v1,3 == hbondEOS1,3 /. { $\phi_2 \rightarrow \phi_2list[[i]]$ ,  $\phi_4 \rightarrow \phi_4list[[j]]$ ,
      T  $\rightarrow$  Tlist[[iT]]}, v2,1 == hbondEOS2,1 /.
      { $\phi_2 \rightarrow \phi_2list[[i]]$ ,  $\phi_4 \rightarrow \phi_4list[[j]]$ , T  $\rightarrow$  Tlist[[iT]]},
      v2,2 == hbondEOS2,2 /. { $\phi_2 \rightarrow \phi_2list[[i]]$ ,  $\phi_4 \rightarrow \phi_4list[[j]]$ ,
      T  $\rightarrow$  Tlist[[iT]]}}, {{ $\rho$ ,  $\rho_{guess}$ , .001, 1}, {v1,1, vguess1,1},
      {v1,2, vguess1,2}, {v1,3, vguess1,3}, {v2,1, vguess2,1},
      {v2,2, vguess2,2}}, MaxIterations  $\rightarrow$  1000000},
      { $\rho \rightarrow -1$ , v1,1  $\rightarrow -1$ , v1,2  $\rightarrow -1$ , v1,3  $\rightarrow -1$ , v2,1  $\rightarrow -1$ , v2,2  $\rightarrow -1$ }}];

For[iT = 1, iT < Tpts + 1, iT++, (*loop over temperature*)
  (*Initialize guess values*)
   $\rho_{guess}$  = .88;
  vguess1,1 = .5;
  vguess1,2 = .02;
  vguess1,3 = .001;
  vguess2,1 = .005;
  vguess2,2 = .02;

  (*Solve first point*)
  i = 1;
  j = 1;
  result = EOSroot[iT, i, j];
   $\rho_{data}[[iT, i, j]] = \rho /. result$ ;
  vdata11[[iT, i, j]] = v1,1 /. result;
  vdata12[[iT, i, j]] = v1,2 /. result;
  vdata13[[iT, i, j]] = v1,3 /. result;
  vdata21[[iT, i, j]] = v2,1 /. result;
  vdata22[[iT, i, j]] = v2,2 /. result;

```



```

(*Solve j=1,i=2*)
i = 2;
ρguess = ρdata[[iT, i - 1, j]];
vguess1,1 = vdata11[[iT, i - 1, j]];
vguess1,2 = vdata12[[iT, i - 1, j]];
vguess1,3 = vdata13[[iT, i - 1, j]];
vguess2,1 = vdata21[[iT, i - 1, j]];
vguess2,2 = vdata22[[iT, i - 1, j]];
result = EOSroot[iT, i, j];
ρdata[[iT, i, j]] = ρ / . result;
vdata11[[iT, i, j]] = v1,1 / . result;
vdata12[[iT, i, j]] = v1,2 / . result;
vdata13[[iT, i, j]] = v1,3 / . result;
vdata21[[iT, i, j]] = v2,1 / . result;
vdata22[[iT, i, j]] = v2,2 / . result;

(*Solve remainder of j=1*)
For[i = 3, i < φ2pts + 1, i++,
  ρguess = -ρdata[[iT, i - 2, j]] + 2 ρdata[[iT, i - 1, j]];
  vguess1,1 = -vdata11[[iT, i - 2, j]] + 2 vdata11[[iT, i - 1, j]];
  vguess1,2 = -vdata12[[iT, i - 2, j]] + 2 vdata12[[iT, i - 1, j]];
  vguess1,3 = -vdata13[[iT, i - 2, j]] + 2 vdata13[[iT, i - 1, j]];
  vguess2,1 = -vdata21[[iT, i - 2, j]] + 2 vdata21[[iT, i - 1, j]];
  vguess2,2 = -vdata22[[iT, i - 2, j]] + 2 vdata22[[iT, i - 1, j]];
  result = EOSroot[iT, i, j];
  ρdata[[iT, i, j]] = ρ / . result;
  vdata11[[iT, i, j]] = v1,1 / . result;
  vdata12[[iT, i, j]] = v1,2 / . result;
  vdata13[[iT, i, j]] = v1,3 / . result;
  vdata21[[iT, i, j]] = v2,1 / . result;
  vdata22[[iT, i, j]] = v2,2 / . result;];

(*Solve j=2*)
j = 2;
For[i = 1, i < φ2pts + 1, i++,
  ρguess = ρdata[[iT, i, j - 1]];
  vguess1,1 = vdata11[[iT, i, j - 1]];
  vguess1,2 = vdata12[[iT, i, j - 1]];
  vguess1,3 = vdata13[[iT, i, j - 1]];
  vguess2,1 = vdata21[[iT, i, j - 1]];

```

```

vguess2,2 = vdata22[[iT, i, j - 1]];
result = EOSroot[iT, i, j];
ρdata[[iT, i, j]] = ρ / result;
vdata11[[iT, i, j]] = v1,1 / result;
vdata12[[iT, i, j]] = v1,2 / result;
vdata13[[iT, i, j]] = v1,3 / result;
vdata21[[iT, i, j]] = v2,1 / result;
vdata22[[iT, i, j]] = v2,2 / result; ];
(*Solve rest of points*)
Clear[j];
For[j = 3, j < φ4pts + 1, j++,
  For[i = 1, i < φ2pts + 1, i++,
    ρguess = -ρdata[[iT, i, j - 2]] + 2 ρdata[[iT, i, j - 1]];
    vguess1,1 = -vdata11[[iT, i, j - 2]] + 2 vdata11[[iT, i, j - 1]];
    vguess1,2 = -vdata12[[iT, i, j - 2]] + 2 vdata12[[iT, i, j - 1]];
    vguess1,3 = -vdata13[[iT, i, j - 2]] + 2 vdata13[[iT, i, j - 1]];
    vguess2,1 = -vdata21[[iT, i, j - 2]] + 2 vdata21[[iT, i, j - 1]];
    vguess2,2 = -vdata22[[iT, i, j - 2]] + 2 vdata22[[iT, i, j - 1]];
    If[ρguess < 0, ρguess = .8, {}];
    If[vguess1,1 < 0, vguess1,1 = .5, {}];
    If[vguess1,2 < 0, vguess1,2 = .01, {}];
    If[vguess1,3 < 0, vguess1,3 = .001, {}];
    If[vguess2,1 < 0, vguess2,1 = .001, {}];
    If[vguess2,2 < 0, vguess2,2 = .001, {}];
    result = EOSroot[iT, i, j];
    ρdata[[iT, i, j]] = ρ / result;
    vdata11[[iT, i, j]] = v1,1 / result;
    vdata12[[iT, i, j]] = v1,2 / result;
    vdata13[[iT, i, j]] = v1,3 / result;
    vdata21[[iT, i, j]] = v2,1 / result;
    vdata22[[iT, i, j]] = v2,2 / result;
  ]];
]

```

EOS Error Correction

- Define smart function testing whether a point is good

```
GoodTest = Function[{iT, i, j},  
  (pdata[[iT, i, j]])1/2 + (vdata11[[iT, i, j]])1/2 + (vdata12[[iT, i, j]])1/2 +  
  (vdata13[[iT, i, j]])1/2 + (vdata21[[iT, i, j]])1/2 +  
  (vdata22[[iT, i, j]])1/2 ==  
  Re[(pdata[[iT, i, j]])1/2 + (vdata11[[iT, i, j]])1/2 +  
  (vdata12[[iT, i, j]])1/2 + (vdata13[[iT, i, j]])1/2 +  
  (vdata21[[iT, i, j]])1/2 + (vdata22[[iT, i, j]])1/2];
```

```
For[iT = 1, iT < Tpts + 1, iT++, (*loop over temperature*)  
  (*Error point correction based on realness tester using  
  interpolation with selected good points in  $\phi_3$  direction*)  
  For[i = 1, i <  $\phi_2$ pts + 1, i++,  
    For[j = 2, j <  $\phi_4$ pts, j++,  
      gindex1 = 1;  
      gindex2 = 1;  
      gtest = 0;  
      hope = 1;  
      If[GoodTest[iT, i, j], {},  
  
        (*Search for good points to use in generating new guess*)  
        While[gtest == 0, (*Continue search*)  
          If[GoodTest[iT, i, j - 1], (*check if lower point is good*)  
            gtest = 1, (*if yes, provisionally set variable to end search*)  
            If[j - gindex1 == 1, gtest = 1; hope = 0, gindex1++]; (*If no,  
            check if seach has reached end of row - if it has ,  
            cancel this attempt- a good guess cannot be generated wit  
            this approach; otherwise, increment lower point search index*)  
          If[GoodTest[iT, i, j], (*check if upper point is good*)  
            {}, (*If yes, do nothing (let end variable stay as is)*)  
            gtest = 0; If[j + gindex2 ==  $\phi_3$ pts, gtest = 1; hope = 0, gindex2++]  
            (*If no, check if seach has reached end of row if it has ,  
            cancel this attempt- a good guess cannot be generated wit  
            this approach; otherwise, increment upper point search index*)  
          ];  
      If[hope == 1,  
        (*calculate new guesses*)
```

```

    pguess =
      (pdata[[iT, i, j + gindex2]] - pdata[[iT, i, j - gindex1]]) /
      (gindex1 + gindex2) gindex1 + pdata[[iT, i, j - gindex1]];
    vguess1,1 =
      (vdata11[[iT, i, j + gindex2]] - vdata11[[iT, i, j - gindex1]]) /
      (gindex1 + gindex2) gindex1 + vdata11[[iT, i, j - gindex1]];
    vguess1,2 =
      (vdata12[[iT, i, j + gindex2]] - vdata12[[iT, i, j - gindex1]]) /
      (gindex1 + gindex2) gindex1 + vdata12[[iT, i, j - gindex1]];
    vguess1,3 =
      (vdata13[[iT, i, j + gindex2]] - vdata13[[iT, i, j - gindex1]]) /
      (gindex1 + gindex2) gindex1 + vdata13[[iT, i, j - gindex1]];
    vguess2,1 =
      (vdata21[[iT, i, j + gindex2]] - vdata21[[iT, i, j - gindex1]]) /
      (gindex1 + gindex2) gindex1 + vdata21[[iT, i, j - gindex1]];
    vguess2,2 =
      (vdata22[[iT, i, j + gindex2]] - vdata22[[iT, i, j - gindex1]]) /
      (gindex1 + gindex2) gindex1 + vdata22[[iT, i, j - gindex1]];
    (*solve with new guesses*)
    result = EOSroot[i, j];
    pdata[[iT, i, j]] = p /. result;
    vdata11[[iT, i, j]] = v1,1 /. result;
    vdata12[[iT, i, j]] = v1,2 /. result;
    vdata13[[iT, i, j]] = v1,3 /. result;
    vdata21[[iT, i, j]] = v2,1 /. result;
    vdata22[[iT, i, j]] = v2,2 /. result;
  , {}
]]];
(*Error point correction based on realness tester using
interpolation with selected good points in φ2 direction*)
For[i = 2, i < φ2pts, i++,
For[j = 1, j < φ4pts + 1, j++,
  gindex1 = 1;
  gindex2 = 1;
  gtest = 0;
  hope = 1;
  If[GoodTest[iT, i, j], {},
    (*Search for good points to use in generating new guess*)
    While[gtest == 0, (*Continue search*)

```

```

If[GoodTest[iT, i - gindex1, j], (*check if lower point is good*)
  gtest = 1, (*if yes, provisionally set variable to end search*)
  If[i - gindex1 == 1, gtest = 1; hope = 0, gindex1++]]; (*If no,
check if seach has reached end of row - if it has ,
cancel this attempt- a good guess cannot be generated wit
  this approach; otherwise, increment lower point search index*)
If[GoodTest[iT, i + gindex2, j], (*check if upper point is good*)
  {}, (*If yes, do nothing (let end variable stay as is)*)
  gtest = 0; If[i + gindex2 ==  $\phi$ 2pts, gtest = 1; hope = 0, gindex2++]]
  (*If no, check if seach has reached end of row if it has ,
cancel this attempt- a good guess cannot be generated wit
  this approach; otherwise, increment upper point search index*)
];
If[hope == 1,
   $\rho$ guess =
    ( $\rho$ data[[iT, i + gindex2, j]] -  $\rho$ data[[iT, i - gindex1, j]]) /
    (gindex1 + gindex2) gindex1 +  $\rho$ data[[iT, i - gindex1, j]];
  vguess1,1 =
    (vdata11[[iT, i + gindex2, j]] - vdata11[[iT, i - gindex1, j]]) /
    (gindex1 + gindex2) gindex1 + vdata11[[iT, i - gindex1, j]];
  vguess1,2 =
    (vdata12[[iT, i + gindex2, j]] - vdata12[[iT, i - gindex1, j]]) /
    (gindex1 + gindex2) gindex1 + vdata12[[iT, i - gindex1, j]];
  vguess1,3 =
    (vdata13[[iT, i + gindex2, j]] - vdata13[[iT, i - gindex1, j]]) /
    (gindex1 + gindex2) gindex1 + vdata13[[iT, i - gindex1, j]];
  vguess2,1 =
    (vdata21[[iT, i + gindex2, j]] - vdata21[[iT, i - gindex1, j]]) /
    (gindex1 + gindex2) gindex1 + vdata21[[iT, i - gindex1, j]];
  vguess2,2 =
    (vdata22[[iT, i + gindex2, j]] - vdata22[[iT, i - gindex1, j]]) /
    (gindex1 + gindex2) gindex1 + vdata22[[iT, i - gindex1, j]];
  result = EOSroot[i, j];
   $\rho$ data[[iT, i, j]] =  $\rho$  /. result;
  vdata11[[iT, i, j]] = v1,1 /. result;
  vdata12[[iT, i, j]] = v1,2 /. result;
  vdata13[[iT, i, j]] = v1,3 /. result;
  vdata21[[iT, i, j]] = v2,1 /. result;
  vdata22[[iT, i, j]] = v2,2 /. result;
  , {}]]];

```

(+Error point correction based on realness tester using the two previous points in ϕ_3 direction for guess+)

```

For[i = 1, i <  $\phi_2$ pts + 1, i++,
For[j = 3, j <  $\phi_4$ pts + 1, j++,
If[GoodTest[iT, i, j], {},
   $\rho$ guess = - $\rho$ data[[iT, i, j - 2]] + 2  $\rho$ data[[iT, i, j - 1]];
  vguess1,1 = -vdata11[[iT, i, j - 2]] + 2 vdata11[[iT, i, j - 1]];
  vguess1,2 = -vdata12[[iT, i, j - 2]] + 2 vdata12[[iT, i, j - 1]];
  vguess1,3 = -vdata13[[iT, i, j - 2]] + 2 vdata13[[iT, i, j - 1]];
  vguess2,1 = -vdata21[[iT, i, j - 2]] + 2 vdata21[[iT, i, j - 1]];
  vguess2,2 = -vdata22[[iT, i, j - 2]] + 2 vdata22[[iT, i, j - 1]];
  result = EOSroot[i, j];
   $\rho$ data[[iT, i, j]] =  $\rho$  /. result;
  vdata11[[iT, i, j]] = v1,1 /. result;
  vdata12[[iT, i, j]] = v1,2 /. result;
  vdata13[[iT, i, j]] = v1,3 /. result;
  vdata21[[iT, i, j]] = v2,1 /. result;
  vdata22[[iT, i, j]] = v2,2 /. result;
}];

```

(+Error point correction based on realness tester using the two next points in ϕ_3 direction for guess+)

```

For[i = 1, i <  $\phi_2$ pts + 1, i++,
For[j =  $\phi_4$ pts, j > 2, j--,
If[GoodTest[iT, i, j], {},
   $\rho$ guess = - $\rho$ data[[iT, i, j + 2]] + 2  $\rho$ data[[iT, i, j + 1]];
  vguess1,1 = -vdata11[[iT, i, j + 2]] + 2 vdata11[[iT, i, j + 1]];
  vguess1,2 = -vdata12[[iT, i, j + 2]] + 2 vdata12[[iT, i, j + 1]];
  vguess1,3 = -vdata13[[iT, i, j + 2]] + 2 vdata13[[iT, i, j + 1]];
  vguess2,1 = -vdata21[[iT, i, j + 2]] + 2 vdata21[[iT, i, j + 1]];
  vguess2,2 = -vdata22[[iT, i, j + 2]] + 2 vdata22[[iT, i, j + 1]];
  result = EOSroot[i, j];
   $\rho$ data[[iT, i, j]] =  $\rho$  /. result;
  vdata11[[iT, i, j]] = v1,1 /. result;
  vdata12[[iT, i, j]] = v1,2 /. result;
  vdata13[[iT, i, j]] = v1,3 /. result;
  vdata21[[iT, i, j]] = v2,1 /. result;
  vdata22[[iT, i, j]] = v2,2 /. result;
}];

```

```
(*Error point correction based realness tester using single
previous point in  $\phi_2$  direction for guess*)
```

```
For [i = 2, i <  $\phi_2$ pts + 1, i++,
For [j = 1, j <  $\phi_4$ pts + 1, j++,
If [GoodTest [iT, i, j], {},
   $\rho$ guess =  $\rho$ data[[iT, i, j - 1]];
  vguess1,1 = vdata11[[iT, i, j - 1]];
  vguess1,2 = vdata12[[iT, i, j - 1]];
  vguess1,3 = vdata13[[iT, i, j - 1]];
  vguess2,1 = vdata21[[iT, i, j - 1]];
  vguess2,2 = vdata22[[iT, i, j - 1]];
  result = EOSroot [iT, i, j];
   $\rho$ data[[iT, i, j]] =  $\rho$  /. result;
  vdata11[[iT, i, j]] = v1,1 /. result;
  vdata12[[iT, i, j]] = v1,2 /. result;
  vdata13[[iT, i, j]] = v1,3 /. result;
  vdata21[[iT, i, j]] = v2,1 /. result;
  vdata22[[iT, i, j]] = v2,2 /. result;
]]];
```

```
(*Error point correction based realness tester using single
next point in  $\phi_2$  direction for guess*)
```

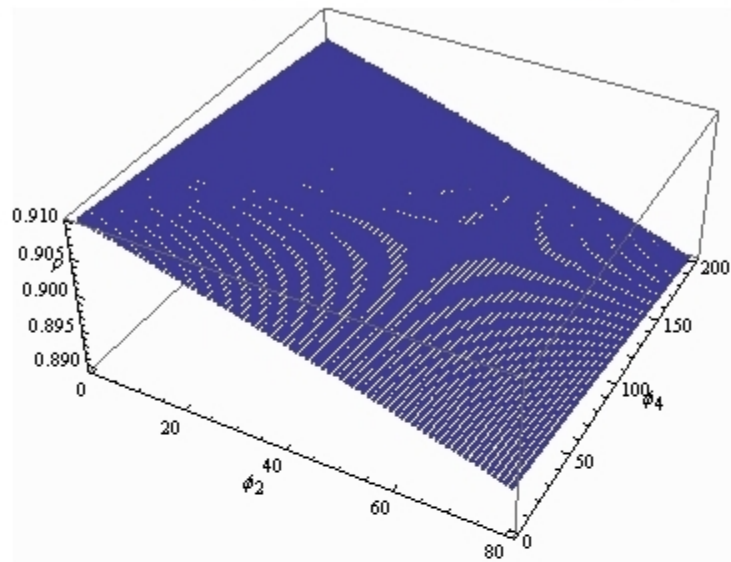
```
For [i =  $\phi_2$ pts - 1, i > 1, i--,
For [j = 1, j <  $\phi_4$ pts + 1, j++,
index = (i - 1)  $\phi_4$ pts + j;
If [GoodTest [iT, i, j], {},
   $\rho$ guess =  $\rho$ data[[iT, i, j + 1]];
  vguess1,1 = vdata11[[iT, i, j + 1]];
  vguess1,2 = vdata12[[iT, i, j + 1]];
  vguess1,3 = vdata13[[iT, i, j + 1]];
  vguess2,1 = vdata21[[iT, i, j + 1]];
  vguess2,2 = vdata22[[iT, i, j + 1]];
  result = EOSroot [iT, i, j];
   $\rho$ data[[iT, i, j]] =  $\rho$  /. result;
  vdata11[[iT, i, j]] = v1,1 /. result;
  vdata12[[iT, i, j]] = v1,2 /. result;
  vdata13[[iT, i, j]] = v1,3 /. result;
  vdata21[[iT, i, j]] = v2,1 /. result;
  vdata22[[iT, i, j]] = v2,2 /. result;
]]]
```

]

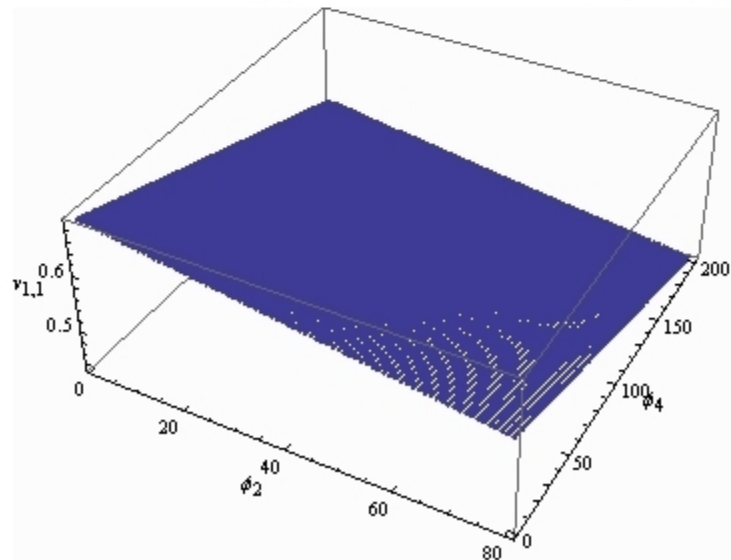
Save[FILENAME, {pdata, vdata11, vdata12, vdata13, vdata21, vdata22}]

Plot EOS data

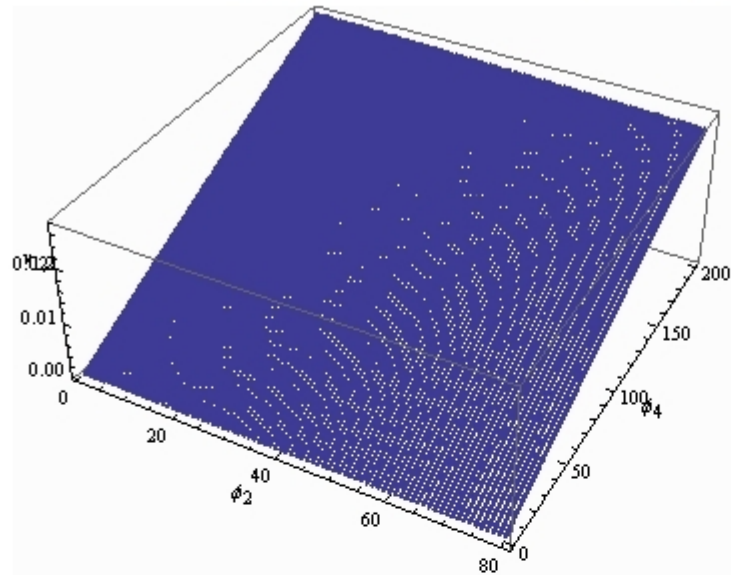
ListPointPlot3D[pdata[[6]], AxesLabel -> { ϕ_2 , ϕ_4 , ρ }



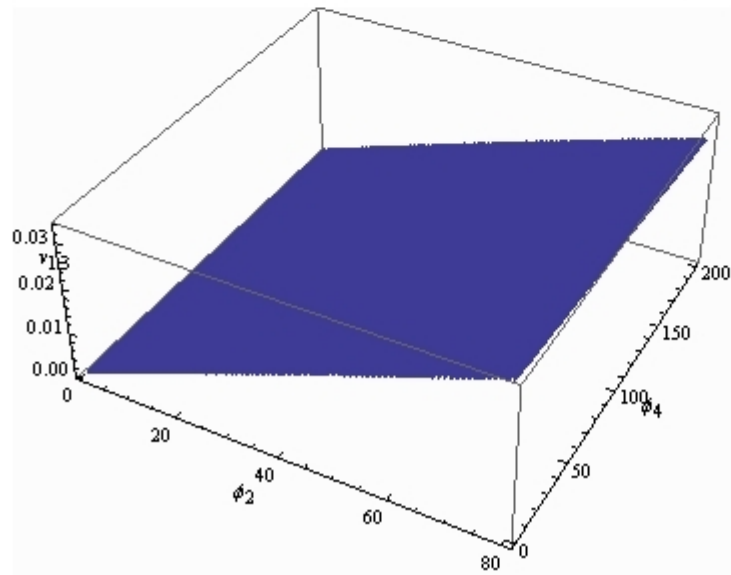
ListPointPlot3D[vdata11[[6]], AxesLabel -> { ϕ_2 , ϕ_4 , $v_{1,1}$ }



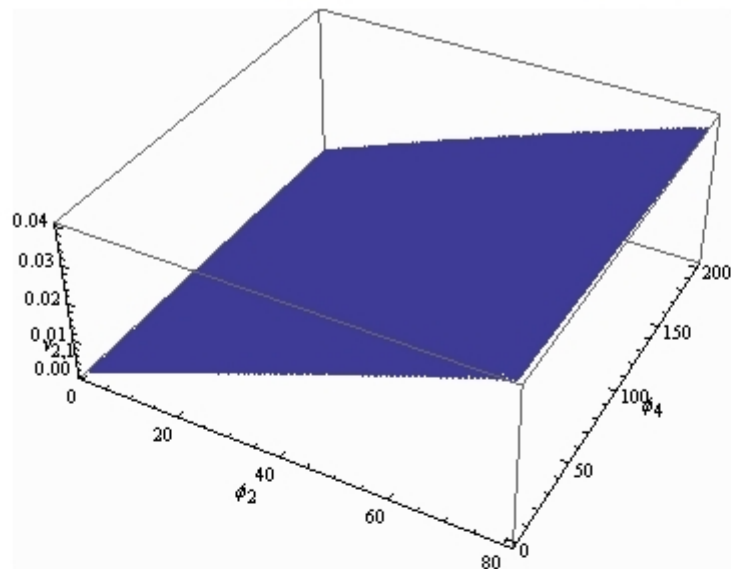
`ListPointPlot3D[vdata12[[6]], AxesLabel -> { ϕ_2 , ϕ_4 , $v_{1,2}$ }]`



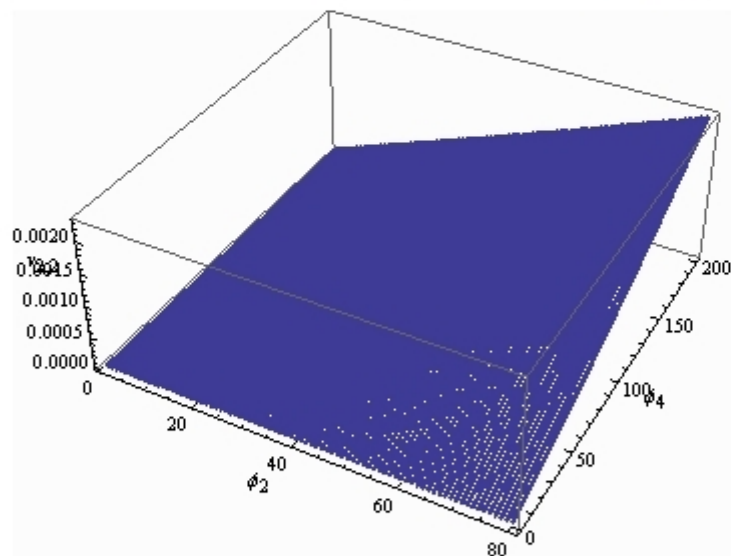
`ListPointPlot3D[vdata13[[6]], AxesLabel -> { ϕ_2 , ϕ_4 , $v_{1,3}$ }]`



```
ListPointPlot3D[vdata21[[6]], AxesLabel -> { $\phi_2$ ,  $\phi_4$ ,  $v_{2,1}$ }
```



```
ListPointPlot3D[vdata22[[6]], AxesLabel -> { $\phi_2$ ,  $\phi_4$ ,  $v_{2,2}$ }
```



Spinodal calculation

- Interpolate 2D isothermal slices of EOS data

```
For[iT = 1, iT < Tpts + 1, iT++,
```

```
  (+Interpolate+)
```

```
  psurfiT =
```

```
  ListInterpolation[pdata[[iT, All, All]],
```

```
    {{ $\phi_{2min}$ ,  $\phi_{2max}$ }, { $\phi_{4min}$ ,  $\phi_{4max}$ }}][ $\phi_2$ ,  $\phi_4$ ];
```

```

v11surfiT =
  ListInterpolation[vdata11[[iT, All, All]],
    {{φ2min, φ2max}, {φ4min, φ4max}}][φ2, φ4];
v12surfiT =
  ListInterpolation[vdata12[[iT, All, All]],
    {{φ2min, φ2max}, {φ4min, φ4max}}][φ2, φ4];
v13surfiT =
  ListInterpolation[vdata13[[iT, All, All]],
    {{φ2min, φ2max}, {φ4min, φ4max}}][φ2, φ4];
v21surfiT =
  ListInterpolation[vdata21[[iT, All, All]],
    {{φ2min, φ2max}, {φ4min, φ4max}}][φ2, φ4];
v22surfiT =
  ListInterpolation[vdata22[[iT, All, All]],
    {{φ2min, φ2max}, {φ4min, φ4max}}][φ2, φ4];
(*Take derivatives*)
dρdφ2surfiT = D[ρsurfiT, φ2];
dv11dφ2surfiT = D[v11surfiT, φ2];
dv12dφ2surfiT = D[v12surfiT, φ2];
dv13dφ2surfiT = D[v13surfiT, φ2];
dv21dφ2surfiT = D[v21surfiT, φ2];
dv22dφ2surfiT = D[v22surfiT, φ2];
dρdφ4surfiT = D[ρsurfiT, φ4];
dv11dφ4surfiT = D[v11surfiT, φ4];
dv12dφ4surfiT = D[v12surfiT, φ4];
dv13dφ4surfiT = D[v13surfiT, φ4];
dv21dφ4surfiT = D[v21surfiT, φ4];
dv22dφ4surfiT = D[v22surfiT, φ4];

(*Calculate spinodal interpolation object*)
SpincurveiT =
  Spinodal /. {ρ → ρsurfiT, v1,1 → v11surfiT, v1,2 → v12surfiT,
    v1,3 → v13surfiT, v2,1 → v21surfiT, v2,2 → v22surfiT, dρdφ4 → dρdφ4surfiT,
    dvdφ4,1 → dv11dφ4surfiT, dvdφ4,2 → dv12dφ4surfiT,
    dvdφ4,3 → dv13dφ4surfiT, dvdφ2,1 → dv21dφ4surfiT,
    dvdφ2,2 → dv22dφ4surfiT, dρdφ2 → dρdφ2surfiT, dvdφ2,1 → dv11dφ2surfiT,
    dvdφ2,2 → dv12dφ2surfiT, dvdφ2,3 → dv13dφ2surfiT,
    dvdφ2,1 → dv21dφ2surfiT, dvdφ2,2 → dv22dφ2surfiT} /. T → Tlist[[iT]];
]

```

```
(*clear original EOS data to reduce memory burden*)
```

```
Clear[pdata];  
Clear[vdata11];  
Clear[vdata12];  
Clear[vdata13];  
Clear[vdata21];  
Clear[vdata22];
```

- Abstract spinodal data grid from interpolated spinodal data

```
Spindata = Table[0, {Tpts}, { $\phi$ 2pts}, { $\phi$ 4pts}];  
  
For[iT = 1, iT < Tpts + 1, iT++,  
  For[i = 1, i <  $\phi$ 2pts + 1, i++,  
    For[j = 1, j <  $\phi$ 4pts + 1, j++,  
      Spindata[[iT, i, j]] = SpincurveiT /. { $\phi$ 2 →  $\phi$ 2list[[i]],  $\phi$ 4 →  $\phi$ 4list[[j]]};  
    ]  
  ]  
]
```

- Reinterpolate in the constant salt planes

```
For[j = 1, j <  $\phi$ 4pts + 1, j++,  
  SaltSpinSurfj =  
    ListInterpolation[Spindata[[All, All, j]],  
      {{Tmin, Tmax}, { $\phi$ 2min,  $\phi$ 2max}}][T,  $\phi$ 2];  
]
```

- Plot spinodal contours in these planes

```
For[j = 1, j <  $\phi$ 4pts + 1, j++,  
  SpinPlotj = ContourPlot[SaltSpinSurfj, { $\phi$ 2,  $\phi$ 2min,  $\phi$ 2max},  
    {T, Tmin, Tmax}, Contours → {0}, ContourShading → None,  
    ContourStyle → Black, FrameLabel → {" $\phi$ p", "T(K)"},  
    FrameStyle → Directive[FontSize → 14],  
    TicksStyle → Directive[Red, FontSize → 12]]  
]
```

```

LCST[[j, 2]] = Min[spin]; (*LCST is minimum of spinodal curve*)
LCSTφ2[[j]] = First[φ2list[[First[Position[spin, LCST[[j, 2]]]]]]];
(*Fix data format*)
LCST[[j, 1]] =  $\frac{\phi_4 r_1}{\phi_1 r_4 M w_1 n_A}$  /. {φ2 → LCSTφ2[[j]], φ4 → φ4list[[j]]};
(*put LCST composition in molality format*)
]

```

InterpolatingFunction::dmval:

Input value {416.052, 0.001} lies outside the range of data in the interpolating function. Extrapolation will be used. ⌘

InterpolatingFunction::dmval:

Input value {416.052, 0.001} lies outside the range of data in the interpolating function. Extrapolation will be used. ⌘

InterpolatingFunction::dmval:

Input value {566.311, 0.001} lies outside the range of data in the interpolating function. Extrapolation will be used. ⌘

General::stop: Further output of InterpolatingFunction::dmval will be suppressed during this calculation. ⌘

FindRoot::lstol:

The line search decreased the step size to within tolerance specified by AccuracyGoal and PrecisionGoal but was unable to find a sufficient decrease in the merit function. You may need more than MachinePrecision digits of working precision to meet these tolerances. ⌘

FindRoot::lstol:

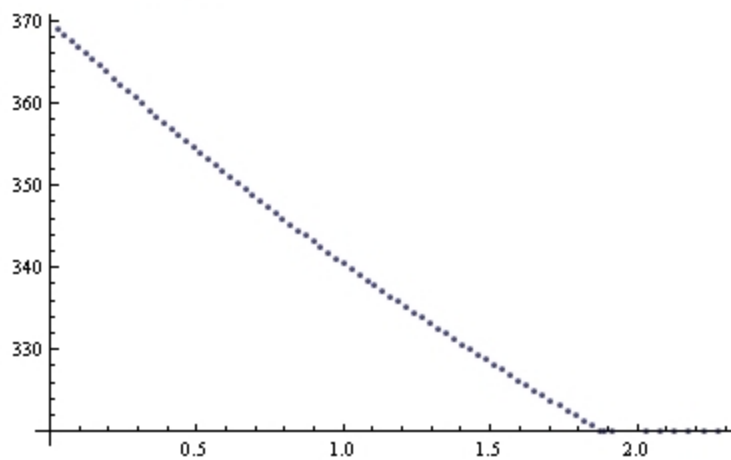
The line search decreased the step size to within tolerance specified by AccuracyGoal and PrecisionGoal but was unable to find a sufficient decrease in the merit function. You may need more than MachinePrecision digits of working precision to meet these tolerances. ⌘

FindRoot::lstol:

The line search decreased the step size to within tolerance specified by AccuracyGoal and PrecisionGoal but was unable to find a sufficient decrease in the merit function. You may need more than MachinePrecision digits of working precision to meet these tolerances. ⌘

General::stop: Further output of FindRoot::lstol will be suppressed during this calculation. ⌘

ListPlot[LCST]



Export["Trange014LCST.xls", LCST]

(+export excel file of LCST data)

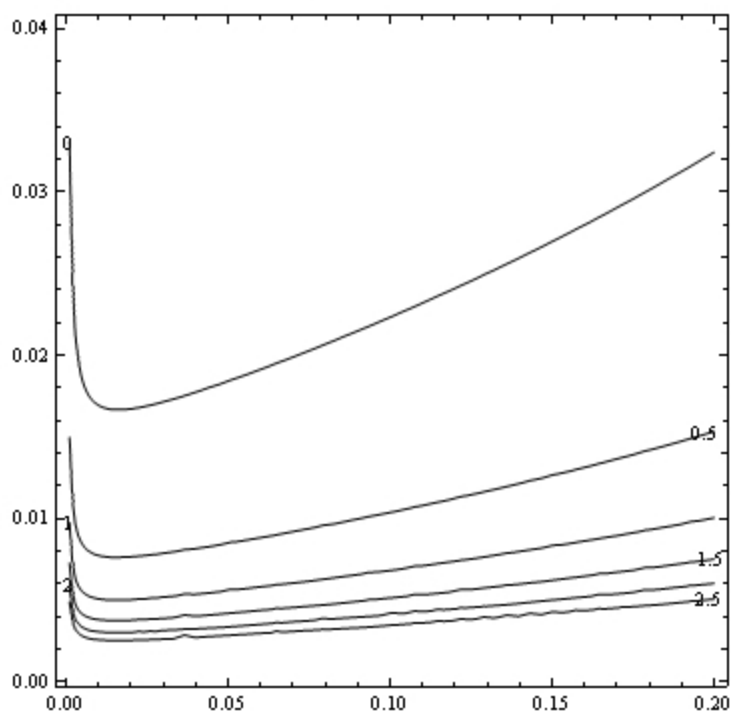
Trange014LCST.xls

ContourPlot[Spincurve₆, { ϕ_2 , ϕ_{2min} , ϕ_{2max} }, { ϕ_4 , ϕ_{4min} , ϕ_{4max} },

AxisLabel → { ϕ_2 , ϕ_4 }, ContourLabels → Automatic, ContourShading → None,

ContourStyle → Black] *

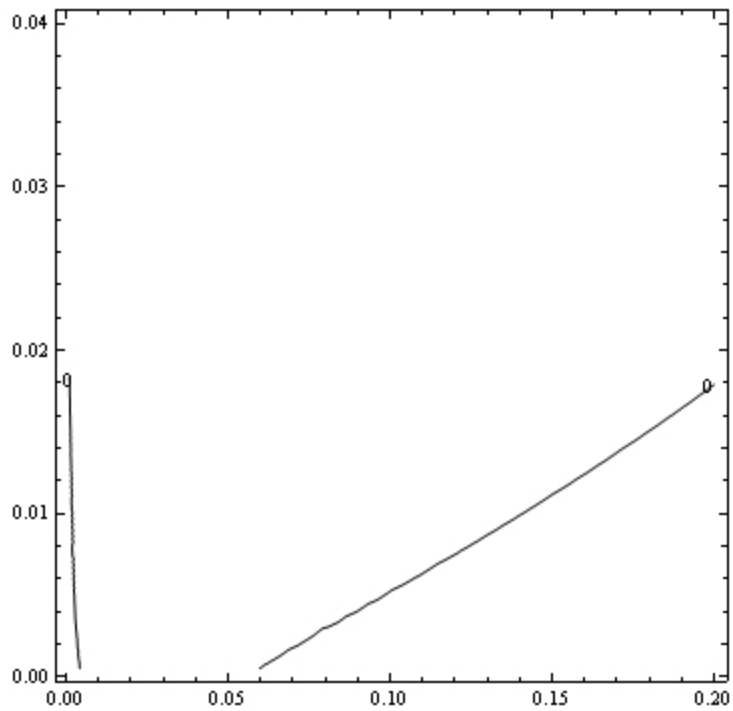
(+Plot isothermal stability curves-positive indicates stability,
negative instability, and zero the spinodal*)



```
Get[FILENAME]; (*recall EOS data*)
```

```
Save[FILENAME, {pdata, vdata11, vdata12, vdata13, vdata21, vdata22,  
  Spindata}] (*resave EOS data along with spinodal data*)
```

```
ContourPlot[Spincurve12, { $\phi_2$ ,  $\phi_{2min}$ ,  $\phi_{2max}$ }, { $\phi_4$ ,  $\phi_{4min}$ ,  $\phi_{4max}$ },  
  Contours → {0}, ContourLabels → Automatic, ContourShading → None,  
  ContourStyle → Black]  
(*Plot isothermal spinodal curves*)
```



A.3.2. Lattice Fluid CGT

Pressure-temperature behavior of the lattice fluid coil-globule transition of a finite chain is numerically determined as described in section 3.1.2 via straightforward numerical solution of equations (3.26), (3.27), and (3.31) over a range of temperatures.

Representative code follows:

Constants

$$k = 1.388 \times 10^{-23};$$

Input Parameters

■ Solvent

$$T_{ss} = 441; \text{ (*Characteristic temperature*)}$$

$$P_{ss} = 3.10 \times 10^8; \text{ (*Characteristic pressure*)}$$

$$\rho_{ss} = 755; \text{ (*Characteristic density*)}$$

$$r_s = 8.09; \text{ (*lattice size*)}$$

■ Polymer

$$T_{ps} = 643; \text{ (*Characteristic temperature*)}$$

$$v_i$$

$$P_{ps} = 354 \times 10^6; \text{ (*Characteristic pressure*)}$$

$$\rho_{ps} = 974; \text{ (*Characteristic density*)}$$

$$M_p = 1.66 \times 10^6 \times 10^{-3} / (6.02 \times 10^{23}) \text{ (*Molecular weight*)}$$

$$2.75748 \times 10^{-21}$$

$$a = \left(\frac{19}{27} \right)^{1/3} \text{ (*gyration radius constant*)}$$

$$\frac{19^{1/3}}{3}$$

Calculated Parameters

$$v_s = \frac{T_{ss} k}{P_{ss}}; \text{ (*solvent characteristic volume*)}$$

$$v_p = \frac{T_{ps} k}{P_{ps}}; \text{ (*polymer characteristic volume*)}$$

$$r_p = \frac{M_p}{\rho_{ps} v_p} \text{ (*polymer lattice size*)}$$

112294.

$$\epsilon_{pp} = T_{ps} k \text{ (*polymer self-interaction energy*)}$$

8.92484×10^{-21}

$$\epsilon_{ss} = T_{ss} k \text{ (*solvent self-interaction energy*)}$$

6.12108×10^{-21}

$$\chi = \frac{(\sqrt{T_{ss}} - \sqrt{T_{ps}})^2}{T} \text{ (*chi-parameter*)}$$

$$\frac{(21 - \sqrt{643})^2}{T}$$

$$\epsilon_{sp} = -\frac{1}{2} (k T \chi - \epsilon_{ss} - \epsilon_{pp}) \text{ (*cross-interaction energy*)}$$

7.39119×10^{-21}

$$P_{\text{crit}} = \left(\frac{2}{(1 + r_s \cdot 5)^2} \right) \left(r_s \text{Log} \left[1 + \frac{1}{r_s \cdot 5} \right] + .5 - r_s \cdot 5 \right)$$

(*solvent critical pressure*)

0.012589

$$T_{\text{crit}} = \frac{2 r_s}{(1 + r_s \cdot 5)^2} \text{ (*solvent critical temperature*)}$$

1.09483

Variable Parameters

Tsred = T / Tss (*Solvent reduced temperature*)

$$\frac{T}{441}$$

Psred = P / Pss (*Solvent reduced pressure*)

$$3.22581 \times 10^{-9} P$$

$\beta = 1 / (k T)$

$$\frac{7.20461 \times 10^{22}}{T}$$

$\alpha = \left(\frac{a}{r_p^{1/3} \phi^{2/3}} \right)^{1/2}$; (*root of expansion factor*)

$$\frac{0.135781}{\phi^{1/3}}$$

$\phi_0 = \frac{a^{3/2}}{r_p^{1/2}}$; (*polymer occupied volume fraction at CGT*)

$$0.00250332$$

Governing Equations

EOSbulk = 1 - Exp $\left[- \left(\frac{\rho_B^2 + Psred}{Tsred} + \left(1 - \frac{1}{rs} \right) \rho_B \right) \right]$

(*bulk solvent equation of state*)

$$1 - e^{-0.876291 \rho_B - \frac{441 (3.22581 \times 10^{-9} P + \rho_B^2)}{T}}$$

chempoteg = $\rho_B \left(\frac{1 - \phi - \rho}{1 - \rho_B} \right)^{rs} \text{Exp}[\beta rs (ess (\rho - \rho_B) + 2 esp \phi)]$

(*condition of solvent chemical potential equality in bulk and in pervaded volume*)

$$e^{\frac{5.82852 \times 10^{22} (6.12108 \times 10^{-21} (\rho - \rho_B) + 1.47824 \times 10^{-20} \phi)}{T}} \rho_B \left(\frac{1 - \rho - \phi}{1 - \rho_B} \right)^{8.09}$$

$$CGT = -rp \left(\beta \epsilon pp \phi 0 + \left(\text{Log} \left[1 - \frac{\phi 0}{1 - \rho} \right] + \frac{\phi 0}{1 - \rho} \right) / \left(\frac{\phi 0}{1 - \rho} \right) \right)$$

(*raw CGT condition*)

$$-112294. \left(\frac{1.60964}{T} + 399.469 (1 - \rho) \left(\frac{0.00250332}{1 - \rho} + \text{Log} \left[1 - \frac{0.00250332}{1 - \rho} \right] \right) \right)$$

$$CGT = \beta \epsilon pp \phi 0^2 + (1 - \rho) \text{Log} \left[\frac{1 - \rho - \phi 0}{1 - \rho} \right] + \phi 0 \text{ (*simplified CGT condition*)}$$

$$0.00250332 + \frac{0.00402945}{T} + (1 - \rho) \text{Log} \left[\frac{0.997497 - \rho}{1 - \rho} \right]$$

Solve governing equations

■ Setup solution grid

```
minT = Tps / 100;
maxT = 2 Tps;
Tint = Tps / 1000;
Tpts = (maxT - minT) / Tint + 1
1991
Tlist = Table[minT + (i - 1) Tint, {i, Tpts}];
```

■ Define data arrays

```
ρBdata = Table[0, {i, 0, Tpts - 1}];
Pdata = Table[0, {i, 0, Tpts - 1}, {2}];
ρdata = Table[0, {i, 0, Tpts - 1}];
```

■ Initialize guesses

```
Pguess = 0;
ρBguess = .001;
ρguess = .001;
```

■ Solve for CGT pressure as function of pressure

```

For[i = Tpts, i > 0, i--, (*loop over temperature*)
(*solve equations*)
chaindata =
Check[FindRoot[{0 == CGT /. T → Tlist[[i]],
  ρ == chempoteg /. {T → Tlist[[i]], φ → φ0},
  ρB == EOSbulk /. T → Tlist[[i]]},
{{P, Pguess}, {ρB, ρBguess, 0, 1}, {ρ, ρguess, 0, 1}},
MaxIterations → 10 000], {P → 0, ρB → 0, ρ → 0}];
(*put results in arrays*)
Pdata[[i, 2]] = (P /. chaindata) / Pss;
ρdata[[i]] = ρ /. chaindata;
ρBdata[[i]] = ρB /. chaindata;
Pdata[[i, 1]] = Tlist[[i]] / Tps;
(*Update guesses with result if appropriate*)
If[(P /. chaindata) != 0, Pguess = P /. chaindata, {}];
If[(ρ /. chaindata) != 0, ρguess = ρ /. chaindata, {}];
If[(ρB /. chaindata) != 0, ρBguess = ρB /. chaindata, {}];
]

```

■ Convert pressure data to dimensional form

```

DimPdata = Table[0, {i, 0, Tpts - 1}, {2}];

For[i = 1, i < Tpts + 1, i++,
  DimPdata[[i, 1]] = Tlist[[i]];
  DimPdata[[i, 2]] = Pdata[[i, 2]] Pss 10-5
]

Max[DimPdata] (*Calculate pressure of Pmax hypercritical
point*)

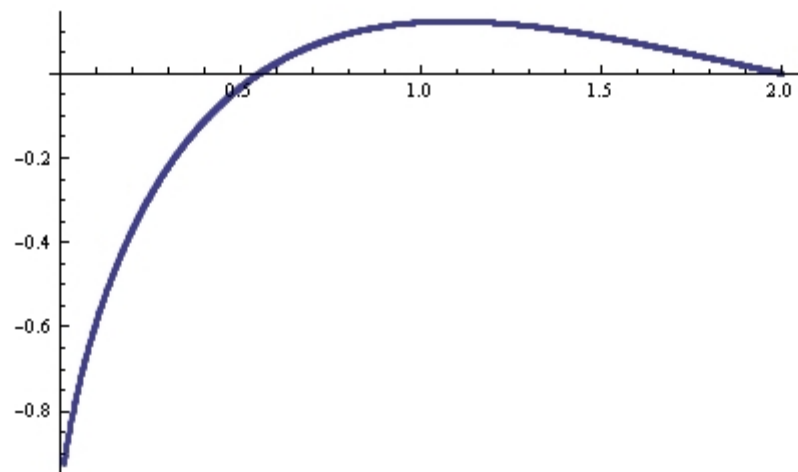
```

1286

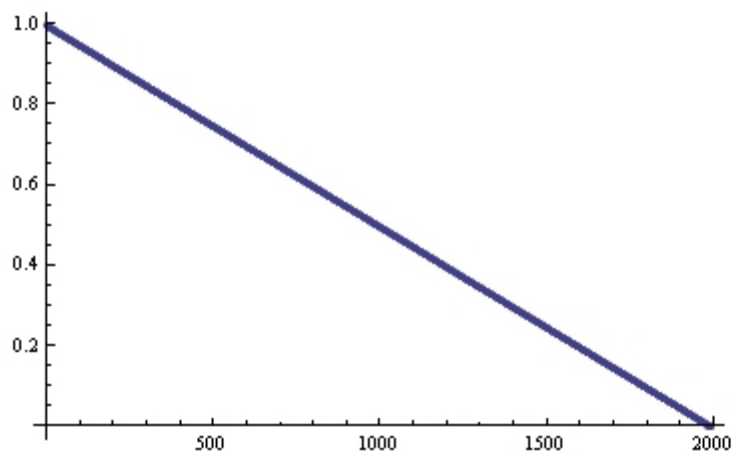
Plot Results

ListPlot[Pdata, PlotRange → Full]

(*Transition pressure as a function of pressure*)

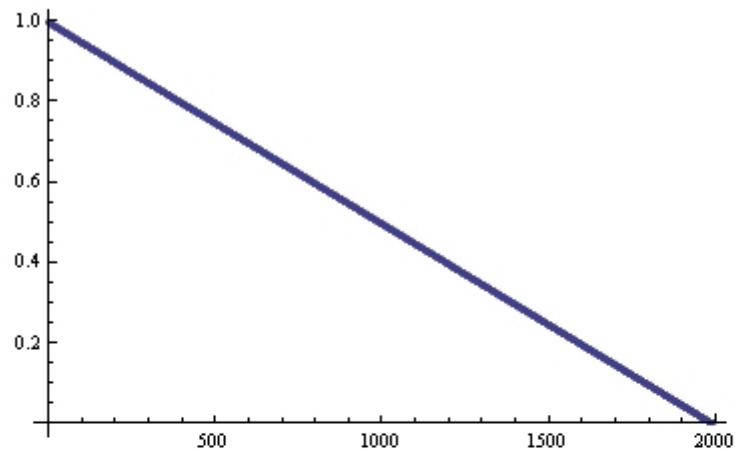


ListPlot[ρ data] (*Solvent density in pervaded volume as a function of pressure at CGT*)

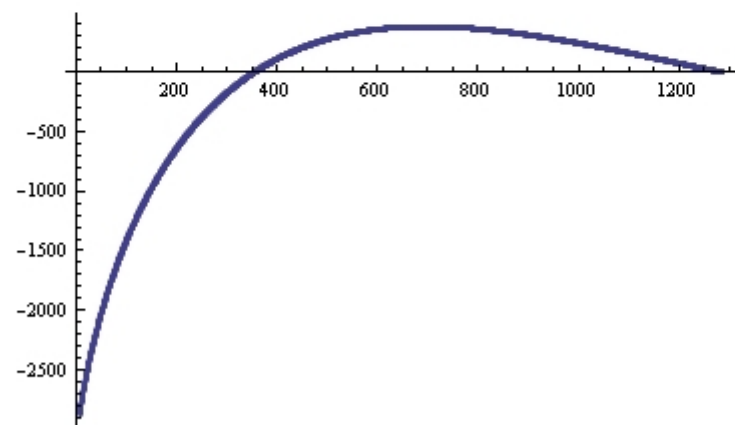


ListPlot[ρ Bdata] (*Solvent density in bulk as a function of pressure at CGT*)

ListPlot[ρ Bdata] (*Solvent density in bulk as a function of pressure at CGT*)



ListPlot[DimPdata, PlotRange -> All]
(*generate dimensional plot of CVT P-T data*)

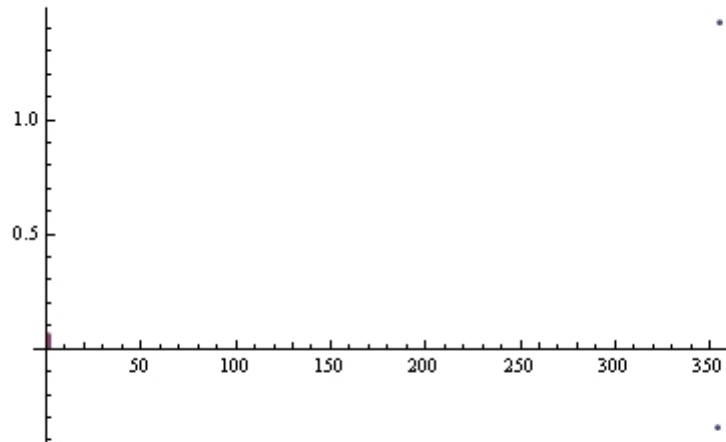


Export["CGT_PIB-nPentane-PTplot.xls", DimPdata]
(*export dimensional P-T data to excel file*)

CGT_PIB-nPentane-PTplot.xls

```
ListPlot[{DimPdata[[542 ;; 543]], Data}]
```

```
(*manually zoom in on two points around zero pressure*)
```



```

$$\frac{\text{DimPdata}[[543, 1]] - \text{DimPdata}[[542, 1]]}{\text{DimPdata}[[543, 2]] - \text{DimPdata}[[542, 2]]}$$

```

```

$$\frac{\text{DimPdata}[[543, 1]] - \text{DimPdata}[[542, 1]]}{\text{DimPdata}[[543, 2]] - \text{DimPdata}[[542, 2]]}$$

```

```
(*based on above manually zoomed plot,  
calculate temperature/pressure slope at p=0*)
```

```
0.36284
```

References

- (1) Freeman, P. I.; Rowlinson, J. S. "Lower Critical Points in Polymer Solutions," *Polymer* **1960**, 1, 20-26.
- (2) Robeson, L. M., *Polymer Blends: A Comprehensive Review*. Hanser Gardner: Munich, 2007.
- (3) Imre, A. R.; Hook, W. A. V.; Wolf, B. A. "Liquid-Liquid Phase Equilibria in Polymer Solutions and Polymer Mixtures," *Macromol. Symp.* **2002**, 181, 363-372.
- (4) Imre, A. R. "Liquid-Liquid Phase Equilibrium of Polymer Solutions and Polymer Blends under Positive and Negative Pressure," *Chinese J. of Poly. Phys.* **2003**, 21, (2), 241-249.
- (5) Lacombe, R. H.; Sanchez, I. C. "Statistical Thermodynamics of Fluid Mixtures," *J. of Phys. Chem.* **1976**, 80, (23), 2568-2580.
- (6) Koningsveld, R.; Stockmayer, W. H.; Nies, E., *Polymer Phase Diagrams: A Textbook*. Oxford University Press: New York, 2001.
- (7) Olabasi, O. "Polymer Compatibility by Gas-Liquid Chromatography," *Macromolecules* **1975**, 8, (3), 316-322.
- (8) Imre, A.; Hook, W. A. V. "Liquid-Liquid Equilibria in Polymer Solutions at Negative Pressure," *Chemical Society Reviews* **1998**, 27, 117-123.
- (9) Konynenburg, P. H. C.; Scott, R. L. "Critical Lines and Phase Equilibria in Binary Van Der Waals Mixtures," *Philosophical Transaction of the Royal Society of London. Series A, Mathematical and Physical Sciences* **1980**, 298, (1442), 495-540.
- (10) Imre, A. R.; Melnichenko, G.; Hook, W. A. V. "Liquid-Liquid Equilibria in Polystyrene Solutions: The General Pressure Dependence," *Phys. Chem. Chem. Phys.* **1999**, 1, 4287-4292.
- (11) Zeman, L.; Biroš, J.; Delmas, G.; Patterson, D. "Pressure Effects in Polymer Solution Phase Equilibria. I. The Lower Critical Solution Temperature of Polyisobutylene and Polydimethylsiloxane in Lower Alkanes," *J. Phys. Chem* **1972**, 76, (8), 1206-1213.

- (12) Folie, B.; Radosz, M. "Phase Equilibria in High-Pressure Polyethylene Technology," *Ind. Eng. Chem. Res* **1995**, 34, 1501-1516.
- (13) Schneider, G. M. "Aqueous Solutions at Pressures up to 2 GPa: Gas-Gas Equilibria, Closed Loops, High-Pressure Immiscibility, Salt Effects and Related Phenomena," *Phys. Chem. Chem. Phys.* **2002**, 4, 845-852.
- (14) Leder, D.; Irani, C. A. "Upper Critical Solution Temperatures in Carbon Dioxide - Hydrocarbon Systems," *J. Chem. and Eng. Data.* **1975**, 20, (3).
- (15) Sanchez, I. C.; Stone, M., In *Polymer Blends*, Paul, D. R.; Bucknall, C. B., Eds. John Wiley & Sons, Inc.: New York, 2000; Vol. 1, p 51.
- (16) Flory, P. J.; Orwoll, R. A.; Vrij, A. "Statistical Thermodynamics of Chain Molecule Liquids. I. An Equation of State for Normal Paraffin Hydrocarbons," *J. Am. Chem. Soc.* **1964**, 87, 3507-3514.
- (17) Flory, P. J.; Orwoll, R. A.; Vrij, A. "Statistical Thermodynamics of Chain Molecule Liquids. II. Liquid Mixtures of Normal Paraffin Hydrocarbons," *J. Am. Chem. Soc.* **1964**, 86, 3515-3520.
- (18) Flory, P. J. "Statistical Thermodynamics of Liquid Mixtures," *J. Am. Chem. Soc.* **1965**, 87, 1833-1838.
- (19) Sanchez, I. C.; Lacombe, R. H. "An Elementary Molecular Theory of Classical Fluids. Pure Fluids," *J. Phys. Chem* **1976**, 80, (21), 2352-2362.
- (20) Sanchez, I. C.; Lacombe, R. H. "Statistical Thermodynamics of Polymer Solutions," *Macromolecules* **1978**, 11, (6), 1145-1156.
- (21) Flory, P. J. "The Configuration of Real Polymer Chains," *J. Chem. Phys.* **1949**, 17, 303-310.
- (22) Flory, P. J., *Polymer Chemistry*. Cornell University Press: Ithaca, 1953.
- (23) de Gennes, P. G., *Scaling Concepts in Polymer Physics*. Cornell University Press: Ithaca, 1979.
- (24) Stockmayer, W. H. "Problems of the Statistical Thermodynamics of Dilute Polymer Solutions," *Die Makromolekulare Chemie* **1960**, 35, (1), 54-74.
- (25) Oono, Y. "On the Unperturbed State of a Polymer Chain," *J. Phys. Soc. Jap.* **1976**, 41, (1), 228-236.
- (26) Oyama, T.; Oono, Y. "Three-Body Intrachain Collisions in a Single Polymer Chain," *J. Phys. Soc. Jap.* **1977**, 42, (4), 1348-1354.

- (27) Sanchez, I. C. "Phase-Transition Behavior of the Isolated Polymer Chain," *Macromolecules* **1979**, 12, (5), 980-988.
- (28) Luna-Barcenas, G.; Gromov, D. G.; Meredith, J. C.; Sanchez, I. C.; Pablo, J. J. d.; Johnston, K. P. "Polymer Chain Collapse near the Lower Critical Solution Temperature," *Chem. Phys. Lett.* **1997**, 278, 302-306.
- (29) Luna-Barcenas, G.; Meredith, J. C.; Sanchez, I. C.; Johnston, K. P.; Gromov, D. G.; Pablo, J. J. d. "Relationship between Polymer Chain Conformation and Phase Boundaries in a Supercritical Fluid," *J. Chem. Phys.* **1997**, 107, (24), 10782-10792.
- (30) Lu, X.; Korgel, B. A.; Johnston, K. P. "Synthesis of Germanium Nanocrystals in High Temperature Supercritical CO₂," *Nanotechnology* **2005**, 16, 389-394.
- (31) Sanchez, I. C. "Phase-Transition Behavior of the Isolated Polymer-Chain," *Macromolecules* **1979**, 12, (5), 980-988.
- (32) Erman, B.; Flory, P. J. "Critical Phenomena and Transitions in Swollen Polymer Networks and in Linear Macromolecules," *Macromolecules* **1986**, 19, (9), 2342-2353.
- (33) Grosberg, A. Y.; Kuznetsov, D. V. "Quantitative Theory of the Globule-to-Coil Transition .1. Link Density Distribution in a Globule and Its Radius of Gyration," *Macromolecules* **1992**, 25, (7), 1970-1979.
- (34) Tanaka, G.; Mattice, W. L. "Chain Collapse by Atomistic Simulation," *Macromolecules* **1995**, 28, (4), 1049-1059.
- (35) Muthukumar, M. "Collapse Transition of a Stiff Chain," *Journal of Chemical Physics* **1984**, 81, (12), 6272-6276.
- (36) Yamakawa, H. "The Radius Expansion Factor and 2nd Virial-Coefficient for Polymer-Chains Below the θ Temperature," *Macromolecules* **1993**, 26, (19), 5061-5066.
- (37) Nakata, M. "Coil-Globule Transition of Poly(Methyl Methacrylate) in a Mixed-Solvent," *Physical Review E* **1995**, 51, (6), 5770-5775.
- (38) Nakata, M.; Nakagawa, T. "Coil-Globule Transition of Poly(Methyl Methacrylate) in Isoamyl Acetate," *Physical Review E* **1997**, 56, (3), 3338-3345.
- (39) Hamurcu, E. E.; Akcelrud, L.; Baysal, B. M.; Karasz, F. E. "Dynamic Light Scattering Studies of Poly(4-Chlorostyrene) and Poly(2-Chlorostyrene) in θ Solvents," *Polymer* **1998**, 39, (16), 3657-3663.

- (40) Nakata, M.; Nakagawa, T. "Kinetics of Coil-Globule Transition of Poly(Methyl Methacrylate) in Isoamyl Acetate," *Journal of Chemical Physics* **1999**, 110, (5), 2703-2710.
- (41) Nakamura, Y.; Sasaki, N.; Nakata, M. "Kinetics of the Coil-Globule Transition of Poly(Methyl Methacrylate) in a Mixed Solvent," *Macromolecules* **2001**, 34, (17), 5992-6002.
- (42) Zhang, G.; Wu, C. "The Water/Methanol Complexation Induced Reentrant Coil-to-Globule-to-Coil Transition of Individual Homopolymer Chains in Extremely Dilute Solution," *J. Am. Chem. Soc.* **2001**, 123, (7), 1376-1380.
- (43) Dogan, M.; Kuntman, A. "Study on Conformational Transition Phenomena of Poly(Methyl Methacrylate) in Acetonitrile near Theta Conditions," *Polymer International* **2000**, 49, (12), 1648-1652.
- (44) Gurel, E. E.; Kayaman, N.; Baysal, B. M.; Karasz, F. E. "Dynamic Light Scattering Studies of Atactic and Syndiotactic Poly(Methyl Methacrylate)S in Dilute Theta Solution," *Journal of Polymer Science Part B-Polymer Physics* **1999**, 37, (16), 2253-2260.
- (45) Polson, J. M.; Moore, N. E. "Simulation Study of the Coil-Globule Transition of a Polymer in Solvent," *Journal of Chemical Physics* **2005**, 122, (2).
- (46) Szleifer, I.; Otoole, E. M.; Panagiotopoulos, A. Z. "Monte-Carlo Simulation of the Collapse-Coil Transition in Homopolymers," *Journal of Chemical Physics* **1992**, 97, (9), 6802-6808.
- (47) Lang, D. "Regular Superstructures of Purified DNA in Ethanolic Solutions," *Journal of Molecular Biology* **1973**, 78.
- (48) Lang, D.; Taylor, T. N.; Dobyhan, D. C.; Gray, D. M. "Dehydrated Circular DNA - Electron-Microscopy of Ethanol-Condensed Molecules," *Journal of Molecular Biology* **1976**, 106, (1), 97-107.
- (49) Vasilevskaya, V. V.; Khokhlov, A. R.; Matsuzawa, Y.; Yoshikawa, K. "Collapse of a Single DNA Molecule in Poly(Ethylene Glycol) Solutions," *Journal of Chemical Physics* **1995**, 102, (16), 6595-6602.
- (50) Melnikov, S. M.; Sergeev, V. G.; Yoshikawa, K. "Transition of Double-Stranded DNA Chain between Random Coil and Compact Globule States Induced by Cooperative Binding of Cationic Surfactant," *Journal of the American Chemical Society* **1995**, 117, (40), 9951-9956.

- (51) Dias, R. S.; Innerlohinger, J.; Glatter, O.; Miguel, M. G.; Lindman, B. "Coil-Globule Transition of DNA Molecules Induced by Cationic Surfactants: A Dynamic Light Scattering Study," *Journal of Physical Chemistry B* **2005**, 109, (20), 10458-10463.
- (52) Pollack, L.; Tate, M. W.; Finnefrock, A. C.; Kalidas, C.; Trotter, S.; Darnton, N. C.; Lurio, L.; Austin, R. H.; Batt, C. A.; Gruner, S. M.; Mochrie, S. G. J. "Time Resolved Collapse of a Folding Protein Observed with Small Angle X-Ray Scattering," *Physical Review Letters* **2001**, 86, (21), 4962-4965.
- (53) Sadqi, M.; Lapidus, L. J.; Munoz, V. "How Fast Is Protein Hydrophobic Collapse?," *Proceedings of the National Academy of Sciences of the United States of America* **2003**, 100, (21), 12117-12122.
- (54) Welker, E.; Maki, K.; Shastry, M. C. R.; Juminaga, D.; Bhat, R.; Scheraga, H. A.; Roder, H. "Ultrarapid Mixing Experiments Shed New Light on the Characteristics of the Initial Conformational Ensemble During the Folding of Ribonuclease A," *Proceedings of the National Academy of Sciences of the United States of America* **2004**, 101, (51), 17681-17686.
- (55) Sherman, E.; Haran, G. "Coil-Globule Transition in the Denatured State of a Small Protein," *Proceedings of the National Academy of Sciences of the United States of America* **2006**, 103, (31), 11539-11543.
- (56) Akasaka, K.; Tezuka, T.; Yamada, H. "Pressure-Induced Changes in the Folded Structure of Lysozyme," *J. Mol. Biol.* **1997**, 271, 671-678.
- (57) Hayakawa, I.; Linko, Y.; Link, P. "Mechanism of High Pressure Denaturation of Proteins," *Lebensm.-Wiss. u.-Technol.* **1996**, 29, 756-762.
- (58) Kunugi, S.; Tanaka, N. "Cold Denaturation of Proteins under High Pressure," *Biochimica et Biophysica Acta* **2002**, 1595, 329-344.
- (59) Dijkstra, M.; Frenkel, D.; Hansen, J. P. "Phase-Separation in Binary Hard-Core Mixtures," *Journal of Chemical Physics* **1994**, 101, (4), 3179-3189.
- (60) Dijkstra, M.; Frenkel, D. "Simulation Study of a 2-Dimensional System of Semiflexible Polymers," *Physical Review E* **1994**, 50, (1), 349-357.
- (61) Luna-Barcenas, G.; Bennett, G. E.; Sanchez, I. C.; Johnston, K. P. "Monte Carlo Simulation of Polymer Chain Collapse in Athermal Solvents," *Journal of Chemical Physics* **1996**, 104, (24), 9971-9973.
- (62) Khalatur, P. G.; Zherenkova, L. V.; Khokhlov, A. R. "Entropy-Driven Polymer Collapse: Application of the Hybrid Mc/Rism Method to the Study of

- Conformational Transitions in Macromolecules Interacting with Hard Colloidal Particles," *European Physical Journal B* **1998**, 5, (4), 881-897.
- (63) Wu, C.; Wang, X. "Globule-to-Coil Transition of a Single Homopolymer Chain in Solution.," *Phys. Rev. Lett.* **1998**, 80, (18), 4092-4094.
- (64) Wang, X.; Qiu, X.; Wu, C. "Comparison of the Coil-to-Globule and the Globule-to-Coil Transitions of a Single Poly(N-Isopropylacrylamide) Homopolymer Chain in Water," *Macromolecules* **1998**, 31, 2972-2976.
- (65) Qiu, X.; Li, M.; Kwan, C. M. S.; Wu, C. "Light-Scattering Study of the Coil-to-Globule Transition of Linear Poly(N-Isopropylacrylamide) Ionomers in Water," *J. Poly. Sci. B: Poly. Phys.* **1998**, 36, 1501-1506.
- (66) Urry, D. W. "Physical Chemistry of Biological Free Energy Transduction as Demonstrated by Elastic Protein-Based Polymers," *Journal of Physical Chemistry B* **1997**, 101, (51), 11007-11028.
- (67) Kubota, K.; Fujishige, S. "Single-Chain Transition of Poly(N-Isopropylacrylamide) in Water," *J. Phys. Chem.* **1990**, 94, 5154-5158.
- (68) Gao, J.; Wu, C. "The "Coil-to-Globule" Transition of Poly(N-Isopropylacrylamide) on the Surface of a Surfactant-Free Polystyrene Nanoparticle," *Macromolecules* **1997**, 30, 6873-6876.
- (69) Xhang, X. Z.; Zhou, R. X.; Cui, J. Z.; Zhang, J. T. "A Novel Thermo-Responsive Drug Delivery System with Positive Controlled Release," *International Journal of Pharmaceutics* **2002**, 235, 43-50.
- (70) Joeong, B.; Kim, S. W.; Bae, Y. H. "Thermosensitive Sol-Gel Reversible Hydrogels," *Advanced Drug Delivery Reviews* **2002**, 54, 37-51.
- (71) Ballauff, M.; Lu, Y. ""Smart" Nanoparticles: Preparation, Characterization and Applications," *polymer* **2007**, 48, 1815-1823.
- (72) Brazel, C. S.; Peppas, N. A. "Pulsatile Local Delivery of Thrombolytic and Antithrombotic Agents Using Poly(N-Isopropylacrylamide-Co-Methacrylic Acid) Hydrogels," *Journal of Controlled Release* **1996**, 39, 57-64.
- (73) Richter, A.; Paschew, G.; Klatt., S.; Lienig, J.; Arndt, K. F.; Adler, H. J. "Review on Hydrogel-Based Ph Sensors and Microsensors," *Sensors* **2008**, 8, 561-581.
- (74) Richter, A.; Howitz, S.; Kuckling, D.; Arndt, K. F. "Influence of Volume Phase Transition Phenomena on the Behavior of Hydrogel-Based Valves," *Sensors and Actuators B* **2004**, 99, 451-458.

- (75) Lowe, C. P.; Dreischor, M. W. "The Size of a Polymer in a Symmetric Solvent," *Journal of Chemical Physics* **2005**, 122, (8), 0849051-0849057.
- (76) Schild, H. G.; Tirrell, D. A. "Microcalorimetric Detection of Lower Critical Solution Temperatures in Aqueous Polymer Solutions," *J. Phys. Chem.* **1990**, 94, 4352-4356.
- (77) Inomata, H.; Goto, S.; Otake, K.; Saito, S. "Effect of Additives on Phase-Transition of N-Isopropylacrylamide Gels," *Langmuir* **1992**, 8, (2), 687-690.
- (78) Suwa, K.; Yamamoto, K.; Akashi, M.; Takano, K.; Tanaka, N.; Kunugi, S. "Effects of Salt on the Temperature and Pressure Responsive Properties of Poly(N-Vinylisobutyramide) Aqueous Solutions," *Colloid and Polymer Science* **1998**, 276, (6), 529-533.
- (79) Hong, J. S.; Nakahara, T.; Maeda, H.; Kikunaga, Y.; Kishida, A.; Akashi, M. "Cloud Points and Phase Separation of Aqueous Poly(N-Vinylacetamide) Solutions in the Presence of Salts," *Colloid Polym. Sci* **1996**, 274, 1013-1019.
- (80) Florin, E.; Kjellander, R.; Eriksson, J. C. "Salt Effects on the Cloud Point of the Poly(Ethylene Oxide) + Water System," *J. Chem. Soc., Faraday Trans. I* **1984**, 80, 2889-2910.
- (81) Park, T. G.; Hoffman, A. S. "Sodium Chloride-Induced Phase-Transition in Nonionic Poly(N-Isopropylacrylamide) Gel," *Macromolecules* **1993**, 26, (19), 5045-5048.
- (82) Annaka, M.; Motokawa, K.; Sasaki, S.; Nakahira, T.; Kawasaki, H.; Maeda, H.; Amo, Y.; Tominaga, Y. "Salt-Induced Volume Phase Transition of Poly(N-Isopropylacrylamide) Gel," *Journal of Chemical Physics* **2000**, 113, (14), 5980-5985.
- (83) Sun, T.; King, H. E. "Pressure-Induced Reentrant Phase Behavior in the Poly(N-Vinyl-2-Pyrrolidone)-Water System," *Phys. Rev. E* **1996**, 54, (3), 2696-2703.
- (84) Muta, H.; Miwa, M.; Satoh, M. "Ion-Specific Swelling of Hydrophilic Polymer Gels," *Polymer* **2001**, 42, (14), 6313-6316.
- (85) Melander, W.; Horvath, C. "Salt Effects on Hydrophobic Interactions in Precipitation and Chromatography of Proteins: An Interpretation of the Lyotropic Series," *Archives of Biochemistry and Biophysics* **1977**, 183, 200-215.
- (86) Takano, K.; Ogata, K.; Kawauchi, S.; Satoh, M.; Komiyama, J. "Ion-Specific Swelling Behavior of Poly(N-Vinyl-2-Pyrrolidone) Gel: Correlations with Water

- Hydrogen Bond and Non-Freezable Water," *Poly. Gels and Networks* **1998**, 6, 217-232.
- (87) Jones, G.; Dole, M. "The Viscosity of Aqueous Solutions of Strong Electrolytes with Special Reference to Barium Chloride," *J. Am. Chem. Soc.* **1929**, 51, (10), 2950-2964.
- (88) Gurney, R. W., *Ionic Processes in Solution*. McGraw-Hill: New York, 1953.
- (89) Debye, P. J. W.; Huckel, E., On the Theory of Electrolytes. I. Freezing Point Depression and Related Phenomena. In *The Collected Papers of Peter J. W. Debye*, Interscience Publishers: New York, 1923; pp 217-263.
- (90) Solis, F. J.; de la Cruz, M. O. "Collapse of Flexible Polyelectrolytes in Multivalent Salt Solutions," *Journal of Chemical Physics* **2000**, 112, (4), 2030-2035.
- (91) Solis, F. J.; Cruz, M. O. d. l. "Flexible Linear Polyelectrolytes in Multivalent Salt Solutions: Solubility Conditions," *Eur. Phys. J. E* **2001**, 4, 143-152.
- (92) Klos, J.; Pakula, T. "Computer Simulations of a Polyelectrolyte Chain with a Mixture of Multivalent Salts," *J. Phys.: Condens. Matter* **2005**, 17, 5635-5645.
- (93) Dobrynin, A. V.; Rubinstein, M. "Theory of Polyelectrolytes in Solutions and at Surfaces," *Prg. Polym. Sci* **2005**, 30, 1049-1118.
- (94) de Gennes, P. G.; Pincus, P.; Velasco, R. M. "Remarks on Polyelectrolyte Conformation," *Journal de Physique* **1976**, 37, 1461-1473.
- (95) Skolnick, J.; Fixman, M. "Electrostatic Persistence Length of a Wormlike Polyelectrolyte," *Macromolecules* **1977**, 10, (5), 944-948.
- (96) Fixman, M.; Skolnick, J. "Polyelectrolyte Excluded Volume Paradox," *Macromolecules* **1978**, 11, (5), 863-866.
- (97) Qian, C.; Kholodenko, A. L. "On Electrostatic Rigidity of Polyelectrolytes," *J. Chem. Phys.* **1988**, 89, (4), 2301-2311.
- (98) Barrat, J. L.; Joanny, J. F. "Persistence Length of Polyelectrolyte Chains," *Europhys. Lett.* **1993**, 24, (5), 333-338.
- (99) Dobrynin, A. V.; Colby, R. H.; Rubinstein, M. "Scaling Theory of Polyelectrolyte Solutions," *Macromolecules* **1995**, 28, 1859-1871.
- (100) Dobrynin, A. V. "Electrostatic Persistence Length of Semiflexible and Flexible Polyelectrolytes," *Macromolecules* **2005**, 38, 9304-9314.

- (101) Flory, P. J. "Molecular Configuration of Polyelectrolytes," *J. Chem. Phys.* **1953**, 21, 162-163.
- (102) Hill, T. H. "Size and Shape of Polyelectrolyte Molecules in Solution," *J. Chem. Phys.* **1952**, 20, 1173-1174.
- (103) Dobrynin, A. V.; Rubinstein, M.; Obukhov, S. "Cascade of Transitions of Polyelectrolytes in Poor Solvents," *Macromolecules* **1996**, 29, 2974-2979.
- (104) Jeon, J.; Dobrynin, A. V. "Necklace Globule and Counterion Condensation," *Macromolecules* **2007**, 50, 7695-7706.
- (105) Ulrich, S.; Laguecir, A.; Stoll, S. "Titration of Hydrophobic Polyelectrolytes Using Monte Carlo Simulations," *J. Chem. Phys.* **2005**, 122, 0949111-0949119.
- (106) Brazel, C. S.; Peppas, N. A. "Synthesis and Characterization of Thermo- and Chemomechanically Responsive Poly(N-Isopropylacrylamide-Co-Methacrylic Acid) Hydrogels," *Macromolecules* **1995**, 28, 8016-8020.
- (107) Vakkalanka, S. K.; Peppas, N. A. "Swelling Behavior of Temperature- and Ph-Sensitive Block Terpolymers for Drug Delivery," *Polymer Bulletin* **1996**, 36, (2), 221-225.
- (108) Yoo, M. K.; Sung, Y. K.; Lee, Y. M.; Cho, C. S. "Effect of Polyelectrolyte on the Lower Critical Solution Temperature of Poly(N-Isopropyl Acrylamid) in the Poly(Nipaam-Co-Acrylic Acid) Hydrogel," *Polymer* **2000**, 41, 5713-5719.
- (109) Kaneko, D.; Gong, J. P.; Osada, Y. "Polymer Gels as Soft and Wet Chemomechanical Systems - an Approach to Artificial Muscles," *J. Mater. Chem.* **2002**, 12, 2169-2177.
- (110) Osada, Y.; Hasebe, M. "Electrically Activated Mechanochemical Devices Using Polyelectrolyte Gels," *Chem. Lett.* **1985**, 14, (9), 1285-1288.
- (111) Murdan, S. "Electro-Responsive Drug Delivery from Hydrogels," *J. Controlled Release* **2003**, 92, 1-17.
- (112) Moschou, E. A.; Peteu, S. F.; Bachas, L. G.; Madou, M. J.; Daunert, S. "Artificial Muscle Material with Fast Electroactuation under Neutral Ph Conditions," *Chem. Mater.* **2004**, 16, 2499-2502.
- (113) Bokias, G.; Staikos, G.; Iliopoulos, I. "Solution Properties and Phase Behavior of Copolymers of Acrylic Acid with N-Isopropylacrylamide: The Importance of the Intrachain Hydrogen Bonding," *Polymer* **2000**, 41, 7399-7405.

- (114) Yin, X.; Hoffman, A. S.; Stayton, P. S. "Poly(N-Isopropylacrylamide-Co-Propylacrylic Acid) Copolymers That Respond Sharply to Temperature and Ph," *Biomacromolecules* **2006**, 7, (5), 1381-1385.
- (115) Jones, M. S. "Effect of Ph on the Lower Critical Solution Temperature of Random Copolymers of N-Isopropylacrylamide and Acrylic Acid," *Eur. Poly. J.* **1999**, 45, 795-801.
- (116) Kuhn, P. S. "A Simple Model for the Collapse of Polyelectrolyte Macromolecules," *Physica A* **2002**, 311, 50-58.
- (117) Winkler, R. G.; Gold, M.; Reineker, P. "Collapse of Polyelectrolyte Macromolecules by Counterion Condensation and Ion Pair Formation: A Molecular Dynamics Simulation Study," *Phys. Rev. Lett.* **1998**, 80, (17), 3731-3734.
- (118) Ullner, M.; Jonsson, B.; Widmark, P. O. "Conformational Properties and Apparent Dissociation Constants of Titrating Polyelectrolytes: Monte Carlo Simulation and Scaling Arguments," *J. Chem. Phys.* **1994**, 100, (4), 3365-3366.
- (119) Tanford, C.; Kirkwood, J. G. "Theory of Protein Titration Curves. I. General Equations for Impenetrable Spheres," *J. Am. Chem. Soc.* **1957**, 79, (20), 5333-5339.
- (120) Neto, A. A.; Filho, E. D.; Fossey, M. A.; Neto, J. R. "Pk Determination. A Mean Field, Poisson-Boltzmann Approach," *J. Phys. Chem.* **1999**, 103, 6809-6814.
- (121) Manning, G. S. "Limiting Laws and Counterion Condensation in Polyelectrolyte Solutions I. Colligative Properties," *J. Chem. Phys* **1969**, 51, (3), 924-933.
- (122) Deshkovski, A.; Obukhov, S.; Rubinstein, M. "Counterion Phase Transition in Dilute Polyelectrolyte Solutions," *Phys. Rev. Lett.* **2001**, 86, (11), 2341-2344.
- (123) Muthukumar, M. "Theory of Counter-Ion Condensation on Flexible Polyelectrolytes: Adsorption Mechanism," *J. Chem. Phys* **2004**, 120, (19), 9343-9350.
- (124) Kundagrami, A.; Muthukumar, M., Theory of Competitive Counterion Adsorption on Flexible Polyelectrolytes: Divalent Salts. In University of Massachusetts at Amherst: Amherst, 2008.
- (125) Ermoshkin, A. V.; Cruz, M. O. d. l. "Polyelectrolytes in the Presence of Multivalent Ions: Gelation Versus Segregation," *Physical Review Letters* **2003**, 90, (12).

- (126) Widom, B. "Some Topics in the Theory of Fluids," *J. Chem. Phys.* **1963**, 39, (11), 2808-2812.
- (127) Sanchez, I. C.; Truskett, T. M.; in 't Veld, P. J. "Configuration Properties and Corresponding States in Simple Fluids and Water," *J. Phys. Chem. B* **1999**, 103, 5106-5116.
- (128) Panayiotou, C.; Sanchez, I. C. "Hydrogen Bonding in Fluids: An Equation-of-State Approach," *J. Phys. Chem* **1991**, 95, 10090-10097.
- (129) Veytsman, B. "Are Lattice Models Valid for Fluids with Hydrogen Bonds," *J. Phys. Chem* **1990**, 94, 8499-8500.
- (130) Panayiotou, C.; Tsivintzelis, I.; Economou, I. G. "Nonrandom Hydrogen-Bonding Model of Fluids and Their Mixtures. 2. Multicomponent Mixtures," *Ind. Eng. Chem. Res.*, **2007**, 46, (8), 2628-2636.
- (131) Kisselev, A. M.; Manias, E. "Phase Behavior of Temperature-Responsive Polymers with Tunable Lcst: An Equation-of-State Approach," *Fluid Phase Equilibria* **2007**, 261, 69-78.
- (132) Sanchez, I. C., Unpublished Work. In 2009.
- (133) Lebowitz, J. L.; Helfand, E.; E., P. "Scaled Particle Theory of Fluid Mixtures," *J. Chem. Phys.* **1965**, 43, (3), 774-779.
- (134) Saeki, S.; Kuwahara, N.; Kaneko, M. "Pressure Dependence of Upper and Lower Critical Solution Temperatures in Polystyrene Solutions," *Macromolecules* **1976**, 9, (101-106).
- (135) Enders., S.; Loos, T. W. d. "Pressure Dependence of the Phase Behavior of Polystyrene in Methylcyclohexane," *Fluid Phase Equilibria* **1997**, 139, 335-347.
- (136) Zeman, L.; Patterson, D. "Pressure Effects in Polymer Solution Phase Equilibria. Ii. Systems Showing Upper and Lower Critical Solution Temperatures," *J. Phys. Chem* **1972**, 76, (8), 1214-1219.
- (137) Zhong, X.; Wang, Y. X.; Wang, S. C. "Pressure Dependence of the Volume Phase-Transition of Temperature-Sensitive Gels," *Chem. Eng. Sci.* **1996**, 51, (12), 3235-3239.

Vita

David Samuel Simmons was born in Miami and attended Miami Killian Senior High School. In 2000, he matriculated at the University of Florida and in 2005 graduated magna cum laude with a Bachelor of Science in Chemical Engineering. During this time, he conducted undergraduate research on the subject of thin film stability, and he also spent several summers employed as a research intern at the biomedical engineering companies Syntheon LLC and Innovia LLC in Miami, Florida. In August, 2009 he began work towards a Ph.D. in the Chemical Engineering Department of the Cockrell School of Engineering at The University of Texas at Austin. Upon completion of his doctoral degree, David plans to join the National Institute of Standards and Technology in Gaithersburg, Maryland as a postdoctoral research associate.

Permanent Address: 9720 SW 121 St., Miami, Florida, 33176

This manuscript was typed by the author.